Title

Experimental Measurement of Residual Stress-Induced In-Plane Displacements of As-Machined Polymer Structures Resultant from Fused Filament Fabrication Additive Manufacturing

Author

Nelson, Daniel

Publication Date

2023

Peer reviewed|Thesis/dissertation

Experimental Measurement of Residual Stress-Induced In-Plane Displacements of As-Machined Polymer Structures Resultant from Fused Filament Fabrication Additive Manufacturing

By

DANIEL NELSON
DISSERTATION

Submitted in partial satisfaction of the requirements for the degree of

DOCTOR OF PHILOSOPHY

in

Mechanical and Aerospace Engineering

in the

OFFICE OF GRADUATE STUDIES

of the

UNIVERSITY OF CALIFORNIA

DAVIS

Approved:

Valeria La Saponara, Chair

Iman Soltani

Anastasia Muliana

Committee in Charge

2023

DEDICATION

To my family (Amy, James, Sam, and Madeline), without your steadfast support through all of the long hours, absences, and stressful events I would never have completed this endeavor. Thank you so incredibly much!

ACKNOWLEDGMENTS

First, I want to thank my advisor Dr. Valeria La Saponara. You inspired me as an undergraduate student to pursue higher learning in engineering. Your unwavering support and mentorship for almost two decades has been invaluable. Not only did you get me started on this path, but you have moved mountains to make sure that I can finish it.

To my dissertation committee members Dr. Anastasia Muliana and Dr. Iman Soltani. Thank you for all your advice and counsel. You always found time in your busy lives to meet with me and shape this project into something useful and achievable.

To the Defense Innovation Unit, LTC Christopher Hetz, Ms. Cherissa Tamayori, Mr. Roshan Jessani, Dr. Nina French, Lt Col Ryan Kappedal, and its former Director Mr. Michael Brown. Thank you for believing in the program and in my ability to complete it. Your foresight in establishing and supporting this investment in educating service members to tackle the toughest DoD problems is truly an example of an organization practicing what it preaches. I only hope my continued service to the organization is worth the effort put forth on my behalf.

To the Air Force Research Lab (AFRL), Mr. Andrew Abbott, Mr. Tyler Lesthaeghe. Dr. Craig Przybyla, Dr. Lorianne Groo, and Dr. Eric Lindgren. Without your support, time, and advice this project would not have been possible. Every single one of you took time from your packed schedules and countless responsibilities to work with me to refine and vet my project plan and never once made me feel like helping me along this journey was a burden.

ABSTRACT

This dissertation documents the research work accomplished to experimentally determine the surface displacements resultant from the manifestation of the internal stresses caused by the thermal flows within the body of a structure created during the act of Fused Filament Fabrication (FFF) manufacturing processes.

One of the most critical technical issues plaguing additive manufacturing (AM) technologies are the effects of warping and dimensional variations found print-to-print in manufactured structures. These issues arise as a result of the creation of manufacturing-induced residual stresses within the body of the structure being created. To overcome these issues, it is necessary to first understand how these stresses manifest and effect the structure of interest during the build process. To establish this level of understanding one needs to utilize a method to locate, quantify, and measure surface displacements over the entire build process in order to develop a means to mitigate the residual stresses causing these problems. This dissertation documents the experimental and analytical processes created to perform these essential measurements. Application of this novel experimental and analysis framework allows for the understanding to be generated as to the behavior of the residual stress induced displacements as well as determining the most significant manufacturing parameters leading to the creation of these displacement events.

Through the execution of the experimental and analysis work presented within the following dissertation, an *in situ* displacement measurement capability was developed for small scale AM FFF manufacturing systems. As part of the design of this overall measurement capability, it was first required to determine the best modalities available to accurately sense and record the surface displacements developed within the AM structure being assembled during

manufacturing. Through a thorough literature review and targeted preliminary experimentation, it was determined that a “no touch” and “no interference” displacement measurement technique was the only viable method to capture full field warping and deformation events created due to thermal discontinuities occurring during the AM process, because it does not interfere with the process. These measurements were accomplished through the use of digital image correlation (DIC) systems which, within the methodology employed, are capable of quantifying the full field surface displacement of the test specimen. This data-capture capability provided a means to determine the magnitude and location of displacement events as they occurred and changed during the act of part manufacture. This novel application of *in situ* DIC monitoring in the 3D printing of small-scale structures was adapted from published works of researchers from the University of Tennessee, Oak Ridge National Laboratory, Vanderbilt University, and The Institute for Advanced Composites Manufacturing Innovation (IACMI). This DIC approach allows for the measurement of surface displacements without the application of an external speckle pattern to the surface of the test specimen. Instead, this application of the DIC technology requires the natural surface roughness of the test specimen itself to act as a replacement for an externally applied speckle pattern. This methodology was found to produce displacement measurements with high correlation to those produced by DIC analysis using an externally applied speckle patterns. Pairing this sensing capability with innovative analysis provided the insight needed to analyze the deformation behavior of the constructed test structure and to work through the determination of the manufacturing parameters that provided the greatest statistical contribution to the generation of those deformation/warping events.

Overall, the experimental and analysis process created through the course of this research effort and detailed within this dissertation provide for the generation of a foundational

understanding of manufacturing-induced residual stresses within the body of FFF polymer structures. The highly robust process designed within this research effort is capable of being adjusted and customized to allow for the displacement assessment of structures composed of a wide variety of filament types across a broad selection of manufacturing systems. This will thereby provide the research and manufacturing communities with an enduring and, I believe, crucial technique.

TABLE OF CONTENTS

LIST OF TABLES

LIST OF FIGURES

CHAPTER 1 - INTRODUCTION

The research conducted for my PhD degree was designed to create an experimentally-based, foundational level-understanding of the effects of residual mechanical stresses developed within the body of additively manufactured (AM) structures. Specifically, my research project consisted of the novel design and demonstration of an experimental architecture that allowed for the *in situ* data capture and analysis of residual stress-induced surface displacements and thermal variations on an AM structure. While the application of the experimental methodology and analysis process presented within this dissertation does not require the use of a specific base material or modality of AM, it has, in this instance, been demonstrated on a Fused Filament Fabrication (FFF) printer utilizing neat Polyethylene Terephthalate Glycol (PETG). Employing this manufacturing system and base material/filament composition allowed for the development of the experimental and analysis processes on a system that represents the most popular and widely used AM variant [1] using a base material/filament mixture (i.e. filaments not containing a polymer matrix with embedded chopped carbon fibers, or filaments comprised of mixture of multiple thermoplastic polymers). This use of an amorphous polymer filament ensured that the creation and initial validation of the experimental and analysis process presented here was not hindered by confounding effects of chopped fiber orientation/bonding or differing amounts of crystallization within the polymer structures print-to-print [2–6].

One of the major deficiencies of polymer-based FFF is the prevalence of part distortion and warpage that occur during part creation as a direct result of this type of manufacturing process [7,8]. The overall goal of this research effort was to design a process that could provide researchers and practitioners of AM technologies a detailed understanding of: 1) the spatial and temporal temperature flow on any point of the surface of a FFF structure during the print

process; 2) the spatial and temporal material displacements for the entirety of the surface imaged, caused by these temperature gradients. Additionally, to more fully understand the problem at hand, it is necessary to determine how the development and magnitude of these measured displacements vary print-to-print, and as certain manufacturing parameters are changed. My research project shows that it is possible to capture and analyze the displacement and thermal data of a structure during the build process, and that statistical analyses determine which manufacturing parameters lead to the largest residual stress-induced surface displacement. These experimental results and data allow for the strategic design of both AM structures and manufacturing strategies, to limit magnitude and effect of these residual stresses.

The research presented within this dissertation concentrates on AM polymer structures, specifically on the manufacturing method of FFF. FFF was chosen as the manufacturing methodology of interest due to its wide proliferation and application. FFF currently accounts for 69% of all 3D printing technologies, and is widely used in a variety of disciplines [1]. Additionally, with the prospect of AM triggering the third industrial revolution, and being an integral part of the industry 4.0 framework [9,10]. There is the potential to generate an enormous impact on this technology when addressing major issues such as warping combined with the ability to tailor mechanical properties during the manufacturing process, through the adjustment of specific printer settings/parameters [11].

As a method of AM, FFF utilizes a thermoplastic filament as its manufacturing base material. This thermoplastic filament is extruded through a nozzle apparatus, where the material is heated to the point that the base material viscosity is low enough to allow for the desired rate of material flow. The heated thermoplastic is then precisely deposited in successive layers, beginning with the build plate, then continuing in a vertical direction with the deposition of new

material onto previously deposited layers, to create the three-dimensional structure desired, as shown in **Figure 1** below.

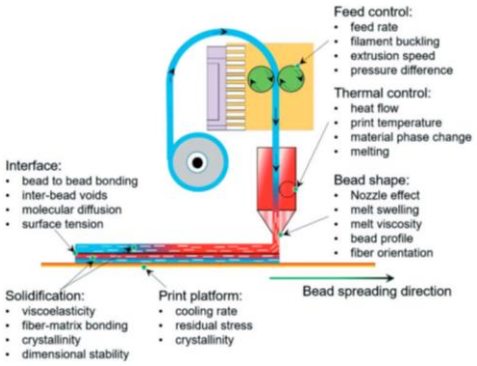

Figure 1. Fused Filament Fabrication Overview [12].

After deposition, the thermoplastic melt solidifies, creating the desired structural configuration. It is this process of repeatedly depositing hot melted thermoplastic upon the previously solidified and cooled layers that leads to significant temperature gradients and interlayer expansion/contraction effects [13]. These temperature gradients, along with the expansion and contraction interactions between deposition layers, can lead to the development of high internal residual stresses, often creating deformation, warping, or reduced mechanical properties of the project piece of interest [12]. The cumulative effect of these residual stresses onto the printed object can often result in severe deformation, shown below in **Figure 2**, causing a complete loss of the structure under construction.

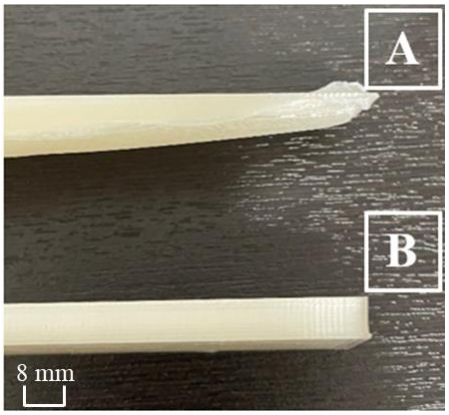

Figure 2. FFF Test Blocks: Block A shows severe edge deformation, Block B shows no edge deformation.

A detailed literature review was conducted to understand the body of work that has been undertaken to measure and model the displacement and warping events that occur in AM. As part of this review, I concentrated on published research that fell into one of two categories. The first category was those research efforts that had been undertaken to model and predict the creation of residual stresses within an AM structure and the resultant deformations that those stresses would cause. The second category was those research efforts that were executed to explore the viability of sensing the effect of the residual stresses created within the structure through a variety of methods.

Within the first category, I found that significant research has been conducted to date to understand, model, and predict the residual stresses developed within polymer structures during the FFF manufacturing process [14–20] . The goal of these research efforts has been focused on building the numerical and analytical modeling of the internal stresses causing these warping occurrences. Overall, there were several shortcomings noted within the overall body of published works, such as:

- Most cited work failed to model the effects of a heated build plate or a build plate that exists at a temperature different from the ambient environment. This oversight can

drastically affect the results that obtained through modeling. The heat supplied by the build plate can limit the amount of contraction occurring within the structure that is in close proximity to the build plate. Additionally, the combined heat supplied by the build plate and the new hot deposition can force a material transition through the glass transition temperature, drastically changing the stiffness of the structure, and reducing its ability to resist residual stress induced deformations;

- Most cited work modeled the structures as a linearly elastic system, not a non-linear viscoelastic system. This shortcoming can reduce the overall accuracy of the modeling results produced. The simplification of a linear elastic assumption can allow for the production of "ballpark" displacement/warping predictions to be made. However, it fails to fully capture the dependence on strain and displacement history and the generation of irreversible displacements within the end state of the cooled structure;
- To the best of my knowledge, no cited work described a model developed in conjunction with a robust and tailored experimental setup, to generate input parameters or to ensure validation of the end-to-end processes described. This shortcoming drastically reduces the potential viability and accuracy of the numerical and analytical models produced. Without a dedicated experimental effort to validate and anchor the models produced, the results produced remain anecdotal. Additionally, without a comprehensive experimental validation process, and an understanding of the behavior of the model compared to physical realities, the utilization of the model on new materials or manufacturing conditions can drastically increase uncertainty in the results obtained; and

- Most cited work that estimated interlayer forces modeled only the residual stresses resulting from a total of 2-4 layers of material deposition. When utilizing small scale FFF manufacturing systems deposition, layer heights can vary from 0.06 to 0.4 mm. By restricting modeling and prediction capabilities to a maximum structure height to 1.6 mm, the usability and applicability of the models generated will be severely limited.

Overall, there is no published work found to date that documents the development of a non-linear viscoelastic model able to account for the effects of the realities of a heated build plate, ambient cooling, multi-layer structures (>4 layers), and created/validated through a tailored experimentation process designed to accurately determine input values, validate model predictions, as well as provide a deeper understanding of the physical processes to shape and inform the simulation construction. A modeling capability without the above mentioned subcomponents will provide little real-world usability, or insight to manufacturers and designers utilizing FFF AM systems in an effort to create more consistent and lower deformation-prone structures.

In addition to the extensive research that has been conducted to create numerical and analytical models describing the stresses developed during the manufacturing process, there has also been a significant amount of research work to experimentally measure the effects of the thermally-induced residual stresses within the body of FFF polymer structures [21–26] . These experimental methodologies have taken the form of devising innovative approaches of measuring the physical strain resultant from the generation of the residual stresses within the structure of interest. Within the published literature, the strain measurement methods employed

by the research teams can be divided into two categories: 1) physical measurements, and 2) remote sensing methodologies. Each strain methodology employed within these works possesses inherent strengths and weaknesses. **Table 1** shown below summarizes the methods utilized within the cited works, along with the noted strengths and weaknesses in measuring the effects of the residual stresses within the body of an AM structure.

Table 1. Experimental Strain Measurement Overview.

Categorical Method	**Specific Sensing Device**	**Strength(s)**	**Weakness(es)**
Physical measurement	*In Situ* Fiber Bragg Grating (FBG) Sensor	Highly accurate, localized strain sensing, temperature sensing can be accomplished using FBG devices	Measurement is highly localized. Sensing device can influence/change the thermal flow through the structure under test
Physical measurement	Hole Drilling	No foreign bodies within the structure under test to change the stress patterns/temperature flow	Destructive method, difficult to detect layer to layer strain differences, cutting can affect the polymer structure
Physical measurement	Sectioning with Digital Image Correlation (DIC)	No foreign bodies within the structure under test to change the stress patterns/temperature flow	Destructive method, the DIC as used is only able to collect data on surface strain measurement
Remote sensing	Coherent Gradient Sensing (CGS)	No foreign bodies within the structure under test to change the stress patterns/temperature flow	Non-representative substrate, strain measurement on bottom surface only
Remote sensing	Acoustic Emission	No foreign bodies within the structure under test to change the stress patterns/temperature flow	Low accuracy, not able to generate the necessary data at the time of the article publication
Remote Sensing	Digital Image Correlation (DIC)	No foreign bodies within the structure under test to change the stress patterns/temperature flow, and layer by layer displacement map was created	Demonstrated in a large-scale manufacturing scenario; was initially unable to produce strain values

Review of these works leads to the conclusion that a remote sensing system should be employed to allow for the creation of a full field displacement monitoring capability resulting in little to no thermal interference.

To confirm this, I conducted a preliminary experimental effort of integrating strain sensors into the body of an AM structure during the manufacturing process. This experimental effort was designed to address following objectives:

1) Determine a process of successfully surface-mounting strain sensing devices onto additively manufactured polymer structures

2) Determine the process of integrating strain sensing devices into the structure of a FFF manufactured item during the printing process to correctly measure mechanical properties of the finished structure

For this experiment, two different test structures were manufactured, which were built in accordance with ASTM D6272-17 (Standard Test for Flexural Properties by Four-Point Bending) [27]. For this preliminary experiment, two total test structures were created: they were identical in their design, but for one test structure the manufacturing process was paused for a period of five minutes, in order to install a strain gage within the body of the manufactured structure. Once the strain gage was installed, the manufacturing process was resumed, and the remaining part of the test structure was added above the layer which included the strain gage. While the second test structure was manufactured without pause as no strain gages were included within its body. Strain gages were installed onto the uppermost surface of both test structures. The completed test structures, equipped with their installed strain gages, were subjected to a four-point bending load executed in accordance with ASTM D6272-17, until structural failure.

This was performed in order to determine the viability of installing sensing devices during the manufacturing process, as well as making a determination of the impact of the embedded strain gage on the overall strength of the as-manufactured structure. The test structures were created using 3DXTech's EcoMAX Natural PLA [28], while Omega SGT-3BH/350-XY41 strain gages were installed on the exterior and within our AM test body, shown below in **Figure 3**.

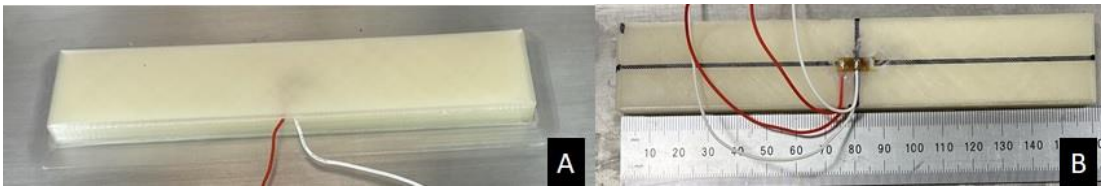

Figure 3. ASTM D6272-17 Test Articles A and B. A: internally installed strain gage after printing completion; Test Article B: externally installed strain gage after installation.

The purpose of this experiment was to measure the strains created within and on the surface of the PLA test beam due to bending through two different methodologies. The first methodology utilized the force and displacement information that was captured by the hydraulic testing machine (Material Testing System, MTS 810) during experimentation, to compute the predicted strain values within the structure under test utilizing the procedural calculations contained within ASTM D6272-17. The second methodology was the experimental measurements taken directly from the installed strain sensing devices on the test structure. It was then possible to compare these predicted values with the data captured by the surface and internally installed strain sensing devices. This demonstrated the ability to install strain sensing devices during and after manufacture, and gather accurate mechanical data on an AM polymer.

A summary of the results of our testing showed the following:

- Exterior surface mounted strain gages (in both cases) and interior strain gages showed good adherence to the PLA test beam;
- For Test Article A (**Figure 3**), the exterior gage showed a strain rate that was 31.2% higher than that of the calculated strain rate, while the interior strain gage showed a strain rate 87.6% higher than the calculated strain rate within the linear response region;
- For Test Article B (**Figure 3**), the measured strains showed a strain rate that was approximately equal to the calculated strain rate with near identical strain values within the linear response region;
- The process of installing the strain gage during the printing process (five-minute pause in printing) resulted in a 14.9% decrease in initial failure strength, when compared to test structure that did not undergo a pause in printing.

For Test Article A, the consistency in the aberrant behavior of both installed strain gages suggests that the error was due to a factor introduced during the manufacturing/pausing process, rather than a repeated error introduced through strain gage installation/orientation failures. This conclusion is strengthened through the examination of the calculated failure stresses found in both cases: 64.0 MPa for Test Article A, and 75.9 MPa for Test Article B. Both compressive loads calculated for the upper surface of the beam during ASTM 6272-17 Four-Point Bending testing. These results lead to the hypothesis that a pause in the printing process, even as short as five minutes, can create conditions that result in significantly altered mechanical properties of the manufactured part. Therefore, it can be hypothesized that the installation of sensing devices into the body of an AM polymer structure has the potential to create reduced mechanical properties due to both the manufacturing pause related effects as well as physical effects resulting from a strain gage inclusion [29]. Further experimentation and investigation would be required to

determine the precise reason(s) for the lower mechanical properties. A more complete understanding of the causes behind these results and how to overcome them would potentially allow for the continued use of embedded sensing devices that would require a disruption in the additive manufacturing process. These results agree with the conclusions made during the course of the literature review, and support the determination that inclusion of a physical strain sensing devices within the body of the test structure could be both potentially damaging to the structure being created and could taint the displacement data obtained, confirming the decision to pursue a remote "no touch" sensing displacement monitoring capability with the means of capturing full field surface displacement data.

To build a high-fidelity model that can be used to determine the internal residual stresses of any polymer based FFF structure, it is first necessary to understand and document the thermally-induced displacements created during the manufacture of a known shape with a known composition. To accomplish this, I created an experimental and analysis architecture that builds upon the previously published research, to remotely sense surface displacements on the body of an AM structure during the manufacturing process. Through the capture and analytical decomposition of these residual stress-induced displacements, print specific data (temperature profile, deposition rate, raster angle, and build plate temperature), and ambient environmental data (build chamber temperature and humidity conditions) that led to these values, it would be possible to develop and validate a numerical model capable of predicting the magnitudes and locations of residual stresses with the bodies of future structures, given filament material properties.

In addition to the core research work stated above, this dissertation also contains a discussion of work undertaken to validate an experimental and analysis process to determine the

coefficient of thermal expansion (CTE) of as-manufactured AM structures. This work was designed to present a methodology that could be used not only as a means to easily derive a critical material property needed to understand the behavior of AM structures, but also as a means of evaluating the viability of utilizing external strain sensing devices (strain gages) on AM structures. The overall viability of this experimental and analysis process was demonstrated on AM FFF polymer structures of both simple and complex geometries, and was validated using traditionally manufactured metal structures.

The following chapters of this PhD dissertation will describe in detail, through the inclusion of academic articles submitted for publication, a detailed description of the experimental and analysis methodology developed within this research project (Chapter 2), a follow on the article presented in Chapter 2 which presents in-depth results of this experimental construct and the conclusions that can be drawn from its use with a PETG test structure (Chapter 3), and finally a detailed description of the adaptation of an experimental and analysis construct designed to derive the CTE of as-manufactured AM structures utilizing dissimilar test specimens (Chapter 4).

CHAPTER 2 - A NOVEL CONSTRUCT TO PERFORM *IN SITU* DEFORMATION OF FUSED FILAMENT-FABRICATED STRUCTURES DURING MANUFACTURE

Authors: Daniel L. Nelson, Valeria La Saponara

Authors contributions: DLN designed and conducted experiments, carried out data analysis, secured funding for supplies and tests at the Air Force Research Laboratory, and wrote the document. VLS advised DLN, provided equipment and laboratory space, and edited the document.

ABSTRACT

Fused filament fabrication (FFF) is an additive manufacturing modality that continues to show great promise in the ability to create low cost, highly intricate, and highly useful structural elements. As more capable and versatile filament materials are devised and the resolution of manufacturing systems continues to increase, the need to understand and predict manufacturing-induced warping will gain ever greater importance. The following study presents a novel *in situ* remote sensing and data analysis construct that allows for the *in situ* mapping and quantification surface displacements induced by residual stresses on a specified test structure. This experimental and analysis process will provide designers and manufacturers with insight into the manufacturing parameters that lead to the manifestation of these deformations, and a greater understanding of the behavior of these warping events over the course of the manufacturing process.

Keywords: Additive Manufacturing: Extrusion-based 3D printing; Fused Filament Fabrication (FFF); Digital Image Correlation (DIC); Residual Stress; Warping; Deformation

Nomenclature	
AM	Additive manufacturing
FFF	Fused Filament Fabrication
CTE	Coefficient of Thermal Expansion
OFS	Optical Fiber Sensors
DIC	Digital image correlation

DED	Directed Energy Deposition
PETG	Polyethylene Terephthalate Glycol
IR	Infrared
FOV	Field of View

INTRODUCTION

One of the core components of the third industrial revolution (industry 4.0), additive manufacturing (AM) technologies [1,2] continue to penetrate a greater variety of applications, as printing base materials are devised, and more capable/complex manufacturing systems are created [30,31] . This continued advancement of AM systems and materials, specifically within the domain of Fused Filament Fabrication (FFF), is due to the relative ease in the prototyping, flexibility in design, and other competitive advantages, when compared to those of subtractive manufacturing [1,32–34]. FFF is an extrusion-based 3D printing technique, and one of the most widely used and available variations of this manufacturing technology [1]. As a method of AM, FFF utilizes a thermoplastic filament as its base material. This thermoplastic filament is extruded through a nozzle apparatus where the material is heated to melting or a sufficiently fluid point. The requirement of heating the filament material to a high temperature within the nozzle section results in a varying and non-uniform thermal profile within the body of the material structure, and in the development of residual stresses that build up within the part under construction. This causes deformation of the printed part, and a reduction of structural accuracy during the manufacturing process [25,35,36]

The creation of these residual stresses is due to the nature of the manufacturing processes, where hot viscous material is deposited layer-by-layer onto previously solidified layers, which then undergoes a period of rapid cooling. These extreme thermal gradients within the structure and swift temperature swings of the structural materials cause contractions within the layers of the

body, which lead to the development of interlayer stresses [19,20,24,25,37]. This phenomenon is further compounded by the conduction of heat through the solidified structure, as new melt layers are added to the body [38–40]. This heated material addition and resultant cooling events result in asymmetric expansion and contraction between layers of the fabricated structure. The cumulative buildup of these residual stresses within the body of the fabricated structure during the manufacturing process can often result in part warping and deformation, as noted in Refs. [13,35]. The buildup of residual stresses and manifestation of the warping/deformation are primarily a thermally-driven process, with the feedstock material coefficient of thermal expansion (CTE) governing the magnitude of the material response to previously described thermal stimuli.

One of the first steps to combat these warping effects is to study the thermo-mechanical properties of such displacement events during the FFF manufacturing processes. This understanding is best achieved through *in situ* measurement of the warping displacements within AM structures, specifically their magnitude, location in the part, as well as the time during the manufacturing process. To date, significant research has been conducted to measure the resultant manufacturing-induced residual stresses post printing [24,25]. Nonetheless, by only viewing the end state displacements, there is little insight into when the displacements were created, and the variability behavior patterns of those displacements/deformations during the manufacturing process. Additionally, the majority of the *in situ* sensing methodologies and their applications within AM have almost entirely relied on the inclusion of physical sensors, such as Optical Fiber Sensors (OFS), to provide highly accurate but highly localized data [21–23,41,42]. This results in a high potential to influence/alter the thermal flow patterns of the FFF printed samples. Thus, in order to capture the desired data and minimize the effect on the body of an embedded sensor, only remote sensing capabilities are considered herein, specifically Digital Image Correlation (DIC).

As a measurement method, DIC refers to the class of no-contact methods that acquire images of an object. Images are stored in a digital form, and image analysis is performed to extract full-field shape, deformation and/or motion measurements of the structure under test [43]. Within the realm of advanced manufacturing, DIC has been employed in many different iterations. Reference [44], for instance, utilized DIC as a quality control, real-time defect detection of the 3D printed parts, by comparing the geometry of the computer model versus that of the printed parts. This would allow *in situ* detection of localized and global defects when they develop during the manufacturing process. Similarly, Ref. [45] combined a DIC sensing capability with a convolutional neural network as a deep-learning method for the real-time detection of warps. In the mentioned study, the printer is automated in a way that after warp detection, it automatically stops the printing process. While these studies utilized DIC as a sensing technique for deformation detection during the course of small-scale FFF manufacturing, neither of the studies provided a detailed understanding of the occurrence, change over time, and location within the printed structured of warping and deformation events.

Within other AM disciplines (large scale FFF and Directed Energy Deposition, DED), e.g., [26,46], DIC-based data capture and analysis procedures have showed great potential in providing time-dependent full-field surface displacement data throughout the course of manufacturing processes. This would allow for an understanding of the development and behavior of the manufacturing-induced residual stresses as they are manifested in terms of surface displacements as the test article is created. Based on the above research review and the demonstrated capabilities of DIC methodologies for 3D-printed applications, this article describes adapting DIC-based experimental methodologies to validate process applicability within small-scale FFF regimes. Further, this article gathers *in situ* surface displacement and thermal data of small-scale neat

polymer structures during an FFF build process. The inclusion of a thermal monitoring capability into the experimental construct allows for greater insight to be gained into the cause of observed mechanical behavior within this thermally driven process. Additionally, this article combines those experimental developments with novel analysis techniques designed to provide greater insight into both the time- and location-dependence of developed displacements/deformations, as well as the print-to-print variation of realized deformations. Overall, the described experimental and analytical methods can provide a full-field surface displacement understanding, a calibrated thermal time history of the surface of the test structure, insight into the variation of displacements realized with identical print parameters, and a statistical determination into the print most significant parameters causing deformations within the test structure.

EXPERIMENTAL METHODS

Typically, the use of DIC measurement requires the application of an externally applied speckle pattern to the surface of the body undergoing deformation. This speckle pattern should possess distinct, unique, non-periodic, and stable grayscale features which would act as the carrier of deformation information within the captured image data [47]. In the case of *in situ* DIC data capture during a FFF manufacturing event, it would be an impossible task to achieve repeated and consistent application of a speckle pattern to the surface of the AM test structure during the build process. In this study, the methodologies devised by Spencer et al. (2021) [26], were adapted to the current project by using surface roughness of the constructed part in place of an externally applied speckle pattern, displacement is measured during the printing process. To minimize the potential of print-to-print variations that would result either from differences in fiber orientation and fiber/polymer bonding [2,3,48], or degree of polymer crystallinity [5,6] an amorphous neat polymer was selected as the filament of choice for the process. With these requirements and criteria

in mind, a black semi-matte Polyethylene Terephthalate Glycol (PETG) manufactured by colorFabb [49] was selected.

The next step in the experimental process was to determine if the natural surface roughness of a structure made with this filament would be capable of performing the functions of an externally applied speckle pattern. To make this determination, a rigid body displacement test was performed, where DIC was used to measure rigid body displacements on printed specimens with and without the application of an external speckle pattern. The two conditions (speckle-patterned surface, surface with its as-manufactured roughness) were considered equivalent with a statistical correlation greater than 95% over the rigid body displacements measured. The rigid body displacement tests were conducted using six total specimens measuring 200mm (L) x 40mm (H) x 2.5mm (W) that were printed using an Ultimaker S5 (with the specification of 240°C nozzle, 75°C print bed, and 0.15mm layer height). Three of these specimens were randomly selected for application of an external speckle pattern, shown in **Figure 4**. Externally applied speckle patterns were applied using spray paint, with a white matte base applied first to the specimen onto which a fine mist of matte black speckles were then applied [50].

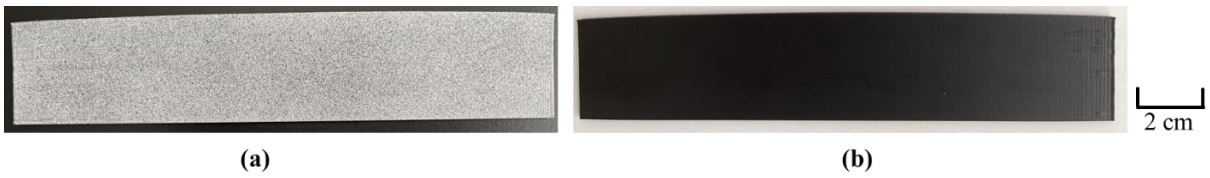

Figure 4. Rigid body test specimens: (a) with applied external speckle pattern, (b) as-manufactured surface.

Rigid body displacements were applied and measured using the apparatus shown in **Figure 5**, which provided a stable consistent platform for the test specimens. Displacements were applied

in a single axial direction and measured using a micrometer dial indicator, and visual data was captured using a Mako G-503B, a 1/2.5-inch monochromatic 5-megapixel CMOS sensor camera equipped with an Edmund Optics 25mm fixed focal length lens. Utilizing a 0.5m working distance to the test specimen, this camera and lens arrangement resulted in an as-designed total resolution of 0.0453 mm/pixel.

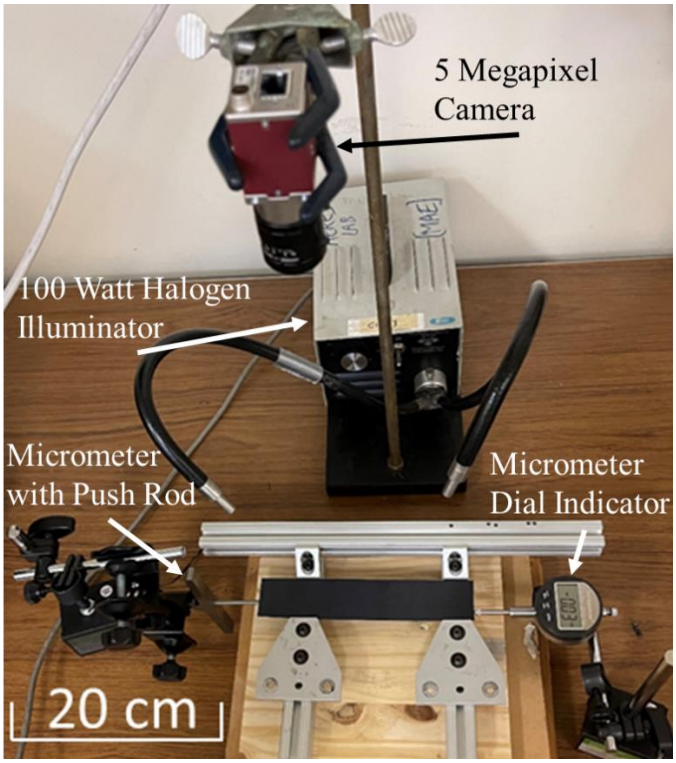

Figure 5. Experimental apparatus for rigid body displacement tests.

A total of 21 displacement measurements were applied to each of the six test specimens with a single visual image taken at every displacement condition. The DIC analysis of the captured images was performed using Correlated Solution VIC 2D-7 software using the prescribed settings within the VIC 2D system for a minimization of uncertainty given the quality and contrast present within the reference image [51]. In this case, the subset size was set for 125 pixels, with a step size

of 3 pixels. At each applied displacement, the DIC-measured displacements were averaged across the entire body of the test piece. These values are shown in **Figure 6**, obtained with the commercial software VIC 2D, along with the results of the statistical correlation analysis that was conducted. These results show high correlation (> 99%, well above the 95% threshold) with an average measurement error of 0.0127mm for test specimens covered by external speckle patterns, and an average measurement error of 0.0318mm, when utilizing the natural surface of the test specimens. These highly correlated, and essentially equivalent, results allow to conclude that this process and the selected filament are capable of replacing an applied speckle pattern for the DIC measurements of rigid body displacements.

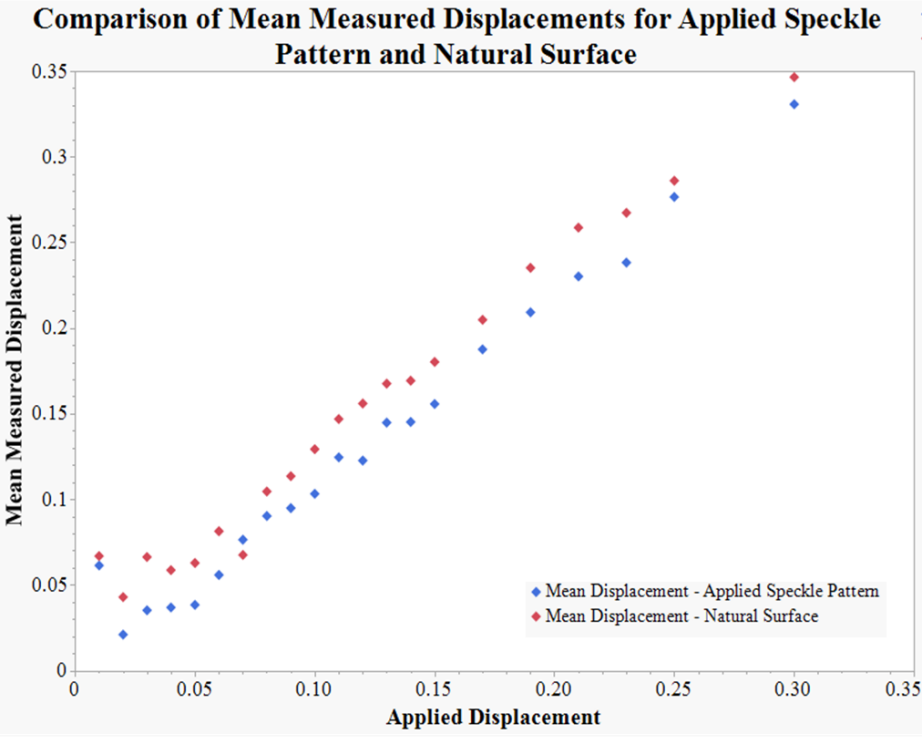

(a)

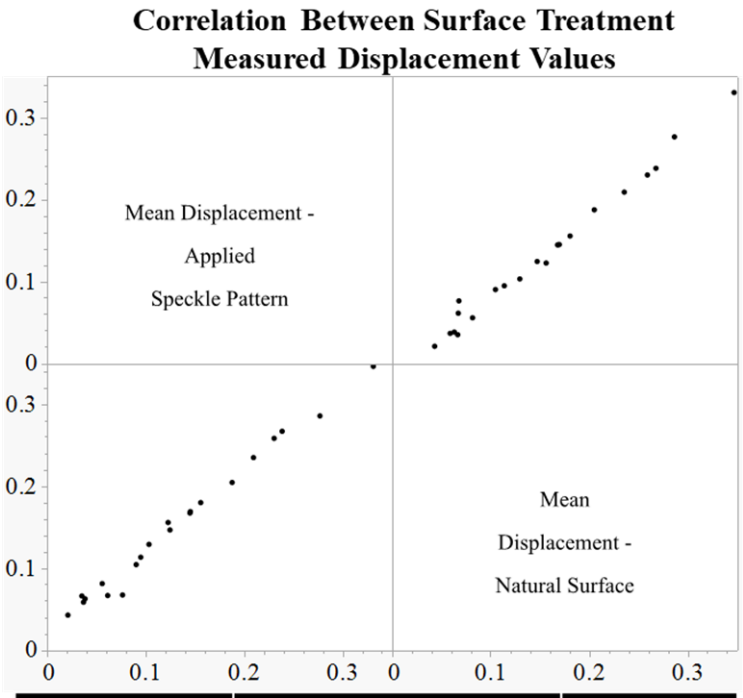

Variable	Variable	Correlation
Natural Surface	Applied Speckle Pattern	0.9939

(b)

Figure 6. Mean rigid body displacement results: (a) comparison between surface treatment results, (b) statistical correlation between the displacement measurement results.

After confirming the viability of the utilization of the natural surface roughness of a party printed with the selected filament, the next step was the *in situ* surface displacement measurement during an ongoing AM process. The printer used for this effort would need to meet the following technical requirements:

1. **Stationary Build Plate** – A build plate that moves in either the vertical or lateral directions has the potential to introduce unwanted image noise and distortion, thereby corrupting the ability to derive meaningful data using DIC analysis.

2. **Unobstructed View of Structure Under Construction** – An unobstructed view of the structure was required in both the visual and infrared (IR) spectra to facilitate data capture.
3. **Nozzle and Build Plate Thermal Monitoring** – When measuring the surface displacements resultant from the AM process, it is critical that the parameters driving the generation of the residual stress are known through the entire period of construction.

The nScript 3Dn-500 printer was selected among those available to the authors, since it met all of the above established requirements, while providing ample space for the positioning of visual, IR, and ambient temperature/humidity data capture equipment [52]. The sizing of the proof-of-concept test article discussed herein is based on the results of the large-scale experimentation conducted by Spencer et al. (2021) [26]: in their work, the displacements of a part constructed with 100 layers have been successfully monitored *in situ* using surface roughness. In the current work, the test structure had nominal dimensions 75mm (L) x 40mm (H) x 1.05mm (W), to be built with the number of layers desired (100), for the largest possible deposition layer height available on the available nScript 3Dn-500 printer (0.4mm layer height). Additionally, the 75mm length selected would ensure a full-field view of the test structure using the camera and lens employed during the rigid body displacement testing. The 1.05mm thickness of the test structure would consist of three deposited lines when employing a 0.4mm extruder nozzle: this was selected to minimize the warping and deformation generated in that dimension.

A key aspect of the application of DIC is the use of uniform and consistent light sources to illuminate the test structure throughout the measurement process [53]. This required the selection of light sources that could provide bright diffuse lighting over a wide area, and could illuminate the body of the test structure as it was both growing and deforming during the manufacturing

process. For this purpose, two Dracast LED500 light panels provided the necessary lighting to meet this requirement [54]. The panels were composed of 512 individual LEDs, and were capable of employing a variable color temperature ranging from 3200K – 5600K. To provide print-to-print imaging consistency with high contrast, the light panels were set to 5600K, and positioned approximately 500mm from the test structure.

Due to the outstanding performance in the rigid body displacement tests of the camera and lens (Mako G-503B with Edmund Optics), that same equipment was utilized, with a 500mm working distance. The field of view of this camera and lens allowed for a complete and continuous view of the test structure, while allowing for a centralization of the structure of interest with a buffer between the edge of the camera field of view (FOV) and the edge of the structure. This is further shown in **Figure 7**, thereby minimizing any potential image distortion [55,56].

For the thermal data capture, it was necessary to select a detection system that was capable of collecting data from structures ranging from 20°C through 250°C, and that possessed the resolution necessary to document the change of temperature of the surface of the test structure. The IR camera adopted for this purpose was the Indigo Systems Merlin MID thermal camera, which possessed both the required thermal imaging range and required FOV to capture full field data of the test structure during its manufacture. Utilizing a working distance of 500mm resulting in a thermal camera resolution of 0.386 mm/pixel. This was considered appropriate for full-field thermal imaging of the entire test structure throughout the manufacturing process, as well as insight into the heat flow through the body and change of temperature of the test structure as new hot melt is extruded onto the structure.

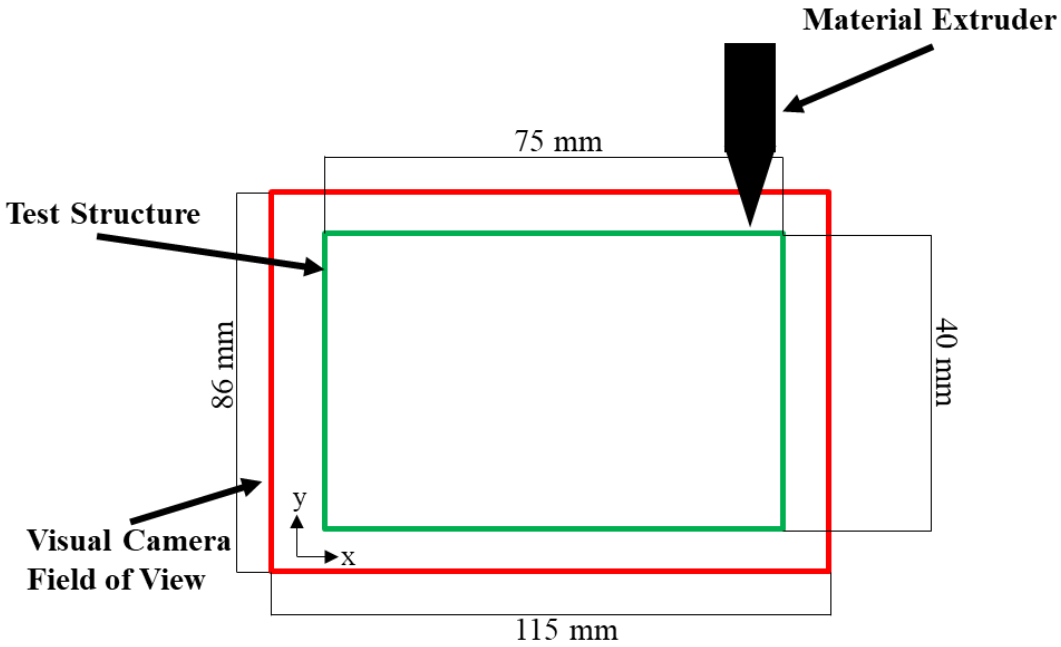

Figure 7. Test structure (x and y are in-plane coordinates) and camera FOV construct.

Finally, to provide a consistent surface and reduce the variability of build plate adhesion from print to print, the nScript 3Dn-500 build plate was coated with a BuildTak Polyetherimide (PEI) self-adhesive sheet and a layer of Elmer's Disappearing Purple glue as shown in **Figure 8**.

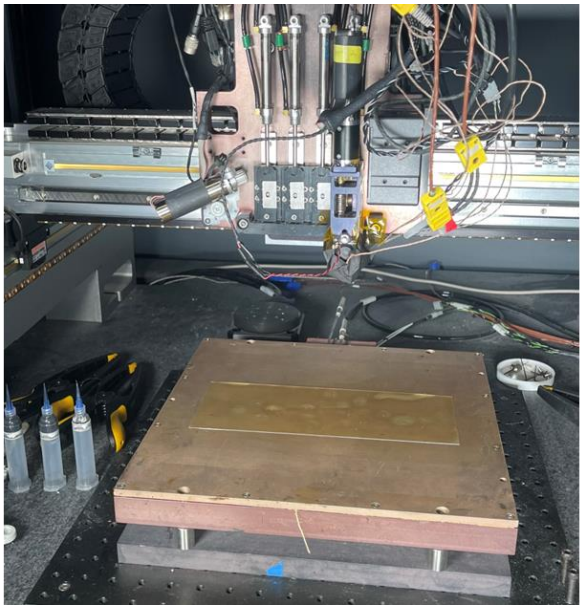

Figure 8. Build plate surface treatments.

Figure 9. Experimental setup: (a) data gathering and lighting equipment positioned 500mm from test structure, (b) data collection during structure manufacture.

The final aspect of data capture critical to correctly understanding and framing the data produced during the *in situ* monitoring is the recording of the ambient temperature and humidity

experienced by the test structure during its build. These factors can significantly affect the material strength of the structure created and while documenting their variations are critical to explaining the data generated through this experimental process [57,58]. For this experimental effort, the Elitech Tlog B100EH temperature and humidity data logger [59] was used. It was mounted inside the manufacturing space of the nScript 3Dn-500 printer.

Figure 10. Placement and installation of temperature and humidity sensor.

RESULTS AND DISCUSSION

Surface Displacements

Surface displacements were analyzed using Correlated Solutions VIC-2D7 software. To correlate surface displacements of the structure as it is being built required the reverse image correlation analysis technique developed by Spencer et al. (2021) [26], utilizing the image of the fully built, cooled structure to act as the DIC reference image. This allows for the computation of

surface displacements of the imaged test structure based on changes found between the location and orientation of grayscale subsets of this referenced image, and the captured images of the test structure during the build. The desired results of these analysis efforts are a subset-by-subset displacement computation across the entire body of the test structure. Those values can be visualized by utilizing a color-coded overlay onto the image of the test structure, an example of which is shown in **Figure 11** for the entire test structure build.

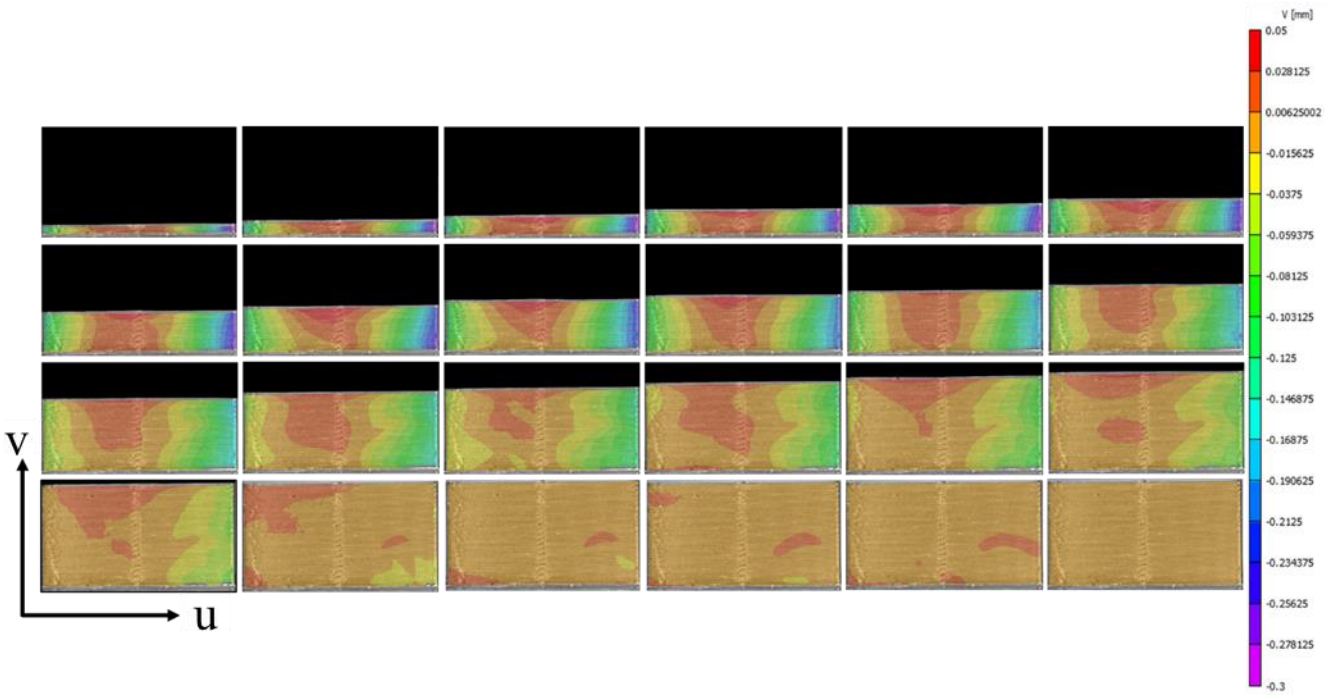

Figure 11. In-plane vertical (v) displacements (mm) measured from the reference image as the test structure was being printed with a layer height of 0.4mm and a nozzle temperature of 230 deg C.

These color-coded overlay outputs allow for a quick assessment of the magnitude and location of the test structure during the build process. To quantitatively compare the displacements of specific areas of all samples and provide insights on the process variability, a different analysis methodology was needed. A method was devised of quantifying the displacements of multiple

prints utilizing the "pixel grid function output" within the Correlated Solutions VIC-2D7 software. This output allows the user to specify the size, in pixels, of an "analysis block" within the DIC analysis area of interest. A depiction of this test structure image division is shown in **Figure 12**. Displacement values are then averaged over each analysis block, providing quantitative displacement values commonly located across the surface of the test structures. These analysis blocks can then be used to compare the measured surface displacements of identical regions of many different test structures of identical construct. This analysis technique enables us to better understand how and when displacements are developed as a function of the addition of new material. Additionally, it may also be possible now to perform statistical studies of the measured surface displacements of AM parts (within the constraints of the hardware, software and materials chosen), to gain insight into how specific print parameter combinations drive the creation of residual stresses and printed part deformations.

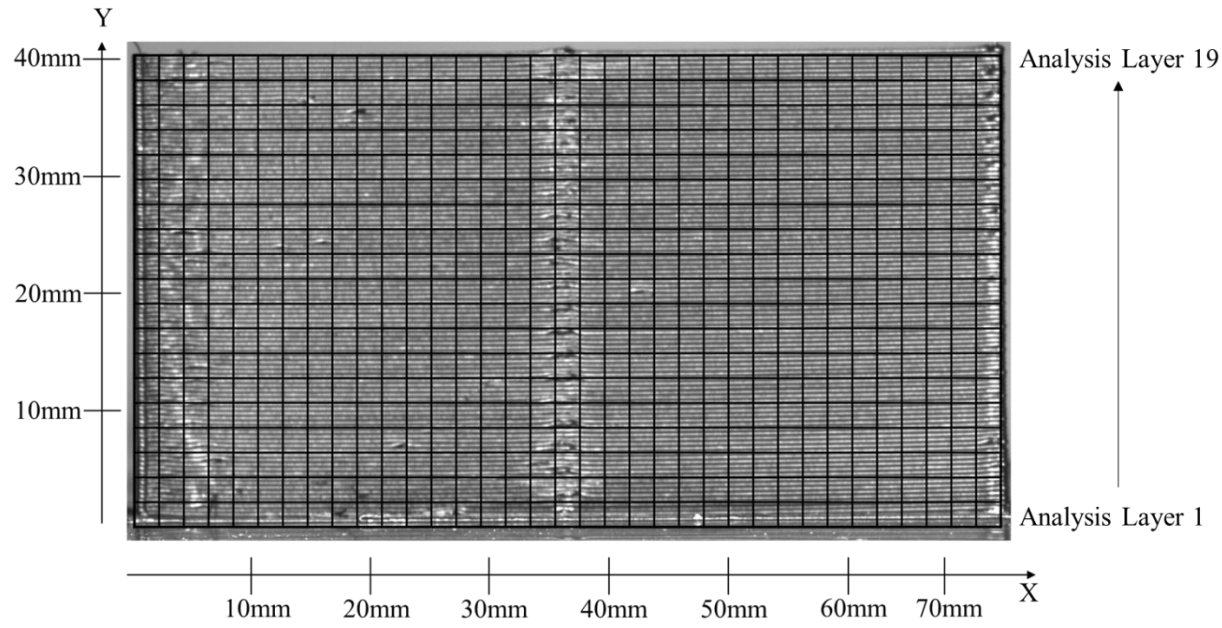

Figure 12. Depiction of a fully constructed test structured divided into 43x43 pixel analysis blocks. The individual rows of analysis blocks are labeled as analysis layers.

Additionally, through this novel analysis methodology it is possible to conduct an analysis layer decomposition of the test articles throughout the manufacturing process. The analysis layer decomposition of the displacement data allows for a determination of the behavior of a specific layer section during the build process. An example of such an analysis layer decomposition is shown in **Figure 13**. Using this type of methodology, it is possible to quickly and easily gain an understanding of the symmetry of the deformation experienced, as well as to when during the manufacturing process residual stresses are developed driving the occurrence and magnitude of deformation for each particular analysis layer. **Figure 13** shows the measured displacement variation of analysis layer 1, which is the analysis layer located closest to the build plate at a height of 4mm above that surface. Additionally, **Figure 13** shows experimental data obtained during the creation of a test structure with a layer deposition height of 0.4mm` (this is the height in the vertical in-plane Y direction of each layer of new material added to the body of the test structure) and a nozzle temperature of 230°C. This analysis layer data can lead to greater insight into the overall performance of a specific filament material, enabling for the adjustment of design and manufacturing parameters to limit the occurrence or magnitude of structural deformations.

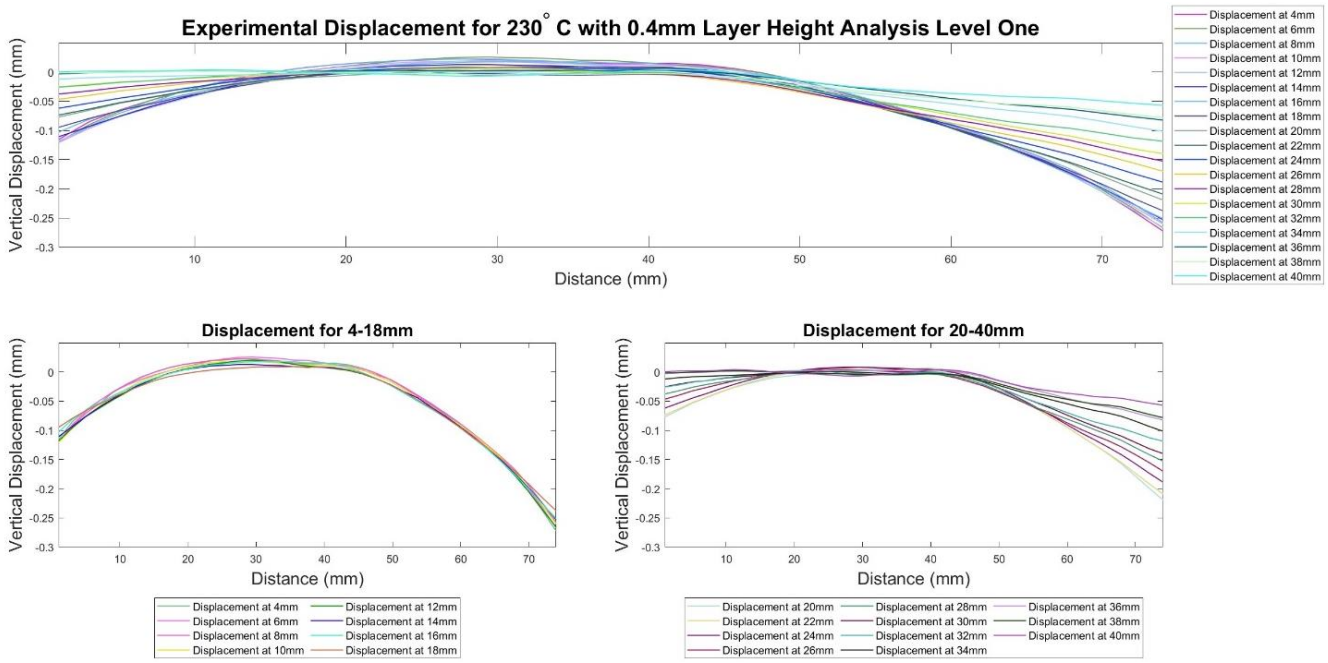

Figure 13. Vertical displacements measured as a difference from the reference image. The plot shows the analysis blocks across analysis layer 1 as the height of test structure increased from 4mm to 40mm. This data was derived from the printing of a test structure with a layer height of 0.4mm and a nozzle temperature of 230 deg C.

The analysis block technique also allows for an in-depth statistical analysis to be conducted into specific manufacturing factors and their contribution to experienced deformations. **Figure 14** shows an example of such statistical analysis: in this case, a two-level two-factor analysis of variance (ANOVA) study was conducted to study the maximum analysis layer deformations for each of three replicates at each of the treatment levels, by using two different nozzle temperatures and two different deposition layer heights. For the ANOVA study conducted on this particular data, vertical in-plane displacements were used as only these values were found to have a normal distribution after the implementation of a Box-Cox transformation, with normality confirmed through the use of an Anderson-Darling normality test. This study allowed us to determine the variance of maximum surface displacements found across the manufactured structures utilizing

the same manufacturing parameters. Further, it allowed a statistical examination of the effect that each of the evaluated treatments (deposition layer height and nozzle temperature) had on the magnitude of vertical surface displacements measured. In this case, the analysis showed that the manufacturing parameters of nozzle temperature and the interaction of nozzle temperature with deposition layer height were significant contributors to the magnitude of measured surface displacements. On the other hand, the deposition layer height as an individual factor was found to be insignificant to the development of surface displacements. This type of information will further allow for a more informed selection of manufacturing parameters of AM structures.

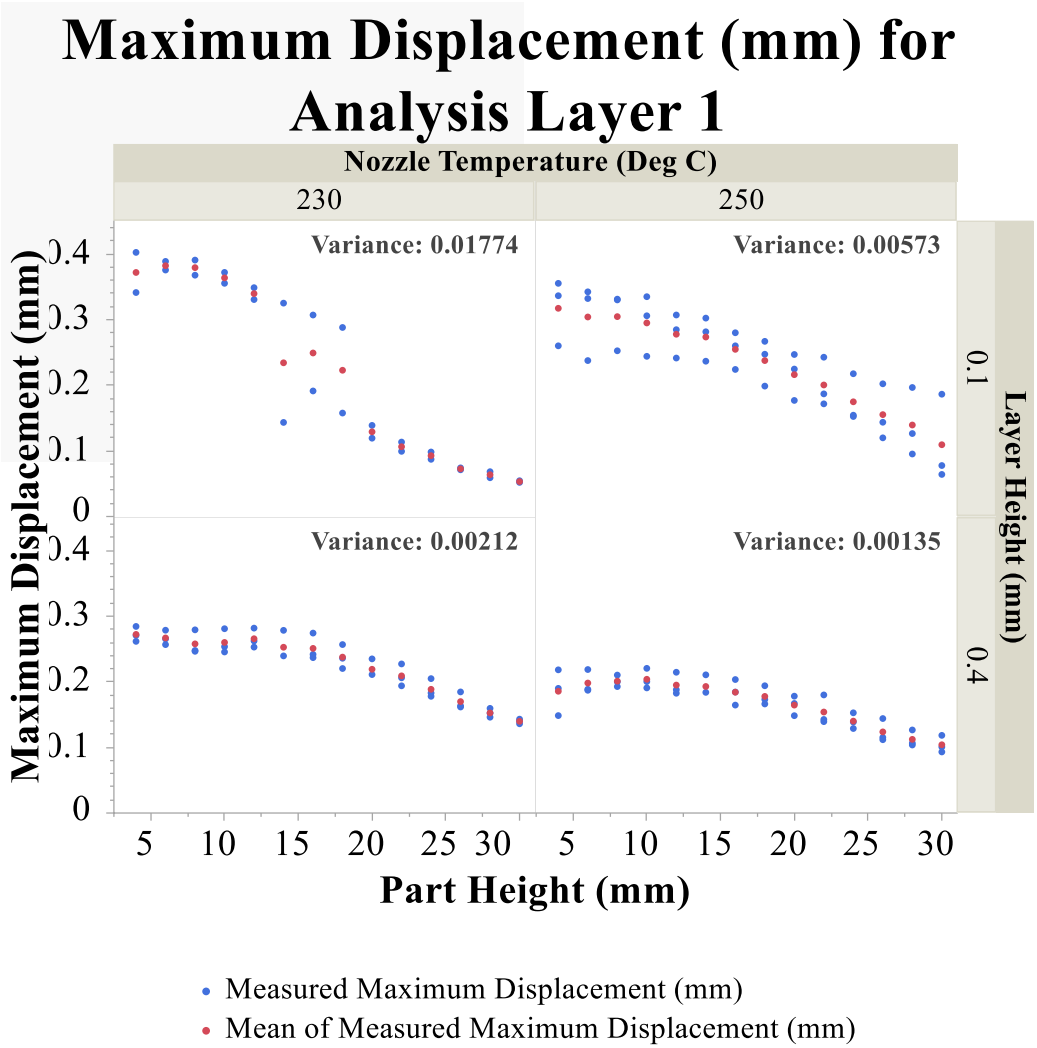

Figure 14. Statistical analysis of maximum displacement for a given analysis layer (Layer 1).

Table 2 shows an example of the results of the ANOVA statistical study. "Degrees of Freedom" describe the number of levels for each treatment minus one. On the other hand, the Degrees of Freedom number for "the nozzle temperature and layer height interaction" describes the degrees of freedom of factor A (nozzle temperature) multiplied by the degrees of factor B (layer height). The "Sum of Squares" describes the individual treatment (nozzle temperature, layer height, and nozzle temperature/layer height interaction), and indicates deviation from the overall mean. The "F Ratio" term within the table describes the mean squares of each factor divided by the mean square error of the data. This data, compared to the F statistic term for each factor, allows for the evaluation of the null hypothesis ("Is this term significant?" $H_O = 0$, no, the effect of each factor is zero). Finally, the "Probability > F" is the reliability to which we can reject the null hypothesis, [60,61]

Table 2. ANOVA results.

Effect Tests				
Source	**Degrees of Freedom**	**Sum of Squares**	**F Ratio**	**Prob > F**
Nozzle Temperature (Deg C)	1	0.0061560	4.1844	0.0410
Layer Height (mm)	1	0.0008806	0.5985	0.4393
Interaction of Nozzle Temperature (Deg C) / Layer Height (mm)	1	0.9813334	667.0403	<.0001
Part Height (mm)	13	3.2365205	169.2273	<.0001

Surface Temperatures

The inclusion of thermal monitoring equipment in the experiment allows for the gathering of critical information that can be used to explain the measured displacements. In fact, as the creation of residual stresses within the body is primarily a thermally-driven process [13,14,17–20,24,25,35,37], an understanding of the structural temperature variations as a function of geometry and time can be used to explain observed behavior. The data captured by the thermal imaging equipment can be analyzed and displayed in a number of ways. The first method is to utilize the captured video, properly calibrated with bodies of known temperature/emissivity. An example of this type of data product is shown in **Figure 15**. This type of data product is highly useful in gaining a broad understanding of the thermal flow through the test body and "big picture" thermal behavior of the entirety of the experimental construct. This refers to the thermal interaction of the hot deposition with the test structure, as well as the thermal interaction of the test structure and the build plate, and large-scale thermal variations across the body of the test structure). This data product, however, may not be sufficient for the highly accurate quantitative study of thermal changes of the test structure during the manufacturing process.

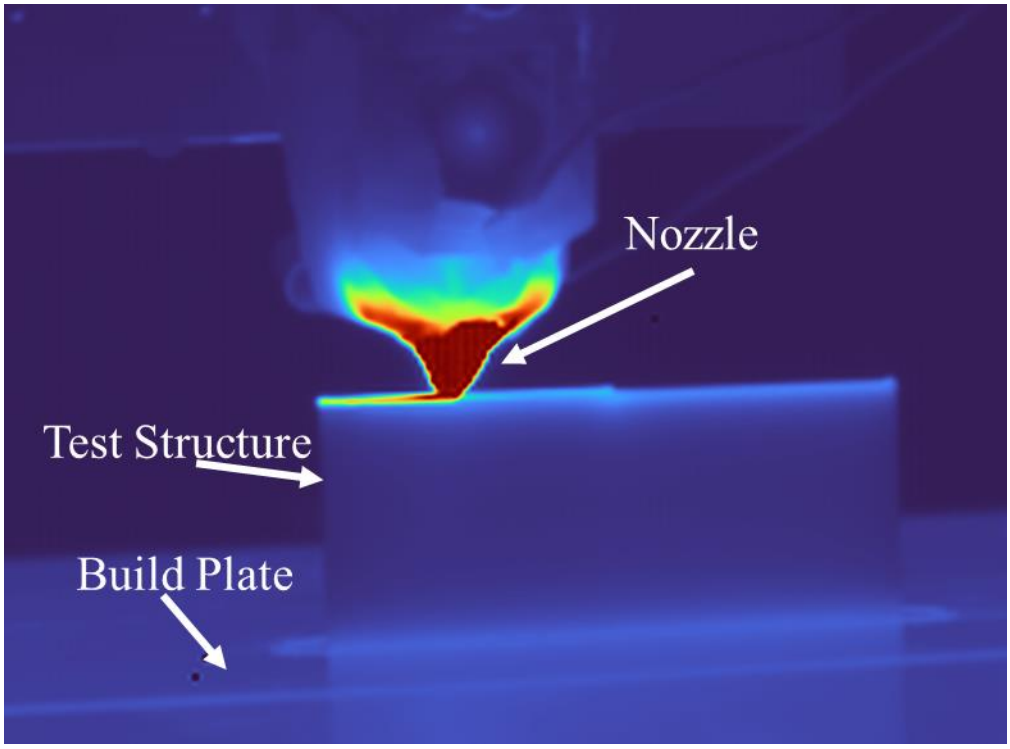

Figure 15. Thermal camera screen shot of test structure during manufacture. This data was derived from the printing of a test structure with a layer height of 0.4mm and a nozzle temperature of 230°C.

In order to conduct a more comprehensive study of the variation of measured temperature values of the surface of the test structure, a different analysis methodology is required. To accomplish this task, pixels within the captured FOV of the thermal camera were selected corresponding to identified regions on the surface of the test structure. The results of this analysis methodology allow for the creation of plots, such as those shown in **Figure 16**. Similar to the analysis layer construct utilized within the displacement study, **Figure 16** shows the variation of temperature across the length of the test structure at a constant height above the build plate for the entirety of the manufacturing process. This type of plot can be used to explain variations described within the displacement data products. For instance, **Figure 16** shows that at a height of 2mm above the build plate, the temperature of the right edge of the test structure experienced greater

heating and heat retention than the heating and heat retention of the left side of the test structure. This observed fact can help to explain the asymmetry found across the length of the test structure for analysis layer 1. This thermal buildup may result in greater local expansion and contraction, and therefore greater local deformation of the right side of the test structure.

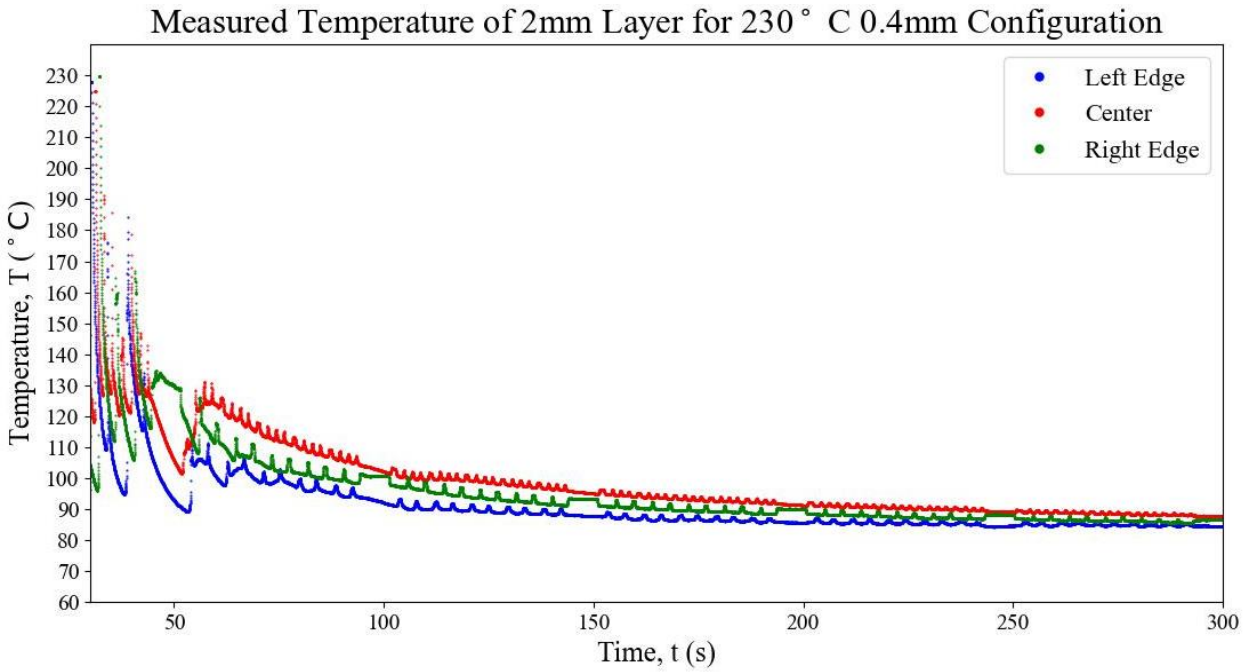

Figure 16. Thermal measurements for the left edge, center, and right edge at 2mm above the build plate. This data was derived from the printing of a test structure with a layer height of 0.4mm and a nozzle temperature of 230°C.

CONCLUSION

This article documented an experimental study to capture *in situ* displacement/thermal data of an AM test structure. Specifically, this research proved that it is possible to utilize the natural surface roughness of an AM part and to employ DIC in order to measure the surface displacements resultant from the buildup of thermally induced residual stresses. This allows for the *in situ* measurement of surface displacements generated during the build process, providing insight into

when and where deformations are occurring. This experimental design also showed the value of pairing displacement and thermal monitoring to better understand and explain the observed displacement results. Finally, this article described the various data analysis techniques and products that can be employed to understand and display the data obtained through the experimentation.

The work and methodologies presented are meant as a proof-of-concept presentation of procedure that can be used to enable the quantification of residual stress manifestation in structures created using filament materials and employing a variety of manufacturing parameters. Through the use of the previously described experimental procedures and analysis methodologies, it would be possible to fine tune the manufacture and design strategies employed when building FFF structures. These explicit and quantitative measurements of FFF bodies will greatly assist designers and users of AM structures to create more consistent and capable structures, reducing potential wrapping effects, maximizing the capabilities of their chosen filaments and printing apparatuses, and assisting the documentation for quality assurance/control and certification.

Additionally, it is also hoped that these methodologies may be used in the creation and validation of an AM simulation/modeling capability. By using these measurements to provide "boundary conditions" and as a method of validating the magnitude, location, and time of creation of deformation predictions, simulations can eventually be developed to predict when, where, and to what extent structural deformations will be created in a structure. This will allow for informed design/material tradeoff decisions to design and certify AM structures.

Acknowledgements

The authors would like to acknowledge the support received from the Defense Innovation Unit (DIU), UC Davis Engineering and Student Design Center (Jose Mojica and Sherry Batin), USAF Research Lab (Mr. Andrew Abbott, Mr. Tyler Lesthaeghe, Dr. Craig Przybyla, Dr. Lorianne Groo, and Dr. Eric Lindgren), Dr. David Slaughter, and the members (Nickolas Loftus and David Guinn) of the UC Davis Advanced Composites, Research, Engineering and Science (ACRES) laboratory who provided critical support and expertise during the development of this study.

CHAPTER 3 - *IN SITU* MANUFACTURING-INDUCED DISPLACEMENT OF POLYETHYLENE TEREPHTHALATE GLYCOL (PETG) FUSED FILAMENT-FABRICATED STRUCTURES

Authors: Daniel L Nelson, Valeria La Saponara

Authors contributions: DLN designed and conducted experiments, carried out data analysis, secured funding for supplies and tests at the Air Force Research Laboratory, and wrote the document. VLS advised DLN, provided equipment and laboratory space, and edited the document.

ABSTRACT

Under the umbrella of additive manufacturing (AM), fused filament fabrication (FFF) stands out as one of the widest proliferated, easy to use, and most versatile manufacturing modalities. A significant challenge with this technology is the deformation and warping that occurs within the manufactured part as a result of the manufacturing induced residual stresses. The following study details a novel remote sensing and data analysis construct that provides a means to locate and quantify surface displacements created during the manufacturing process. Additionally, this study provides and in-depth review of the use of this novel construct in determining the deformation behavior and the most significant manufacturing parameters that drove the formation of surface displacements in a polyethylene terephthalate glycol (PETG) test structure.

Keywords: Additive Manufacturing: Extrusion-based 3D printing; Polyethylene Terephthalate Glycol (PETG); Fused Filament Fabrication (FFF); Digital Image Correlation (DIC); Residual Stress; Warping; Deformation

Nomenclature	
AM	Additive manufacturing
FFF	Fused Filament Fabrication
CTE	Coefficient of Thermal Expansion
OFS	Optical Fiber Sensors
DIC	Digital image correlation

DED	Directed Energy Deposition
PETG	Polyethylene Terephthalate Glycol
IR	Infrared
FOV	Field of View

INTRODUCTION

With the invention of Stereolithography in 1984 [62], additive manufacturing (AM) as an industrial capability was born. Over the last several decades, the methodologies of execution and applications of AM have greatly increased [63]. As we continue to advance as a society there is great expectations that AM technologies will continue to develop and power our future advancement, and the ability to create evermore complex structures and more easily utilized new advanced materials [64]. Additionally, the economic impact and increase in uses of AM is forecast to grow, powering a more agile and sustainable economy [65–68]. However, even with all the benefits associated with their use, AM-produced structures, particularly those created through the use of Fused Filament Fabrication (FFF) with polymer feedstock, routinely suffer from part deformation and a lack of consistent production quality [69,70].

These part deformation and production quality issues arise as a result of the strains caused by the buildup of residual stresses within the body of the AM structure [25,35,36]. The creation of these residual stresses are due to the nature of the manufacturing process, where repeated deposition of new material onto a previously solidified layer is executed and then undergoes a period of rapid cooling. These swift temperature swings within the body of the manufactured structure cause contractions within the material layers leading to the development of interlayer stresses [19,20,24,25,37]. The repeated heating and cooling cycles of the structures due to the conduction of heat through the body [38–40] further complicate the development of these parts. This complexity is most pronounced within the AM modalities that utilize polymer

feedstock, as these materials will transition from a melted/low viscosity phase through the glass transition temperature, to a solidified/high viscosity phase. The glass transition temperature is defined as "the temperature, below which the physical properties of plastics change to those of a glassy or crystalline state. Above T_g they behave like rubbery materials. Below the T_g a plastic's molecules have relatively little mobility […]. The value of the glass transition temperature depends on the strain rate and cooling or heating rate, so there cannot be an exact value for T_g."[71]

Temperature excursions combined with stresses and strains within the structure under construction can cause fluctuations of specific layer stiffness/strength, resulting in displacements and deformations, affecting the adhesion of the structure to the AM build plate [72]. As these interlayer stresses continue to build during the manufacturing process, structural displacements and part deformations are developed within the body under construction [13,35].

The goal of the experimental effort presented within this article is to present a combined methodology to measure and analyze the full-field surface displacements generated within a structure being constructed using small scale FFF. Through the analysis of this captured displacement data, it is possible to gain a deeper understanding of where on the test structure surface displacements are formed, when the surface displacements are manifested during the build process, and to what magnitude the structural displacement develop. This experimental effort utilizes an amorphous polymer filament as the build material of the measured test structure. This material, free from complexities due to fiber/matrix interactions [2,3,48] and polymer crystallinity variations [5,6], provides an excellent baseline material to develop and explore the experimental methods needed to capture the data of interest, as well as the range of analysis approaches available to gain a more complete understanding of the *in situ* deformation

manifestation behavior of AM structures. Overall, the described combined experimental and analytical methods were able to provide a full-field surface displacement understanding, a calibrated thermal time history of the surface of the test structure, insight into the variation of displacements realized with identical print parameters, and a statistical determination into the print parameters most significant to the manifestation of deformations within the test structure.

EXPERIMENTAL METHODS AND ANALYSIS PROCEDURES

The experimental work described within this article was designed to build upon the published work/methodology of Spencer et al. (2021) [26], with the modification and adaptation of that published work for use with small scale FFF AM printers utilizing neat polymer filaments. Spencer et al. showed that, in the case of large-scale, it was possible to measure the surface displacements resultant from the buildup of residual stresses developed within the manufactured structure, as a consequence of the FFF process, through the employment of natural surface roughness-facilitated Digital Image Correlation (DIC). As a measurement method, DIC refers to the class of non-contacting methods that acquire images of an object, store those images in a digital form, and perform image analysis to extract full-field shape, deformation and/or motion measurements of the structure under test [43]. Under standard employment best practices, DIC uses an externally applied speckle pattern to carry deformation information from image to image [43,47,56]. In the case of *in situ* monitoring of deformations on the body of an AM test structure during the build process, application of an external speckle pattern is practically impossible. Therefore, utilization of the random surface characteristics/roughness of the structure itself, as described within [26], could be the best employment methodology currently available to quantify where on the structure, when during the manufacturing process, and to what magnitude surface displacements are created during its print, using DIC measurements. Appendix I

describes the experimental methodology and shows the particular results used to prove that use of the surface characteristics/roughness of the particular neat amorphous polymer utilized within this experimental construct can function in place of an externally applied speckle pattern to carry the necessary deformation and displacement information. Overall, the experimental examination of natural surface roughness viability for DIC applications showed that there was a statistical correlation of >99% between an externally applied speckle pattern and the displacements measured utilizing the natural surface roughness. Additionally, the two surface treatments showed very similar measurement errors, average measurement error of 0.0127 mm for an external speckle pattern and an average measurement error of 0.0318mm utilizing the natural surface of the test specimen. Given these results, the determination was made that the use of the use of the natural surface roughness resultant from the use of this particular filament on small scale AM equipment was sufficiently able to replace an externally applied speckle pattern to facilitate DIC measurements.

In addition to the measurement of surface displacements developed during the manufacturing process, this experimental effort included the continuous capture of thermal data from the surface of the test structure throughout the build process. The creation of the residual stresses which cause the buildup of residual stresses and result in AM part structural deformations is a thermally driven process [19,20,24,25,37], and pairing surface displacement results with thermal measurements will provide greater context into the behavior of the trends observed, offering potential explanations to the type and variations found within the displacement results.

For the experimentation presented within this article, the print filament under evaluation was ColorFabb's back semi-matte Polyethylene terephthalate glycol (PETG) [49], a neat

amorphous thermoplastic. The visual images of the test structure taken during the build process were captured using a Mako G-503B 1/2.5-inch monochromatic five Megapixel CMOS sensor camera equipped with a 25mm fixed focal length Edmund Optics variable aperture lens, shown in **Figure 17**. This visual image capture equipment was positioned 500mm from the test structure, providing an overall visual resolution of 0.0435 mm/pixel. Thermal data was captured through the utilization of the Indigo Systems Merlin MID thermal camera, also shown in **Figure 17**. When positioned next to the visual data capture system, 500mm from the structure under construction, the thermal imaging equipment provided a resolution of 0.386 mm/pixel.

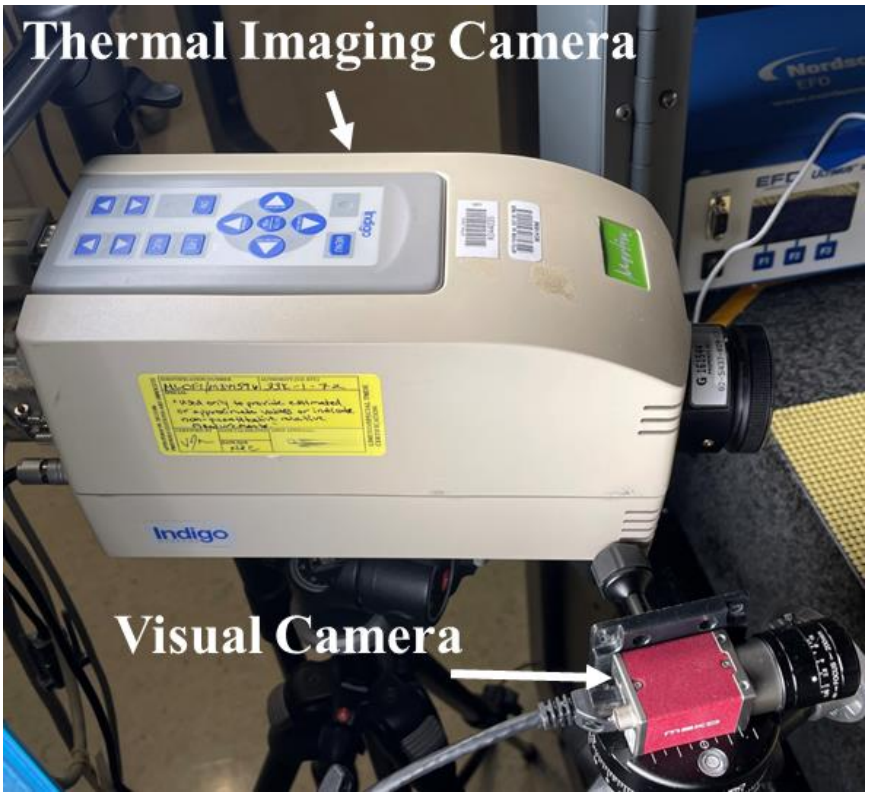

Figure 17. Thermal and visual data capture equipment.

The test structure that was built to measure the surface temperatures and displacements developed during the manufacturing process was designed as a thin wall, with dimensions 75mm

(L) x 40mm (H) x 1.05mm (W). Its design and orientation were selected to maximize the field of view available within both imaging devices, while also ensuring a minimum height of 100 deposition layers at the maximum available deposition height. A hundred deposition layers were selected as a minimum height due to the experimental results reported by [26], where a structure of 100 deposition layers was built showing very enlightening resultant displacements. It was determined that replication of this structural sizing would allow for correlations/comparisons to be made between the displacements developed within small and large scale AM. Additionally, the test structure was sized to include of a buffer between the FOV edge of the structure to prevent image distortion [55,56] A depiction of the visual camera FOV with an outline of the design parameters of the test structure when seen from the visual camera's point of view is shown in **Figure 18**.

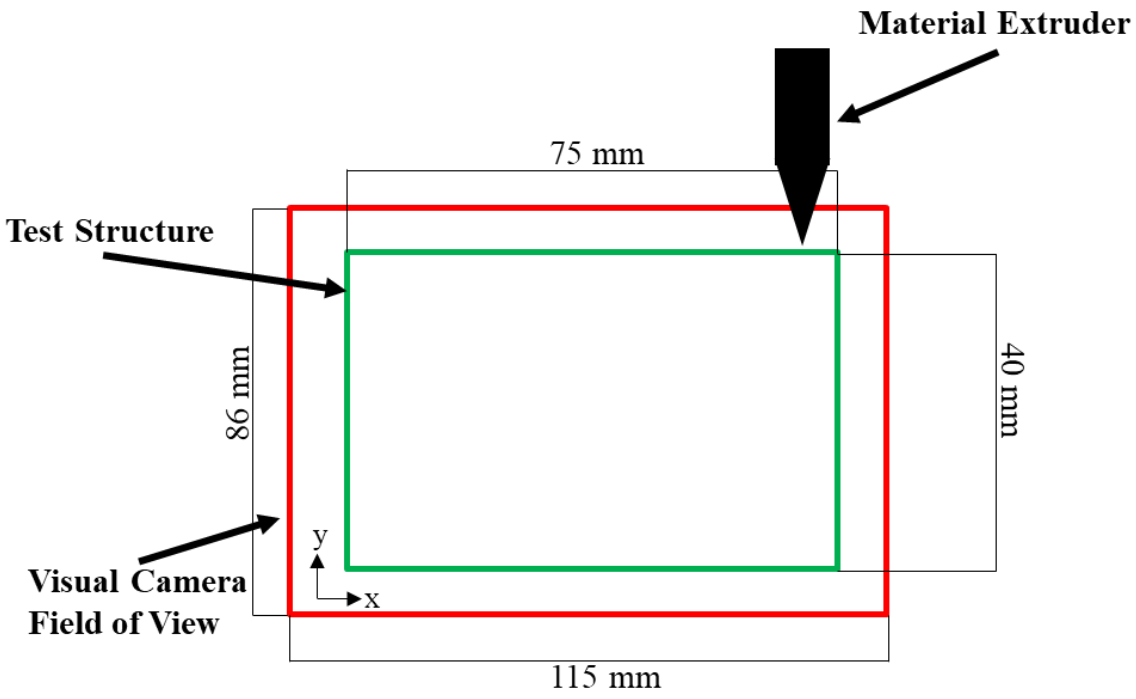

Figure 18. Visual camera FOV and test structure design, with x and y being the in-plane coordinates tracked by the cameras.

The test structure shown in **Figure 18** was designed in this manner to maximize displacements in the X and Y directions, while minimizing deformations generated as a result of the material solidification, expansion, and contraction of the deposited material, as it undergoes initial deposition and subsequent heating and cooling events in the out of plane directions. During the building of the test structure, visual images were captured after the addition of each 2mm of material deposition. In this way, it was possible to track the location and variation of the surface displacements and deformations generated within the X-Y plane during the building of the test structure. In addition to the visual images, thermal data was continuously gathered at a 15 Hz rate for the entirety of the building process.

To allow for capture of the test structure within a consistent area of the camera fields of view, it was necessary to utilize an AM printer that employed a stationary build plate. In the case of visual images, movement of the test structure between image capture events would introduce significant noise and errors into the analysis, impacting the computed surface displacements through the comparison of surface patterning between deformed and undeformed structural images [73]. For thermal imaging, significant movement of the test structure during the data gathering would make analysis of the thermal changes of the structure very difficult. This is due to the fact that the pixels associated with a specified region on the structure would be constantly changing, causing great difficulty in quantitatively tracking thermal variations. To solve this problem, it was determined that the nScript 3Dn-500 FFF printer was the appropriate equipment to prevent these issues: this small-scale AM printer provides a completely stationary heated build plate with a design that allowed for an unobstructed view of the test structure (both in the visual and thermal regimes) during the manufacturing process.

To meet the DIC requirement of uniform and consistent lighting [53] illuminating the test structure samples during visual image capture two Dracast LED500 light panels used. The two light panels were positioned approximately 500mm from the test structure, with each panel set to 5600K color temperature at their maximum brightness level.

The experimentation conducted was designed as a two-factor, two-level full factorial analysis of variables (ANOVA), with a single blocking variable and with three replications created at each configuration. The two factors that varied throughout this experimental construct were nozzle temperature and deposition layer height. For each factor, two distinct levels were used: 230 Deg C and 250 Deg C for nozzle temperature, and 0.1mm and 0.4mm for deposition layer height with all other printing parameters kept constant during all printing events; these are shown in **Table 3**. Additionally, the height of the test structure at each of the displacement measurement intervals was used as the blocking variable. This experiment was designed to evaluate the variability in generated displacements across prints of identical factor configurations, and to determine the specific factor and/or combination of factors that contribute most to the development of the observed structural surface displacements. Given this experimental design a statistical model can be created with the following form (**Eq. 2**):

$$\boldsymbol{Y_{ijkl} = \mu_{...} + \rho_i + \alpha_j + \beta_k + (\alpha\beta)_{jk} + \varepsilon_{ijkl}} \qquad \textbf{(Eq. 2)}$$

where
$\boldsymbol{Y_{ijkl}}$ is the measured displacement value
$\boldsymbol{\mu_{...}}$ is the grand mean
$\boldsymbol{\rho_i}$ is the effect due to the blocking term – Structure height
$\boldsymbol{\alpha_j}$ is main effect A (nozzle temperature)
$\boldsymbol{\beta_k}$ is main effect B (deposition layer height)
$\boldsymbol{(\alpha\beta)_{jk}}$ is the interaction term between A and B
$\boldsymbol{\varepsilon_{ijkl}}$ is the random error

Table 3. Printing parameters that were kept constant across all printing events.

Parameter	Value
Deposition Speed	$40\ mm/s$
Build Plate Temperature	$75\ ℃$
Build Plate Surface Prep	BuildTak PEI Sheet with Elmer's Disappearing Purple Glue Stick
Filament	ColorFabb Black Semi-Matte PETG

Due to the nature of the build and displacement measurement process, taking images of the test structure as it progressively grows, it was necessary to employ reverse image correlation which is the DIC analysis methodology devised by Spencer et al. (2021) [26]. Reverse image correlation is a method of utilizing DIC where the completed, cooled, and deformed test structure is used as the reference image. This DIC analysis methodology is necessary because of the consistent addition of new material onto the imaged structure. Its use allows for the entire body of the structure captured within each image to be compared to the reference image. Displacements can then be computed by calculating the difference in positioning and orientation of the captured grayscale subsets between the image under evaluation and the reference image. The reverse image correlation DIC analysis of the test structures created within this experimental effort was accomplished through the use of the Correlated Solutions VIC-2D7 software suite. In order to ensure commonality between the precision and accuracy of the calculated displacement data obtained across all generated structures, all DIC analyses were conducted using a single subset size (23 x 23 pixels) and a single step size (2 pixels). Additionally, all surface displacement values utilized in the data analysis were uncorrected/unmodified, meaning that no rigid body displacement or rotation post processing/removal were enacted on the generated data.

The need to perform a statistical analysis of the measured displacement values necessitated the creation of a novel analysis methodology. This new analysis methodology utilized the pixel grid [51] functionality present within the Correlated Solutions VIC-2D7 software, to break each of the analyzed regions of the captured images into a series of 43 x 43-pixel grids; an example is shown in **Figure 19**. The analysis block size was selected to correspond to the size (2mm) of the deposition intervals between visual image capture events. Meaning that since visual images were captured every 2mm of material deposition, the analysis blocks were designed to be approx. 2mm x 2mm given the pixel size produced by the visual image data capture equipment. These grids allow for the comparison of measured displacement values across identical regions of all generated test structures. Without the creation and use of this analysis methodology it would have been impossible to ensure that the analyzed displacements of all completed test structures were comparing identical areas. Specific nomenclature for this methodology described each square within the grid as an "analysis block" and each row of analysis blocked as an "analysis layer". With analysis layer 1 being the closest to the build plate at a height of 4mm and analysis layer 19 being the furthest from the build plate at a height of 40mm. The VIC-2D7 analysis suite allows for computation of specific displacement values for each analysis block. This also provides a method to track the specific displacements generated at both a single analysis block and across an entire analysis level as new material is added to the test structure during the manufacturing process. Allowing for the quantification of the distribution of generated displacements in both the X and Y directions as well as the changes in those measured values over time.

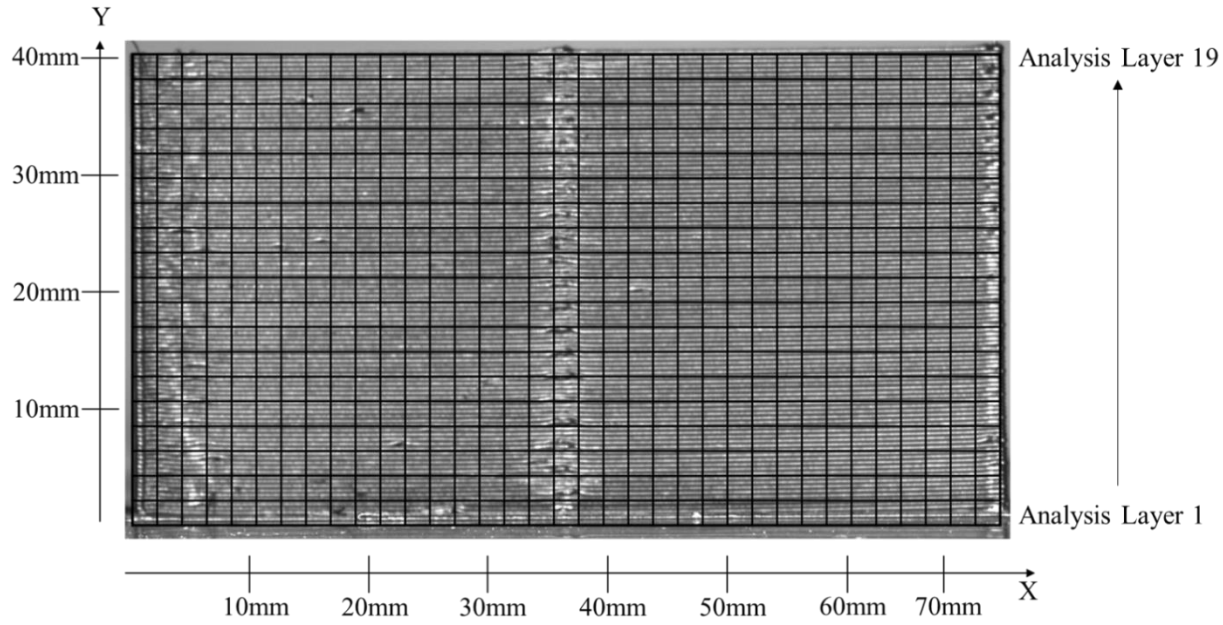

Figure 19. Depiction of the analyzed region of a completed test structure divided into 43 x 43-pixel analysis blocks.

Statistical analyses were conducted by using the maximum displacement values measured within each analysis level, computed at each visual image capture event (after the addition of 2mm of material onto the test structure). Maximum displacement values were used as they show the largest impacts to the structure under construction. Statistical analysis was accomplished through the use of the commercial JMP software suite. This software package allowed for the construct of the ANOVA experimental model, and to determine the factors within the model that contributed most to the variation in surface displacements found as the treatment values were varied. Additionally, this software suite provided a means to quantify the print-to-print variation in surface displacements found between structures created using identical treatment values.

To minimize external environmental (ambient temperature and humidity variations), equipment, and effects caused by potential filament formulation variations all test structures were printed from the same spool of PETG filament on the same day and using the same printer.

Additionally, the ambient thermal and humidity conditions within the build chamber were monitored for the entirety of print execution, to fully document and account for any potential change in material strengths [74] throughout the day, due to prolonged exposure to varying environmental conditions.

EXPERIMENTAL RESULTS

During the single day of test, the ambient temperature varied of 2.6 degrees Celsius within the build chamber (measured temperature ranged from 25.1 to 27.1 degrees Celsius). Ambient humidity tracking within the build chamber showed a relative humidity variation of 5.5% (measured specific relative humidity values ranged from 36.8% to 42.3% relative humidity). These ambient temperature and relative humidity variations were deemed to be insignificant within the overall data obtained for the printed PETG structure, when compared to the effect seen in [74] after prolonged immersion in distilled water.

Within the Correlated Solutions VIC-2D7 system, a common set of analysis parameters were employed across all of the images gathered during experimentation. These specific analysis parameters were: subset size of 23 x 23 pixels and a step size of 2 pixels. The utilization of these parameters provided a mean confidence margin, *s*, equal to 0.0264 across all of the images evaluated. This number is a VIC-2D7 in-system measurement of error [51], with lower numbers indicating a between quality match between data points. While the value of 0.0264 is higher than the ideal value of 0.01 as described in the VIC-2D7 software manual, it is significantly lower than the default confidence margin threshold of 0.05, where data is automatically removed. We felt confident proceeding forward, as this s = 0.0264 compared very favorably with the value of 0.0267 reported within the results obtained by Spencer et al. (2021) [26] in their large-scale AM analysis.

During the manufacturing process, the test structures created with the utilization of a 230 degrees Celsius nozzle and a deposition layer height of 0.1mm experienced significant build plate adhesion issues. As such, it was only possible to build those particular test structures to a height of 30mm instead of the design height of 40mm. Additionally, the deformation in one of the three replications created using these particular printing parameters was so significant that DIC analysis was not possible. Therefore, for the data presented below only two test structures at the 230 degrees Celsius and 0.1mm layer deposition height design condition have been used to compute averaged values.

The DIC analysis allowed for the simultaneous measurement of both in-plane vertical and horizontal displacements across the full field of the test structure. **Figure 20** and **Figure 21** provide a visual depiction of those measured displacements in the form of a color-coded overlay onto the body of the test structure. These color-coded overlays have been termed as "displacement heat maps", as they use colors to denote areas of varying displacements. **Figures 20 and 21** show a subset of the images analyzed across a representative test structure utilizing each of the print parameter treatments evaluated.

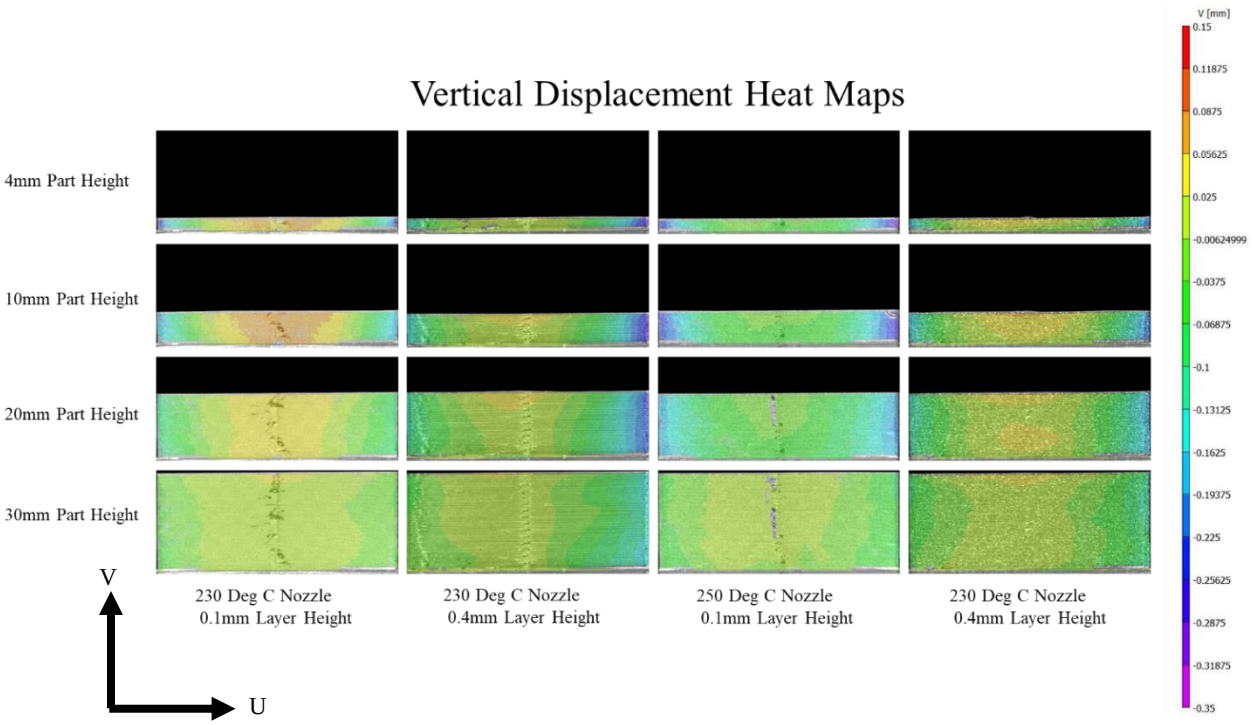

Figure 20. In-plane vertical v displacement maps. Note the 230 deg. C nozzle and 0.1mm test structure builds were terminated at 30mm to build plate detachment.

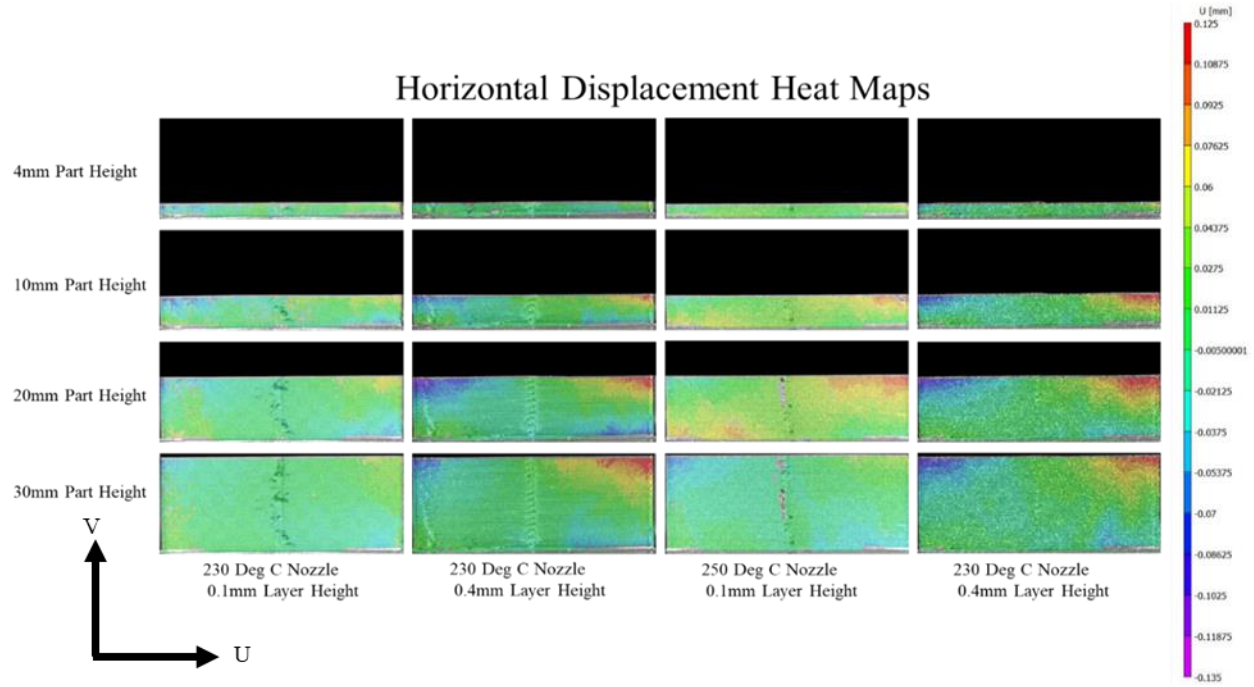

Figure 21. In-plane horizontal u displacement maps. Note the 230 deg. C nozzle and 0.1mm test structure builds were terminated at 30mm to build plate detachment.

The above displacement maps provide a highly useful method of understanding of the overall patterning and magnitudes of surface displacements on individual structure builds. **Figure 20** shows the vertical displacements measured at discrete intervals of the build process over a single replication of each of the print parameter variations, using the cooled fully built test structure as the reference. From this figure, it is possible to discern a symmetric patterning to the vertical displacements, observed with higher deformations on the edges of the structure, while the central region of the test structure shows little to no surface displacements across the entirety of the test structure construction. In **Figure 20**, the measured vertical displacements appear to remain relatively constant in the vertical direction (v) and only vary across the horizontal span (u) of the test structure at each measurement interval. With the magnitudes of the measured displacements, as measured from the cooled final structure, consistently decreasing as the test structure is built.

In examining **Figure 21**, it is possible to see that the measured horizontal displacement magnitude is increasing as the height of the test structure increases. Additionally, there is a symmetrical behavior about the center of the test structure, with both edges contracting toward the middle of the test structure. Unlike the displacement heat maps shown in **Figure 20**, the horizontal displacements in **Figure 21** exhibit extensive magnitude variations by the time the structure is printed.

To develop a more complete understanding of the measured displacements created during the AM build process, we utilized the novel analysis block methodology described previously, where the measured displacements of the test structure are computed over a series of 43 x 43-pixel blocks across the surface of each of the imaged test structures. This allows for the quantitative comparison of measured displacements on identical areas of different imaged test

structures. An example of the use of this methodology is shown in **Figure 22**, which depicts the mean vertical displacement analysis block values for a particular permutation of print parameters (in this case a nozzle temperature of 230 degrees Celsius and a layer deposition height of 0.4mm), plotted across the horizontal span of the test structure for analysis layer 1, where the analysis layer is composed of all the analysis blocks in a horizontal row, with analysis layer 1 being the closest to the build plate at a height of 4mm (successive analysis layers would be located 2mm above each preceding layer). Each line within **Figure 22** shows the vertical displacements measured after the deposition of 2mm of test structure onto the previously deposited layers. From this example plot, it is possible to see location in analysis layer 1, and magnitude of the vertical displacements during the addition of every 2mm of material, during the manufacturing process. When inspecting these analysis plots, it is important to remember that the displacements are measured from completed, cooled structure. Therefore, displacement values will approach zero as the configuration of the imaged structure approaches that of the completed, cooled, and deformed structure; displacement values describe either an undeformed or differently deformed structure from that of the complete body.

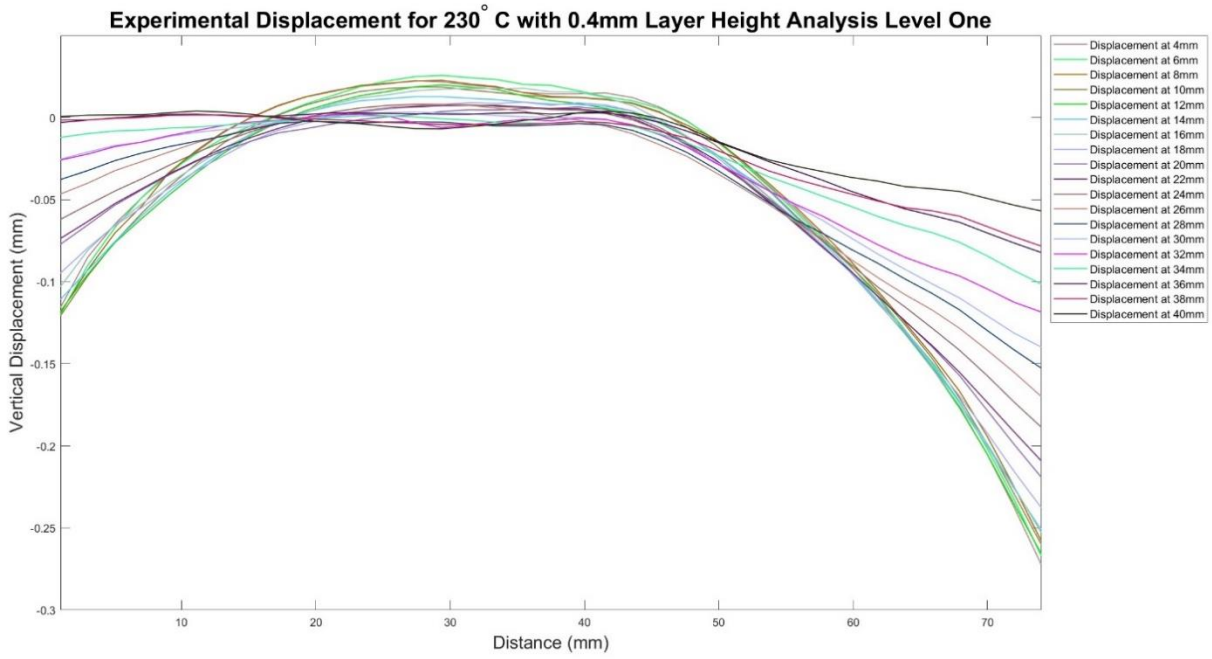

Figure 22. Example analysis block displacement plot showing mean vertical displacements across analysis level 1 for the complete build of the test structure. The displacement values shown are for a specific analysis layer and how the material comprising the individual analysis blocks has moved in relation to the reference DIC image.

Figures 23-26 show clear behavior patterns during the construction process of the test structure. When we examine the structures created using 0.1mm layer depositions for both nozzle temperature treatments, the vertical displacements fall into very discrete groups with large jumps between imaging intervals, followed by periods of little to no vertical displacements. The vertical displacement values measured in structures created using 0.1mm layer depositions remain constant initially, with some slight gradual movement followed by discrete steps with very small displacements created in between these discrete steps. On the other hand, the test structures created using 0.4mm layer depositions show significantly less discrete displacement behavior: the vertical displacements remain initially constant, but then undergo a series of small and consistent vertical displacements throughout the entire manufacturing process. Regardless of

the specific expression of the displacement behavior, the following overall observations can be made of the vertical displacements measured during the construction of test structures within small scale AM printers utilizing the neat amorphous polymer-PETG:

1. This experimentation did not reveal the existence of a height limit above the analyzed analysis layer, where the addition of new material would not cause vertical displacements/deformation within that particular layer.
2. Vertical displacements showed the greatest magnitude away from the center of the test structure.
3. Initial manifestation of vertical displacements was highly dependent on the height of the structure: within the choice of print parameters and their values, there was an initial region of the test structure (at slightly varying heights) where no vertical deformations were created during the print. It can be concluded that a number of material deposition/heating/cooling events were required to create the cumulative residual stresses needed to cause vertical deformations. The number of these deposition/heating/cooling events observed prior to initial vertical deformation were significantly higher when utilizing a deposition layer height of 0.1mm (100-120 events for 0.1mm deposition layer heights compared to 45 events for 0.4mm deposition layer heights).

Maximum observed vertical displacement for each of the evaluated print parameter permutations are reported in **Table 4**.

Table 4. Analysis block maximum measured vertical displacement.

230 deg C nozzle w/ 0.1mm layer height	230 deg C nozzle w/ 0.4mm layer height	250 deg C nozzle w/ 0.1mm layer height	250 deg C nozzle w/ 0.4mm layer height
0.402544 mm	0.287647 mm	0.35539 mm	0.220505 mm
At analysis layer 1	At analysis layer 3	At analysis layer 1	At analysis layer 1

It was seen that, for a given deposition layer, the vertical deformations measured were larger when the nozzle temperature was held at 230 degrees Celsius with respect to the case of 250 degrees Celsius. Finally, the largest observed vertical displacements were found to occur within analysis blocks located at or near the bottom of the test structure (closest to the build plate), and decreased for analysis blocks located higher up on the structure (farther from the build plate).

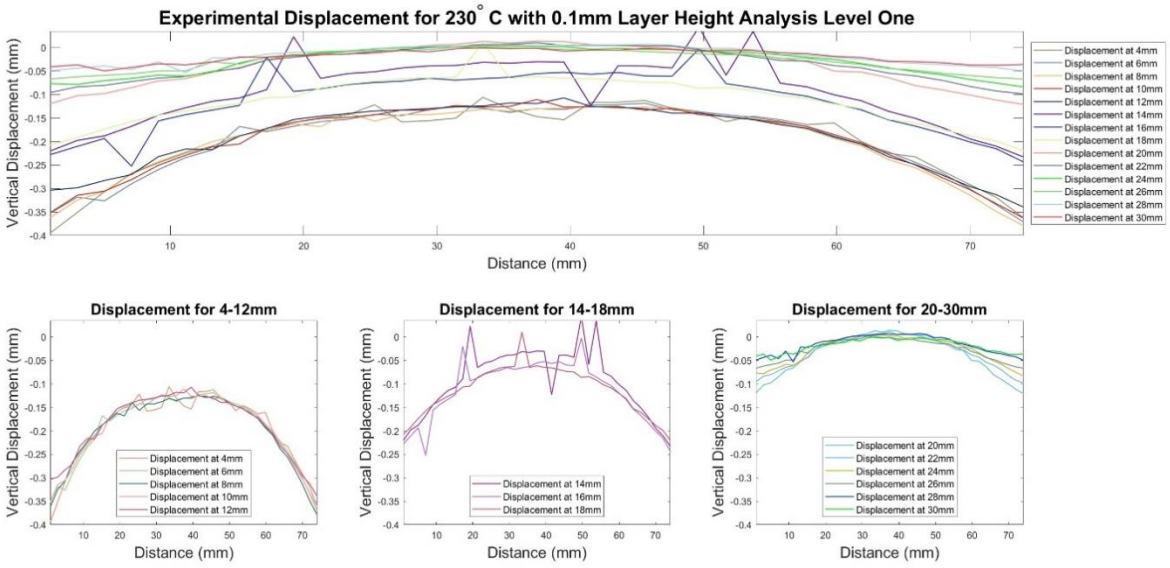

Figure 23. Analysis level 1 mean in-plane vertical displacement behavior plot for 230 deg. C with 0.1mm layer deposition. Note the 230 deg. C nozzle and 0.1mm test structure builds were terminated at 30 mm to build plate detachment.

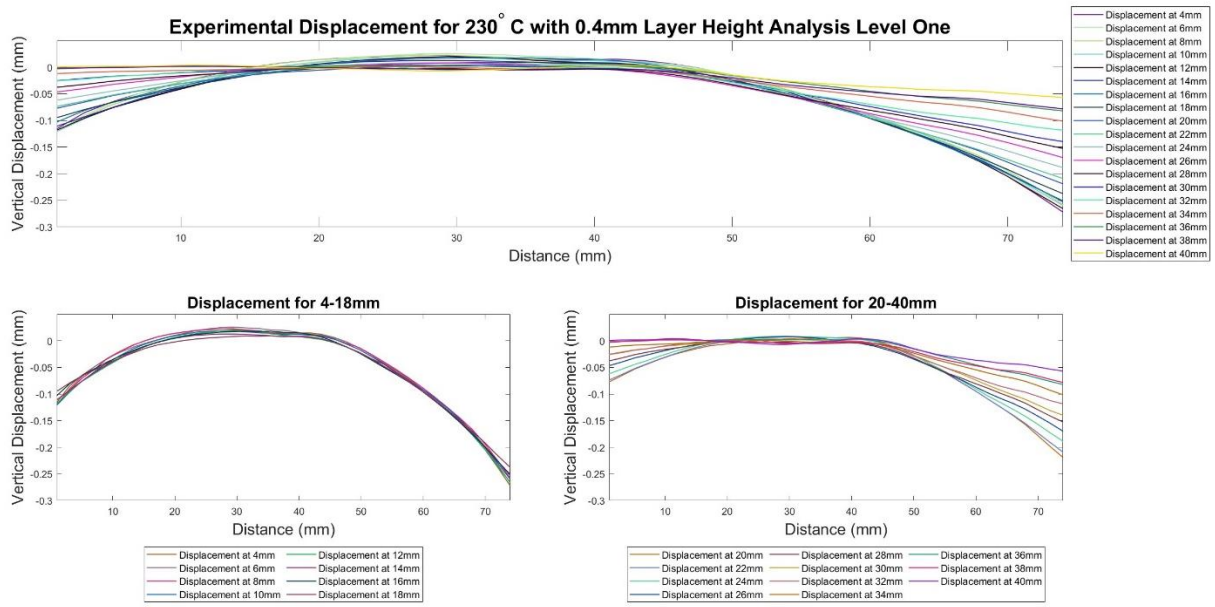

Figure 24. Analysis level 1 mean in-plane vertical displacement behavior plot for 230 deg. C with 0.4mm layer deposition.

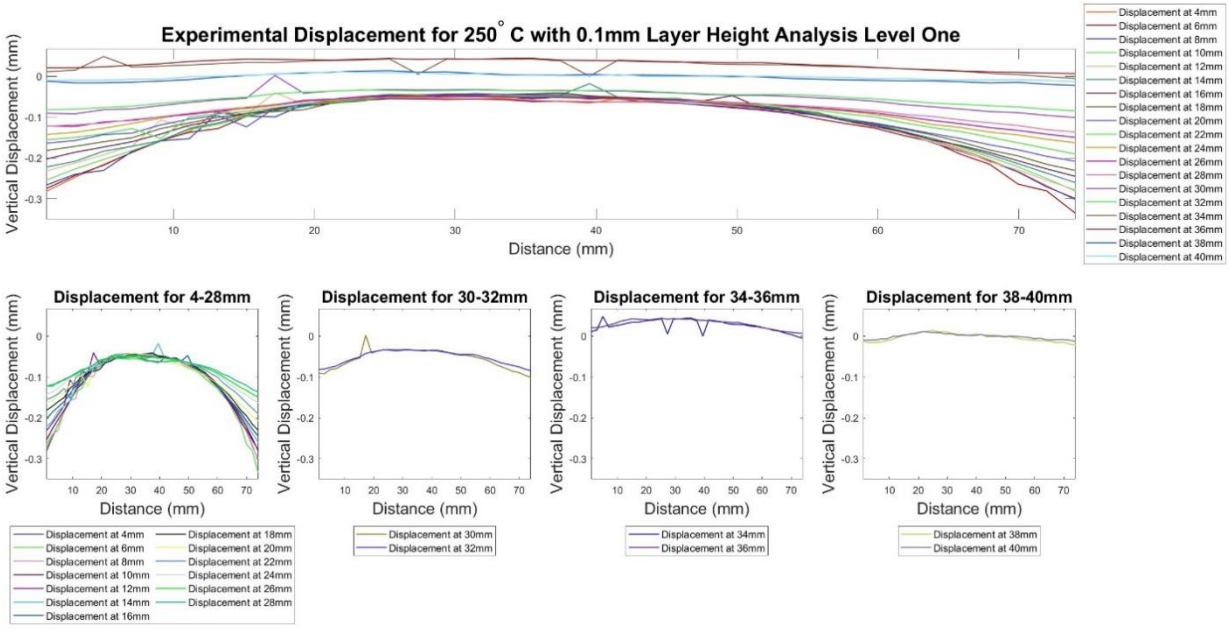

Figure 25. Analysis level 1 mean vertical displacement behavior plot for 250 deg. C with 0.1mm layer deposition.

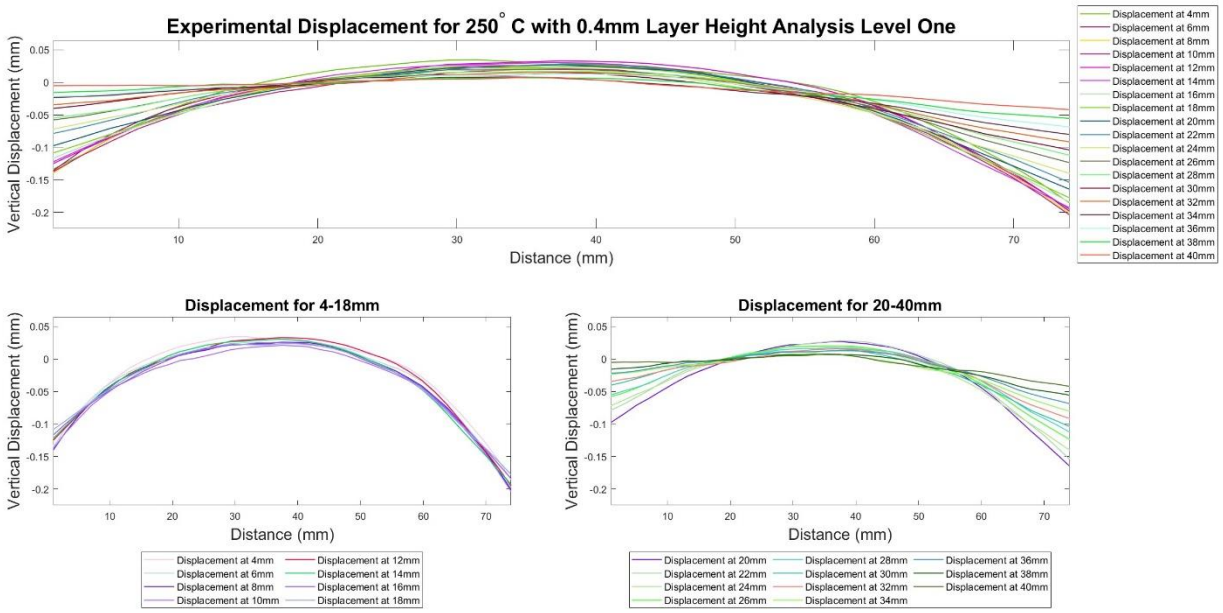

Figure 26. Analysis level 1 mean vertical displacement behavior plot for 250 deg. C with 0.4mm layer deposition.

In addition to the observations above, **Figures 23-26** indicate that test structures created using a 0.4mm layer deposition have a slightly less symmetric displacement pattern than the patterns resultant through the utilization of a 0.1mm layer deposition. In the earlier case, the right-hand side of the test structure shows a consistently larger displacement than the left-hand side of the test structure for across both evaluated nozzle temperatures. One potential reason for this asymmetric behavior is a thermal variation within the structure, with the right side of the test structure undergoing a slightly different heating/cooling profile than that of the other sections of the test structure. To verify this hypothesis, **Figures 27-30** were created using the data gathered through the thermal imaging system. These figures show the calibrated thermal measurements taken during the complete manufacturing process at 4mm above the build plate (the same height

as analysis layer 1) at three locations along the horizontal span of the test structure. These figures clearly show that for all print parameter treatment configurations, the center of the test structure exists at a higher temperature than that of either the right- or left-hand side; the right-hand side of the test structure maintains a consistently higher temperature than that of the left-hand side. This temperature delta between the two sides of the test structure, shown in **Figure 31**, was found to be greatest in the test structures created using a 0.4mm layer deposition height, and has the potential to lead to greater shape change due to thermal stimuli [75,76], and thus greater displacement on the right-hand side compared to the left-hand side.

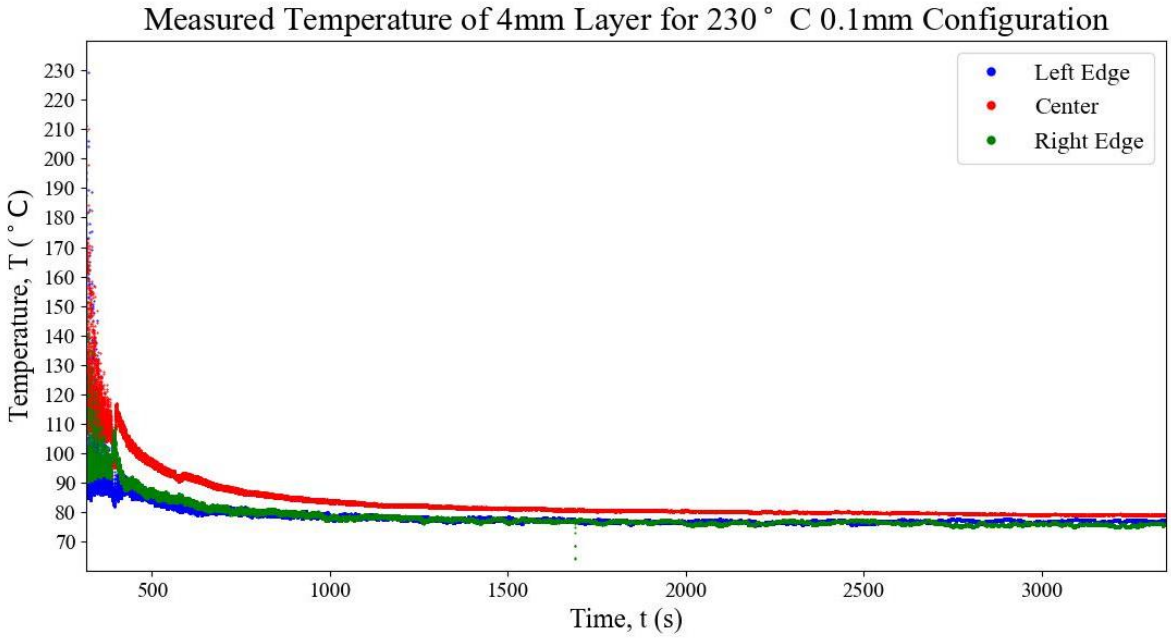

Figure 27. Thermal history plot for the left, center, and right edge of the test structure built using 230 deg. C nozzle with 0.1mm layer deposition.

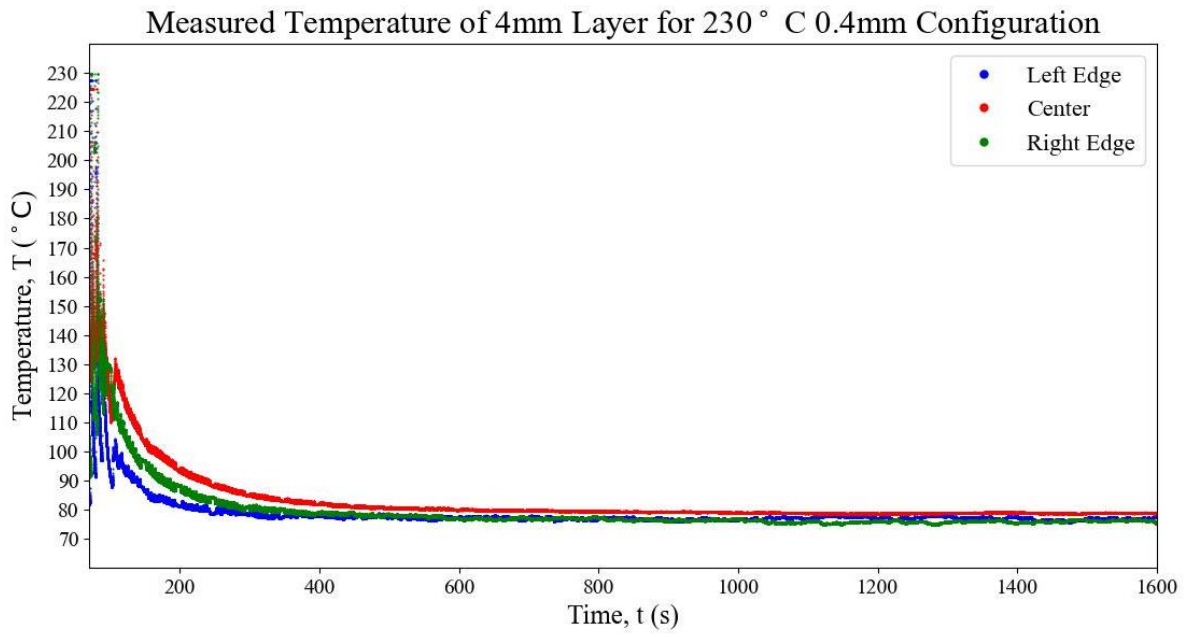

Figure 28. Thermal history plot for the left, center, and right edge of the test structure built using 230 deg. C nozzle with 0.4mm layer deposition.

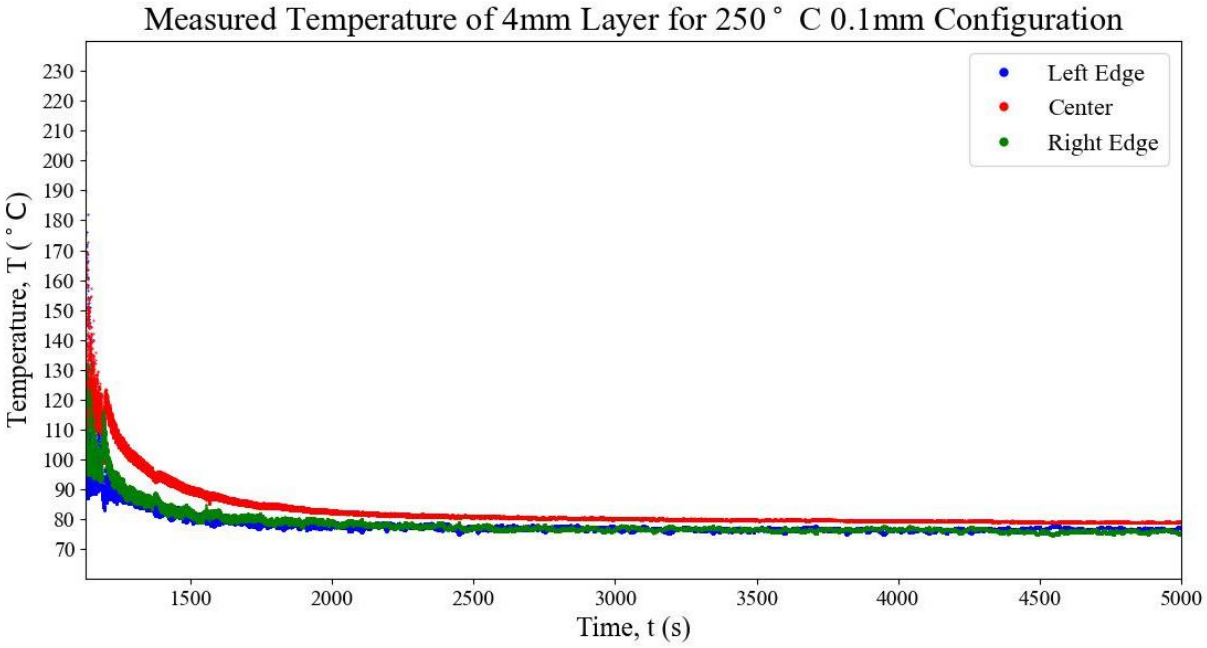

Figure 29. Thermal history plot for the left, center, and right edge of the test structure built using 250 deg. C nozzle with 0.1mm layer deposition.

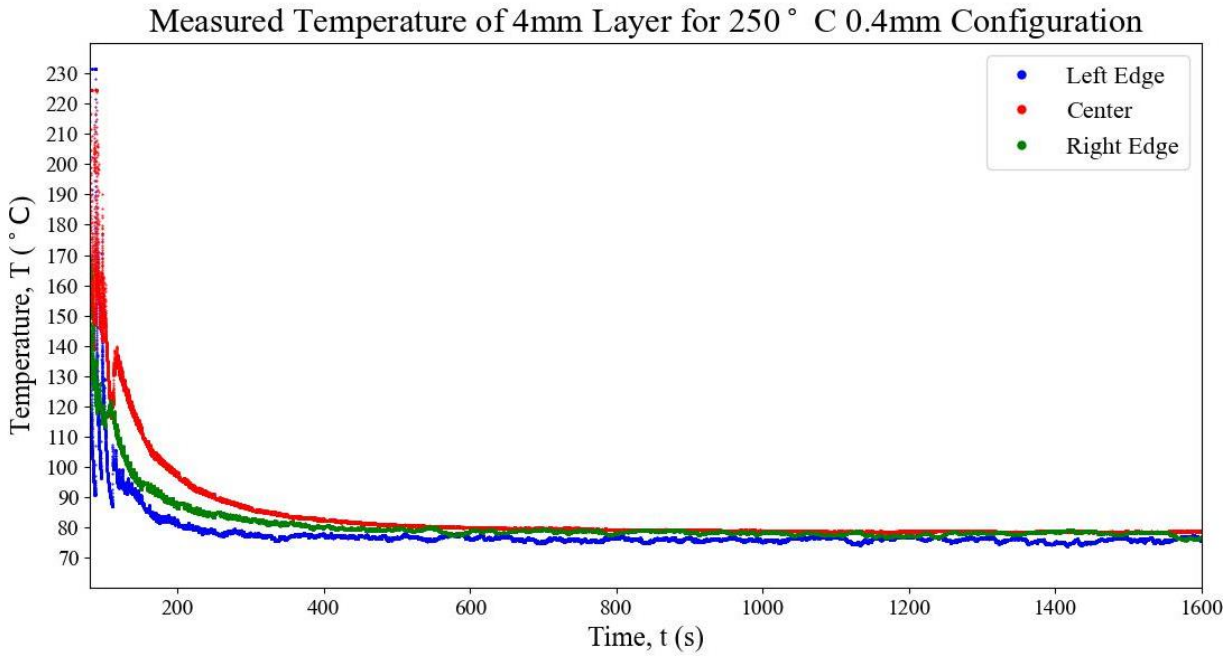

Figure 30. Thermal history plot for the left, center, and right edge of the test structure built using 250 deg. C nozzle with 0.4mm layer deposition.

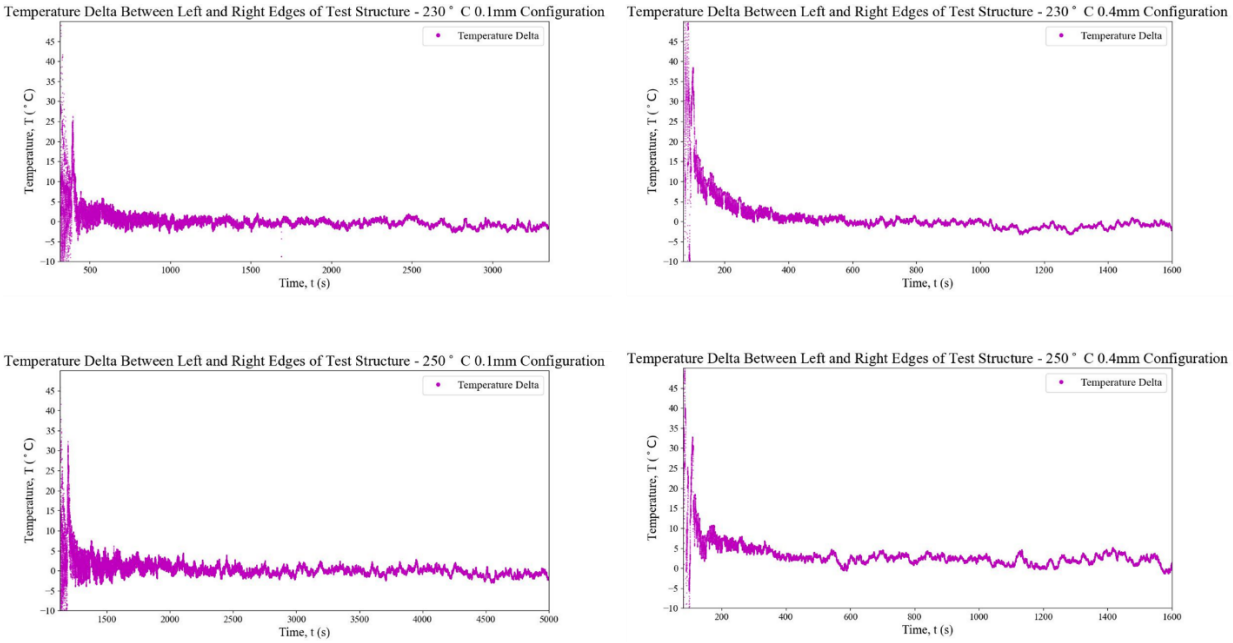

Figure 31. Calibrated temperature difference between the right and left hand side of the test structure.

As seen previously within the horizontal displacement heat maps, **Figure 21**, there were variations in both the horizontal (u) and vertical (v) displacements. Therefore, it was determined that the best method to analyze and understand the data captured was to build time history plots describing the creation and change of horizontal displacements (**Figure 32**) for a series of particular analysis layers, as material is added to the test structure. For these plots, the analysis layers located at 4mm, 10mm, 20mm, 30mm above the build plate were chosen to best illustrate the observed behavior of the horizontal displacements. Overall, across all print parameter variations, analysis layer 1 exhibits different behavior than observed layers higher (farther from the build plate) on the test structure.

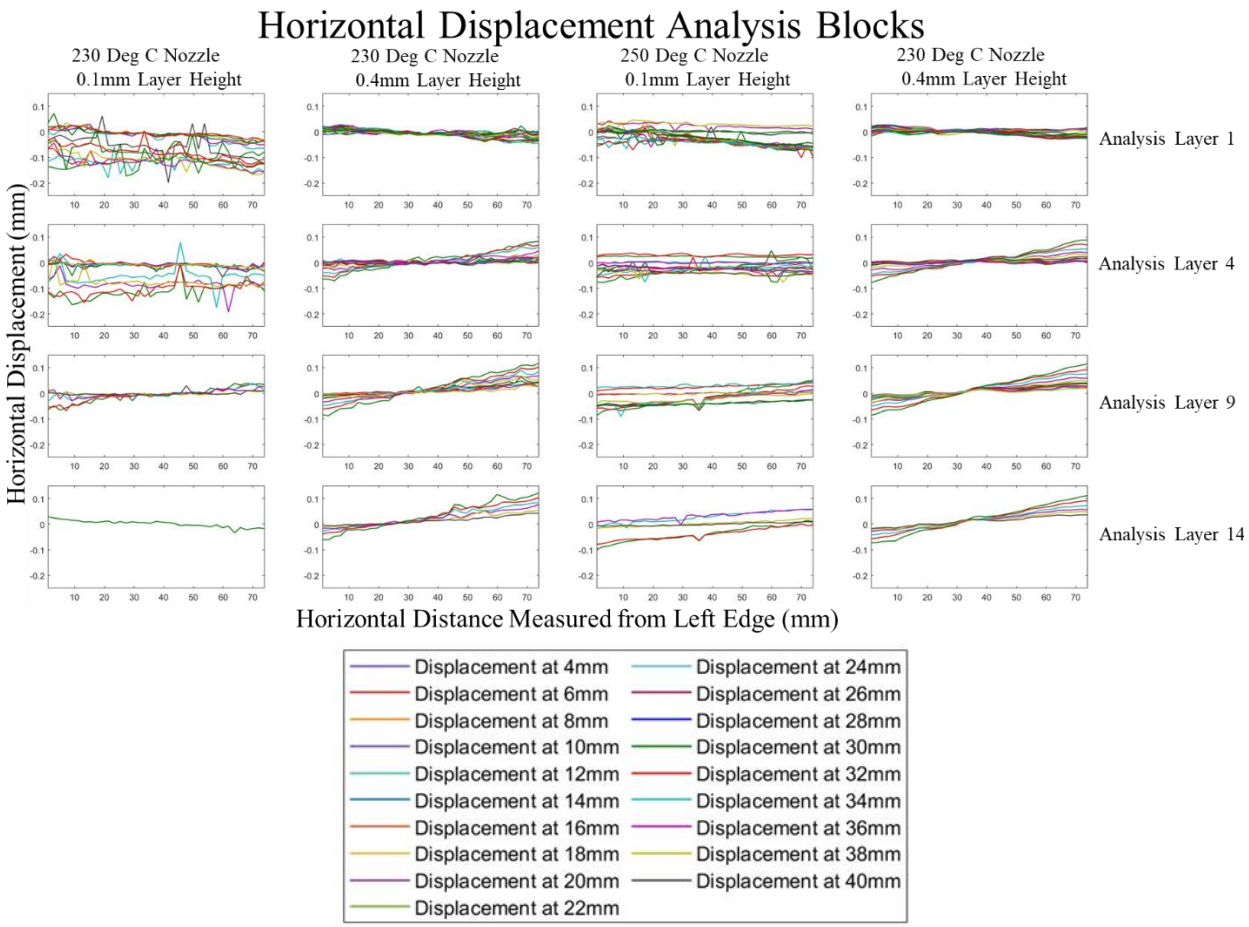

Figure 32. Analysis block horizontal displacements. Note the 230 deg. C nozzle and 0.1mm test structure builds were terminated at 30mm to build plate detachment.

Additionally, the first analysis layer has a different pattern depending on the deposition layer height used in the construction of the test structure. For test structure builds utilizing a 0.1mm layer deposition height, analysis layer 1 shows a small variation between the left- and right-hand side of the test structure; it does however show comprehensive horizontal shifts in the entire test structure during the build process. In the case of the structures built using a 230 degrees Celsius nozzle, these large magnitude horizontal shifts combined with the previously discussed vertical deformations led to the termination of the manufacturing process at a test structure height of 30mm due to build plate detachment. Conversely, test structures built utilizing

a layer deposition height of 0.4mm showed little to no variation or displacement within analysis layer 1. This process leads to the overall observation that test structures created with a layer deposition height of 0.1mm with the given equipment and print parameters experienced a series of total repeated horizontal shifts in both the positive and negative horizontal (u) directions. While observed in all 0.1mm deposition layer height test structures, the magnitude of these total body shifts was larger in those structures that also utilized a nozzle temperature of 230 degrees Celsius.

As the height of the test structures increased, analysis layers further away from the build plate began exhibiting a new consistent behavior pattern: an initial negative displacement on the left-hand side of the structure, and an initial positive displacement on the right-hand side of the structure, with a zero-magnitude displacement measured at center of the test structure. As new material was added to the test structure, the magnitudes of these measured displacements steadily reduced to zero for the entire analysis layer. It was seen that the onset of this consistent behavior pattern occurred at a lower overall height for the 0.4mm case (transition occurred by a structure height of 10mm) than for the 0.1mm case (transition occurred by a structure height of 20mm).

Based on the data captured through the course of this experimental effort it is possible to make the following observations, within the selected equipment and print parameters:

1. Test structures manufactured with a deposition layer height of 0.1mm were observed to exhibit repeated and persistent structure-wide horizontal shifts throughout the entire build process. The magnitude of these shifts was seen to be greatest in the test structures that combined a 0.1mm deposition layer height with a nozzle temperature of 230 degrees Celsius.

2. The manifestation of horizontal displacements within the body of the test structures was seen to be highly dependent on the height of the test structure, meaning that from the build plate to the top surface of the completed and cooled test structure, differing horizontal behavior patterns were observed. Lower analysis levels (closer to the build plate) showed little to no analysis layer horizontal displacements, and absent wholesale structural shifting observed in those structures built with a 0.1mm layer deposition height. During the development of a consistent initial negative left-hand side, the initial positive right-hand side displacement pattern evolved as the height of the test structure increased.
3. At analysis layers above the build plate, where the horizontal displacement behavior began exhibiting a consistent behavior (above 10mm for structures built with a deposition layer height of 0.4mm and above 20mm for structures built with a deposition layer height of 0.1mm), the analysis layers showed a steady contraction towards the center of the structure, as new material was added. This steady contraction was seen to cease after the addition of 8mm (20 material deposition layers) for structures built with a deposition layer height of 0.4mm and 10mm (100 material deposition layers), for structures built with a deposition layer height of 0.1mm.

Maximum observed vertical displacement for each of the evaluated print parameter permutations are reported in **Table 5**.

Table 5. Analysis block maximum measured horizontal displacement.

230 deg C nozzle w/ 0.1mm layer height	**230 deg C nozzle w/ 0.4mm layer height**	**250 deg C nozzle w/ 0.1mm layer height**	**250 deg C nozzle w/ 0.4mm layer height**
0.238634mm	0.1590296mm	0.190950394mm	0.131307138mm
At analysis layer 3	At analysis layer 9	At analysis layer 9	At analysis layer 10

Maximum measured analysis block horizontal displacements developed on the surface of the test structures exhibited a behavior similar to that observed with maximum measured vertical displacements. Specifically, the largest analysis block horizontal displacements were found within the test structures built with a layer deposition height of 0.1mm, with reductions in maximum displacement seen as the nozzle temperature was increased from 230 degrees Celsius to 250 degrees Celsius. It is also worth noting that the maximum expression of horizontal displacement occurred towards the middle height of the structure (with the exception of the test structures created using a 230 degrees Celsius nozzle and a 0.1mm layer deposition height), with maximum displacements seen at the left- and right-hand edges of the test structures under evaluation.

In addition to the ability to compute and compare displacements measured across all print parameter variations, the analysis block methodology allows for the conduct of statistical studies to gain additional insight into the results obtained. These statistical studies were created by using the maximum reported analysis block displacements within each analysis layer at each imaging interval. The first of the studies undertaken was an examination of the print-to-print variability of maximum displacements found within each of the factorial configurations evaluated. This study provides insight into the variance in displacements generated in the creation of identical test structures using identical print parameters, how those variances changed during the test structure construction, and how that variability compares across all the print parameter permutations evaluated.

Figure 33 provides the results of this statistical study focusing specifically on the maximum measured vertical displacements within each analysis level. This figure shows very

clearly that, with the exception of test structures created with a nozzle temperature of 230 degrees Celsius and a layer deposition height of 0.1mm (discussed below), the print-to-print variability in maximum vertical displacements measured during the manufacturing process was fairly consistent across all analysis layers. To contrast this observation, test structures created with a nozzle temperature of 230 degrees Celsius and a layer deposition height of 0.1mm had significant variability in displacements at different analysis layers: this variability was the highest in analysis layers 6-8 (overall structure height of 14-18mm), with low variations noted within analysis layers 1-5 and 9-14. Overall print to print vertical maximum displacement variance showed clear behavior patterns as a function of the manufacturing treatments used. **Table 6** shows an ordered list of the specific treatment configurations examined along with the specific variances found in the maximum measured vertical displacements (with the lowest variation treatment configuration listed topmost and those configurations with greater variation listed in descending order).

Table 6: Print to Print Vertical Displacement Variance

Print to Print Vertical Displacement Variance	
Configuration	**Maximum Variance**
250 deg C with 0.4 mm layer deposition height	0.00115
230 deg C with 0.4 mm layer deposition height	0.00202
250 deg C with 0.1 mm layer deposition height	0.00512
230 deg C with 0.1 mm layer deposition height	0.01285

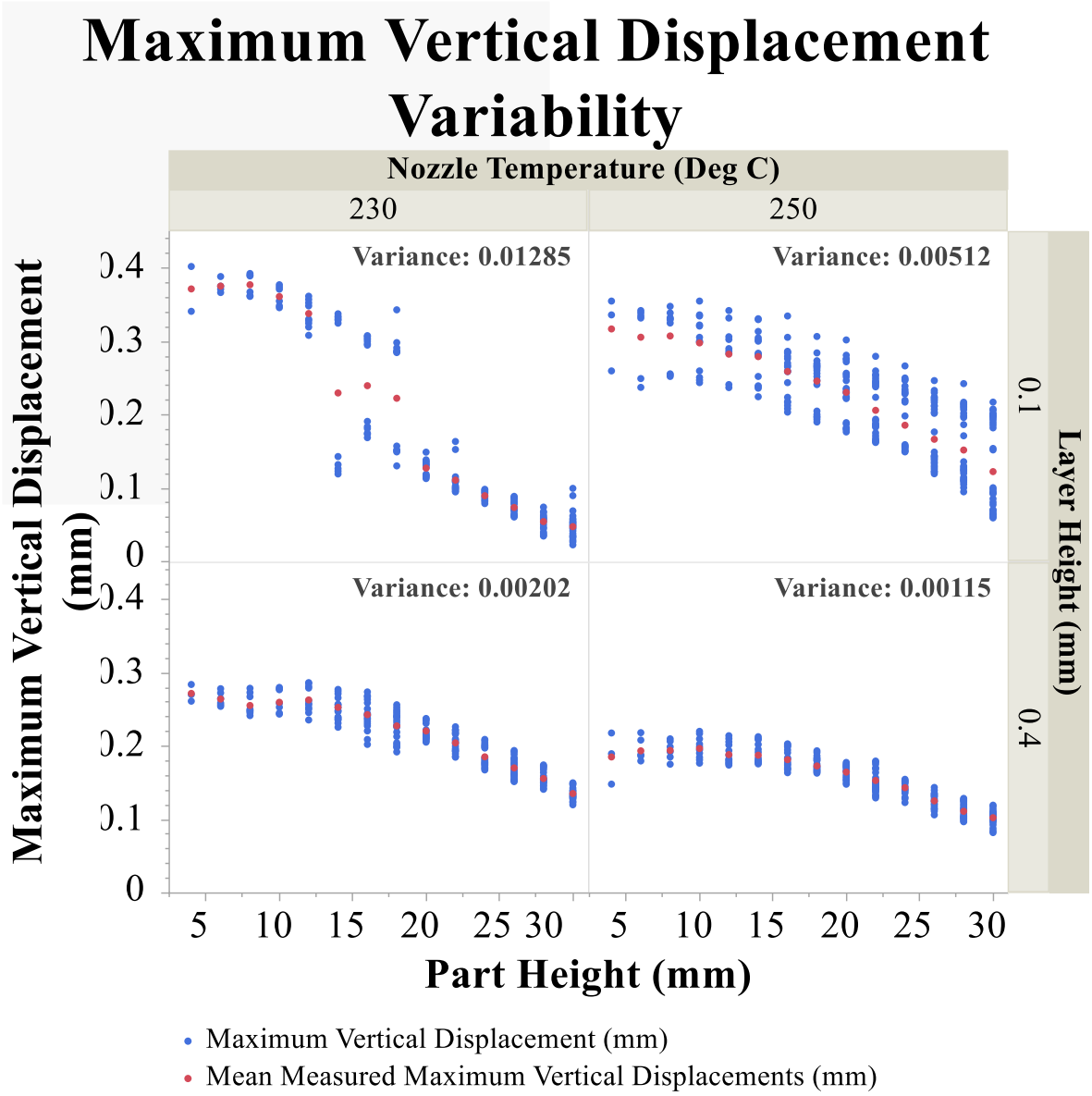

Figure 33. Variance in maximum measured vertical displacements.

Figure 34 continues the statistical study discussed above, and applies it to the maximum horizontal displacements measured within each analysis layer at each measurement interval. It indicates less overall consistency of variance between analysis layers. Test structures created with a nozzle temperature of 230 degrees Celsius and a layer deposition height of 0.1mm showed high levels of variance initially, but once the structure reached a height of 20mm, the variance

found between prints drastically reduced. Similar behavior was noted for test structures built with nozzle temperature of 230 and 250 degrees Celsius and a layer deposition height of 0.4mm, except the structures started with a very low variance that progressively increased until the structure reached a height of 10mm, at which point the variance stabilized at a more consistent value. **Figure 34** shows that test structures built with a nozzle temperature of 250 degrees Celsius and a layer deposition height of 0.1mm showed a consistent variance in horizontal displacements between prints over the entire manufacturing process. The reported variances of maximum measured horizontal displacement across the selected print parameter permutations show the same behavior pattern as the variances associated with vertical displacements and are shown in **Table 7**. With the lowest variation treatment configuration listed topmost and those configurations with greater variation listed in descending order.

Table 7: Print to Print Horizontal Displacement Variance

Print to Print Horizontal Displacement Variance	
Configuration	**Maximum Variance**
250 deg C with 0.4 mm layer deposition height	0.00091
230 deg C with 0.4 mm layer deposition height	0.00111
250 deg C with 0.1 mm layer deposition height	0.00263
230 deg C with 0.1 mm layer deposition height	0.00398

Finally, it is worth noting that the calculated variances for each parameter permutation with respect to horizontal displacements were found to be significantly lower than those calculated with respect to vertical displacements, showing a lower level of print-to-print

horizontal deformation variation than print-to-print vertical deformation variation with the utilization of identical manufacturing processes.

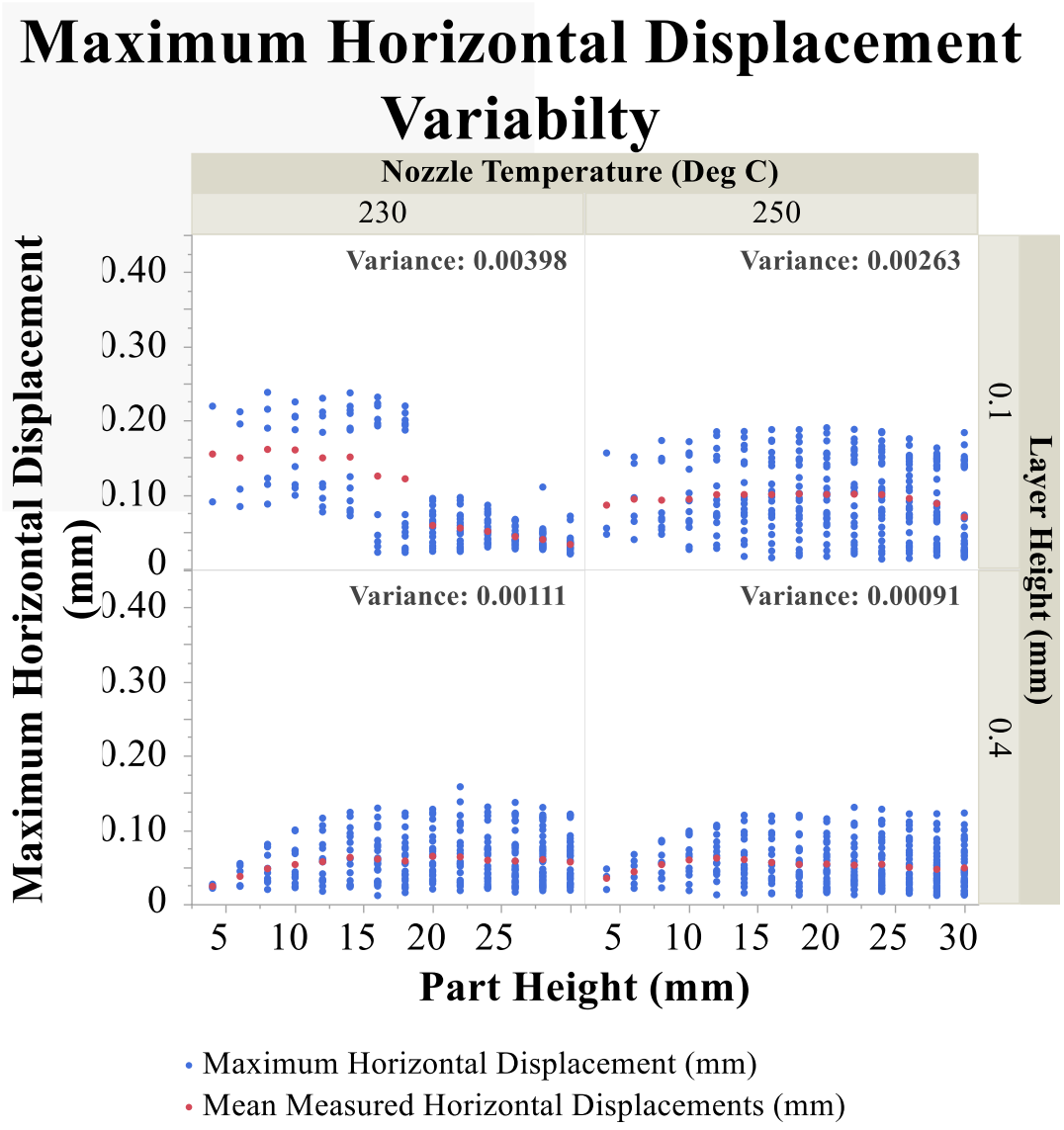

Figure 34. Variance in maximum measured horizontal displacements.

The final statistical study undertaken utilizing the data gathered and analyzed from this experimental construct was the application of ANOVA. This statistical model allowed for the understanding as to which of the print parameters had statistically relevant impacts on the

displacement results obtained. For this study, only vertical displacements (not the horizontal displacements) were used, as they were the only set of the two that were found to be normal, through the use of an Anderson-Darling normality test, after completion of a Box-Cox transformation, and therefore were viable for ANOVA [61]. The results of the ANOVA study are shown in **Table 6**. These results showed that the deposition layer height did not significantly contribute to the differences in vertical displacements found within the conducted experiment. Instead, nozzle temperature and the interaction factor (nozzle temperature and deposition layer height) were found to be significant contributors to the displacements measured. Additionally, the statistical study found that the inclusion of part height as a blocking term recorded at each particular imaging interval was a statistically significant factor to include within the model. Taken all together, these statistical results show that the development of vertical displacements within the body of an AM structure created using small scale printing with PETG filaments are highly dependent on the height of the constructed body, as well as the combination of the nozzle temperature and layer height. Nozzle temperature as a singular factor provides a lesser but still significant impact.

Table 8. Statistical print parameter effects test results.

Effect Tests				
Source	**Degrees of Freedom**	**Sum of Squares**	**F Ratio**	**Prob > F**
Nozzle Temperature (Deg C)	1	0.0061560	4.1844	0.0410
Layer Height (mm)	1	0.0008806	0.5985	0.4393
Nozzle Temperature (Deg C) x Layer Height (mm)	1	0.9813334	667.0403	<.0001
Part Height (mm)	13	3.2365205	169.2273	<.0001

Table 6 shows the results of the ANOVA statistical study. Within this table, we see the "Degrees of Freedom" describing the number of levels for each of the treatments minus one, with the exception of the nozzle temperature/layer height interaction, which describes the degrees of freedom of factor A (Nozzle Temperature) multiplied by the degrees of factor B (layer height). The "Sum of Squares" describes the individual treatment (nozzle temperature, layer height, and nozzle temperature/layer height interaction) mean deviation from the overall mean. The "F Ratio" term within the table describes the mean squares of each factor divided by the mean square error of the data. This data compared to the F statistic term for each factor allows for the evaluation of the null hypothesis ("Is this term significant?" $H_O = 0$, the effect of each factor is zero). Finally, the "probability > F" is the reliability to which we can reject the null hypothesis [60,61]. The results presented within this section show a complete and detailed description of deformations and displacements created within the body of the PETG test structures created through small scale AM and exposed to ambient environmental conditions during the manufacturing process. Additionally, these methodologies allowed for the development of a greater level of understanding of print-to-print variability of deformations and displacements created, as well as the discovery of the print parameter factors that contribute most to the deformations and displacements produced (within the selected equipment). From the totality of these results, it is clear that to minimize both the magnitude of displacements generated and the variability in structures produced using small scale AM printers with PETG filaments, the largest possible layer deposition height (in the case evaluated above, this was 0.4mm) and the hottest possible nozzle temperature recommended by the filament manufacturer should be utilized. Additionally, in cases where extreme printed part accuracy is required,

individual sub-parts of an overall structure should be limited in height below 18mm, while instead utilizing the length and width dimensions as much possible.

CONCLUSIONS

This article has described a detailed experimental process and novel data analysis methodologies to analyze results across a number of AM builds with a variety of print parameters. These analysis methodologies enabled the understanding and documentation of the displacement behavior patterns as a function of the location on the constructed test structure and time during the manufacturing process. Through the utilization of the "analysis block" data architecture, it was shown that it is possible to gain greater insight into the print-to-print variability and print parameter contribution to the displacements/deformations generated during the AM process. We prove that, within the selected equipment and print parameters, the interaction between nozzle temperature and layer deposition height and nozzle temperature are the most statistically significant print parameters.

It is our hope that the experimental construct, analysis methodologies, and conclusions drawn here build foundational steps in the further exploration and understanding of the deformation phenomena discussed. Through the continued utilization of the methods presented and the creation of new experimental/analysis methods it will be possible to discover insights into a wider range of polymers and AM parameters (i.e., build plate temperature, infill construct, and print speed). The ultimate goal is the ability to model and predict the formation of these structural deformations, and utilize the flexibility and capability of the AM systems to account for and overcome these stress formation events. This will thereby allow for the use of AM systems to create more capable, consistent, and critical structures, where and when they are

needed. As AM creation techniques and available materials continue to advance, it is crucial that an in-depth understanding be developed to evolve alongside these systems, to sense, understand, and predict the formation of manufacturing-induced residual stresses, and to minimize and counteract their detrimental effects on the structures we design and build.

Acknowledgements

The authors would like to acknowledge the support received from the Defense Innovation Unit (DIU), UC Davis Engineering and Student Design Center (Jose Mojica and Sherry Batin), USAF Research Lab (Mr. Andrew Abbott, Mr. Tyler Lesthaeghe, Dr. Craig Przybyla, Dr. Lorianne Groo, and Dr. Eric Lindgren), Dr. David Slaughter, and the members (Nickolas Loftus and David Guinn) of the UC Davis Advanced Composites, Research, Engineering and Science (ACRES) laboratory who provided critical support and expertise during the development of this study.

APPENDIX I

This appendix details the experimental effort that was undertaken to validate the use of the natural surface roughness of an AM structure to be used in place of an externally applied speckle pattern for use with DIC measurements. Typically, DIC measurements aimed at capturing surface displacements and strains of the structure of interest require the application of an externally applied speckle pattern to the surface of the body undergoing deformation. This speckle pattern should possess distinct, unique, non-periodic, and stable grayscale features which would act as the carrier of deformation information within the captured image data [47]. In the case of *in situ* DIC data capture during a FFF manufacturing event, repeated and consistent application of a speckle pattern to the surface of the AM test structure during the build process would be a very challenging task: it would be impossible to apply a speckle pattern to individual layers of an AM structure during the build, without disrupting/changing the speckle pattern applied to previous layers. Additionally, the act of speckle pattern application would require the pausing of the manufacturing process, which has been shown to cause profound effects on the interlayer bonding and overall structure strength of the created object. In this validation study, the methodologies devised by Spencer et al., 2021 [26], were adapted for use with small-scale manufactured structures. An amorphous neat polymer was selected as the filament of choice for this process, to minimize the potential of print-to-print variations due to differences in fiber orientation and fiber/polymer bonding [2,3,48], or degree of polymer crystallinity [5,6]. With these requirements and criteria in mind, a black semi-matte Polyethylene Terephthalate Glycol (PETG) manufactured by colorFabb [49] was selected.

The next step in the experimental process was to determine if a structure created with this filament would have a natural surface roughness capable of performing the functions of an externally applied speckle pattern. To make this determination, a rigid body displacement test was

performed, where DIC methodologies were used to measure rigid body displacements on printed specimens with and without the application of an external speckle pattern. The goal of this testing is to show equivalency between results obtained through the use of objects with and without an externally applied speckle pattern, by capturing and comparing data obtained in both instances. The two conditions (speckle-patterned surface, surface with its as-manufactured roughness) were considered equivalent with a statistical correlation greater than 95% over the rigid body displacements measured. The rigid body displacement tests were conducted using six total specimens measuring 200mm (L) x 40mm (H) x 2.5mm (W) that were printed using an Ultimaker S5 (with the specification of 240°C nozzle, 75°C print bed, and 0.15mm layer height). Three of these specimens were randomly selected for application of an external speckle pattern, shown in **Figure 35**. Externally applied speckle patterns were applied using spray paint, with a white matte base applied first to the specimen onto which a fine mist of matte black speckles were applied [50].

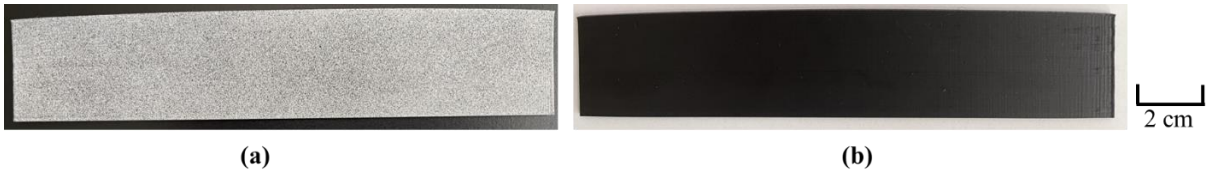

Figure 35. Rigid body test specimens: (a) with applied external speckle pattern, (b) as-manufactured surface.

Rigid body displacements were applied and measured using the apparatus shown in **Figure 36**, which provided a stable consistent platform for the test specimens. Displacements were applied in a single axial direction and measured using a micrometer dial indicator, and visual data was captured using a Mako G-503B, a 1/2.5-inch monochromatic 5-megapixel CMOS sensor camera equipped with an Edmund Optics 25mm fixed focal length lens. Utilizing a 0.5m working distance

to the test specimen, this camera and lens arrangement resulted in an as-designed total resolution of 0.0453 mm/pixel.

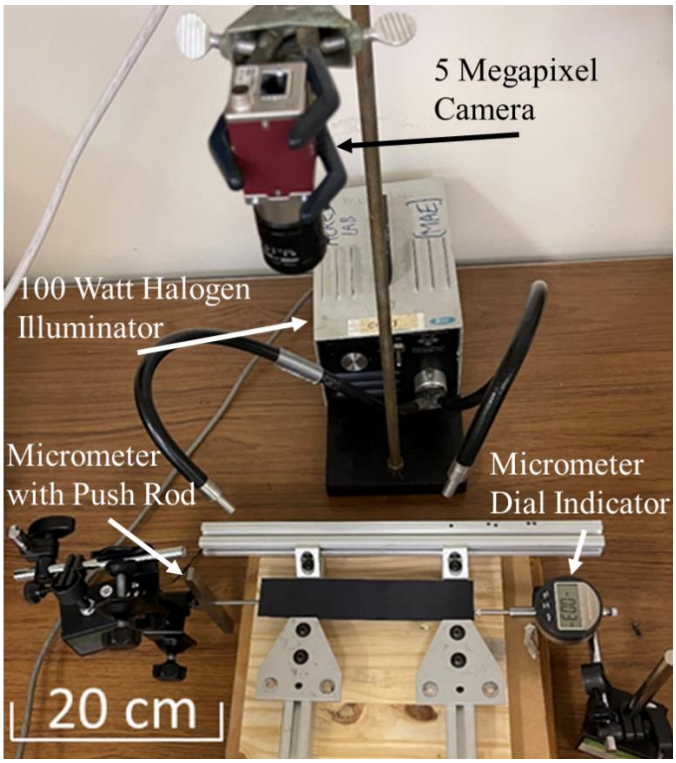

Figure 36. Experimental apparatus for rigid body displacement tests.

A total of 21 displacement measurements were applied to each of the six test specimens with a single visual image taken at every displacement condition. The DIC analysis of the captured images was performed using the commercial Correlated Solution VIC 2D-7 software, using the prescribed settings within the VIC 2D system for a minimization of uncertainty given the quality and contrast present within the reference image [51]. In this case, the subset size was set for 125 pixels, with a step size of 3 pixels. At each applied displacement, the DIC-measured displacements were averaged across the entire body of the test piece as the entire structure was undergoing uniform rigid body displacement. These values are shown in **Figure 37**, along with the results of

the statistical correlation analysis that was conducted. These results show high correlation (> 99%, well above the 95% threshold) with an average measurement error of 0.0127mm for test specimens covered by external speckle patterns, and an average experimental measurement error of 0.0318mm, when utilizing the natural surface of the test specimens. These highly correlated, and essentially equivalent, results allow us to conclude that this process and the selected filament are capable of replacing an applied speckle pattern for the DIC measurements of rigid body displacements.

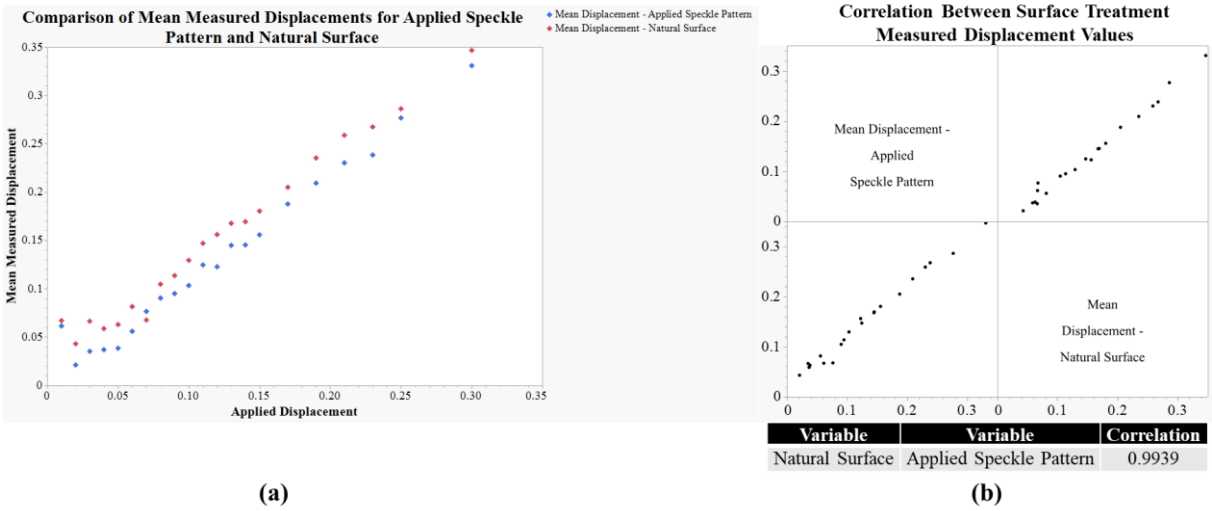

Figure 37. Mean rigid body displacement results: (a) comparison between surface treatment results, (b) statistical correlation between the displacement measurement results.

Therefore, having met our equivalence criteria between surface treatments for this particular material type and their use in supporting the execution of DIC measurements, we determined that utilization of the natural surface roughness of the test structure was sufficient to allow for the *in situ* usage of the demonstrated technique.

CHAPTER 4 - DEMONSTRATION OF AN EXPERIMENTAL PROCESS FOR THE DETERMINATION OF THE COEFFICIENT OF THERMAL EXPANSION OF ADDITIVELY MANUFACTURED STRUCTURES

Authors: Daniel L. Nelson, Santiago Mejia, Valeria La Saponara

Authors contributions: DLN designed and conducted experiments, carried out data analysis, secured funding for supplies, and wrote the document. SM assisted with the experiments. VLS advised DLN, provided equipment and laboratory space, and edited the document.

ABSTRACT

Additive Manufacturing (AM) of complex structures that are able to maximize functionality is poised to become the future of vehicle of creation for advanced vehicles, systems, and structures. A current major limiting factor in the adoption and greater use of this technology is reduced understanding of the overall macro-level mechanical/material properties within the finished products. This reduced understanding is due to the nature of the manufacturing process, especially with respect to complex geometries, where material deposition patterns within the structure of interest can vary based on the design of the body. These differing patterns of deposition can create interlayer interactions that affect the overall behavior of structure created by AM means. This study sought to demonstrate the viability of an experimental and analysis procedure, that was adapted for use with AM created structures, to determine the macro-level Coefficient of Thermal Expansion (CTE) of structures with complex geometries. Within this study, it is shown that the initial iteration of this procedure was capable of producing usable and consistent results, and that its continued refinement could prove highly useful in the advancement of AM capabilities.

Keywords: Additive Manufacturing; Extrusion-based 3D printing; Fused Filament Fabrication (FFF); Coefficient of Thermal Expansion

Nomenclature	
AM	Additive manufacturing
FFF	Fused Filament Fabrication
CTE	Coefficient of Thermal Expansion
PLA	Polylactic Acid

INTRODUCTION

As Additive Manufacturing (AM) technologies approach a fourth decade of development [77] their integration into an ever-greater variety of applications has continued to increase [30,31,78–82]. The persistent expansion of this technology is due to an extensive array of printer types and materials that can be employed to generate structures ranging from rapid prototypes to advanced structural elements [83,84]. These AM systems are able to create highly complex objects utilizing a flexible digital design and manufacture paradigms, resulting in a minimization of material and energy waste [85,86]. These factors make AM technologies a core component of the fourth industrial revolution (”industry 4.0”) that has only begun to unfold [9,10]. Despite the many benefits, however, one major drawback of this manufacturing capability continues to be the buildup of residual stresses from high deposition/melting temperatures [25,35,36]. The creation of these residual stresses is due to the nature of the manufacturing process: the layer-by-layer deposition of either hot viscous material or the deposition of material undergoing an exothermic curing reaction onto previously deposited layers results in interlayer thermal gradients. These extreme thermal gradients and swift temperature swings cause contractions within the material layers, leading to the development of interlayer stresses [19,20,24,25,37]. This phenomenon is further compounded by the conduction of heat through the solidified structure, as new melted layers are added to the body [38–40]. This heat flow and resultant

cooling events lead to an asymmetric expansion and contraction between layers of the fabricated structures. The cumulative buildup of these residual stresses within the AM body can often result in part warping, and deformation, as reported in Refs. [13,35]. The buildup of residual stresses and manifestation of the warping/deformation are primarily a thermally driven process, with the feedstock material coefficient of thermal expansion (CTE) governing the magnitude of the material response to these thermal stimuli. In order to overcome the warping and deformation events caused by these manufacturing-induced residual stresses, it is necessary to fully understand the thermomechanical properties of the as-manufactured structures. Only through this complete material understanding will it be possible to model and predict when and where the resulting warping and deformations will occur [12,14,87,88]. Thus, this understanding will allow for production teams to adjust their design strategies and/or print parameters, in an effort to offset and reduce the magnitude and overall negative effect of the induced residual stresses within the AM body. In addition, the thermomechanical performance of AM structures is highly dependent on the orientation and deposition tool path used in its creation [3,89,90]. This is especially true of structures utilizing complex geometries, or those employing fiber reinforcement within the base matrix, where the orientation and path of material deposition vary through the body, leading to differing performance within the same body to thermomechanical stimuli. The development of a macro-level understanding of the behavior of AM structures is needed if the true benefits of this manufacturing technology are to be realized within our society. Additionally, without the establishment of foundational experimental processes and procedures to derive the core structural and materials properties, it will continue to be very challenging to build capable and complete modeling and simulation capabilities for these structures.

With all of these factors in mind, the following study was undertaken to create and demonstrate a low-cost and highly accessible experimental process to derive the CTE of an as-manufactured 3D-printed test body, regardless of printer or material type. This is especially useful for AM systems that generate highly complex structural shapes assembled through the deposition of material in a variety of patterns (raster angle, infill percentage and patterns), with measurable effects on developed structural properties [91–96]. Additionally, many printers are incapable of generating viable test specimens that meet the size limitations of many standard thermomechanical analysis systems. This research effort was developed to expand the range of test specimen sizes and shapes that could be easily assessed without the need to resort to cutting/trimming of structures that can prove costly and destructive to the specimens of interest. Overall, this study examines the viability of an experimental method and analysis technique demonstrated on 1) traditionally manufactured aluminum samples, and 3D-printed neat thermoplastic polymer test specimens, comprised of Polylactic Acid (PLA). This study evaluated the viability of this technique on AM simple shapes, as well as the use of this technique on more complex structural shapes.

EXPERIMENTAL METHODS

In this study, the experimental program was adapted from techniques originally developed at Oak Ridge National Lab (ORNL), described in Ref. [97]. Within this experimental setup, strain sensing (strain gages) and thermal sensing devices (thermocouples) are attached to dissimilar materials, one acting as the reference sample and the other the unknown test specimen. Those two materials are subjected to temperature cycling within a controlled environmental chamber, for the purpose of experimentally deriving the unknown CTE value of the test specimen. A visual depiction of the setup is in **Figure 38**. In addition to the thermal sensing

devices attached to the reference sample and test specimen, a hygrometer/thermometer sensor (Mocreo ST3) was utilized during the experiments to monitor the ambient environmental conditions within the controlled environmental chamber.

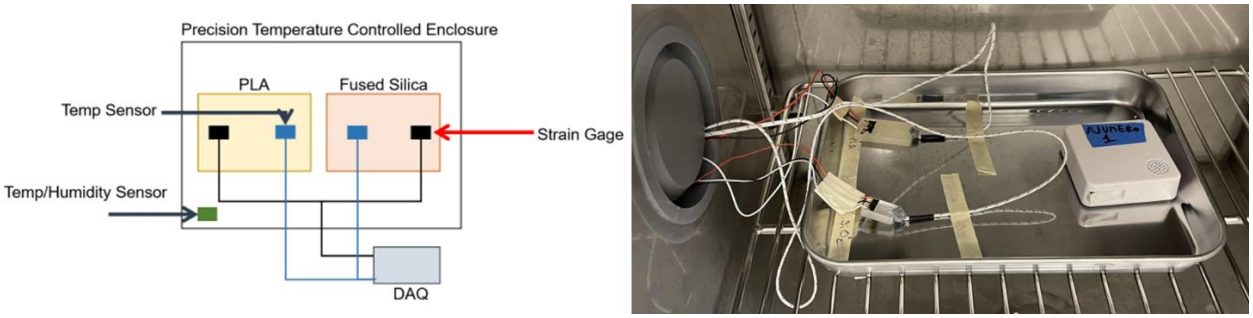

Figure 38. Experimental setup for the determination of the CTE.

Within this experimental construct, we attempted to measure the strain induced within the unknown sample through the expansion of that sample, as it is subjected to a repeatable ambient thermal profile. Given the fact that the strain sensing devices themselves are subjected to the sample's thermal variations, it becomes necessary to understand and remove the thermal expansion effects of the strain gages. The reason for such removal was to isolate the strain values associated with only the sample and specimen of interest. To accomplish this, identical type and model strain gages of the two samples were connected to each other in a quarter Wheatstone bridge configuration (specifically a quarter Wheatstone bridge configuration II, as described within Ref. [98]). This quarter bridge configuration allowed for a simultaneous isolated uniaxial strain measurement for each of the two samples, with the thermal effects of the strain gages themselves removed.

To induce expansion events within our samples, it was necessary to create a repeatable thermal profile within the environmental chamber. In this case, the available Tenney T2

environmental chamber [99] was used. In the chamber, all samples and specimens were subjected to the same pre-programmed thermal profile. The goal of the selected thermal profile was to induce a thermal expansion event within the samples under investigation, while operating within any known temperature limits of the equipment and materials used. For the experimentation conducted within this study, we wanted to keep the maximum temperature within the chamber below 55°C for two reasons: avoid the published temperature limit of the Mocreo ST3 monitoring sensor (60°C), and remain below the published glass transition temperature of the PLA thermoplastic utilized (published value of 55°C). The steps below detail the thermal profile that was executed for all samples and specimens:

1. 10 min cold soak at 15°C (strain gage calibration is conducted at the end of this stage)
2. Ramp from 15 – 55°C
3. Hold for 2 min at 55°C

The next action was the validation of this experimental procedure. To accomplish this task, a traditionally machined aluminum 6061 sample was used as the test specimen, while fused silica (SiO2) was used as the reference sample. In fact, aluminum 6061 was selected as it possesses a well-known CTE value with well-documented thermal strain response curves within the thermal evaluation range shown previously, while fused silica possesses a well-documented low average CTE value, $0.57\frac{\mu m}{m \times K}$, with a highly linear response within the temperature range examined (15-55°C), [100]. An external strain gage (Omega SGT-3BH/350-XY41) was installed onto the surface of each of the two test specimens and reference sample. The strain gages were installed by following Omega Engineering's user manual as in Ref. [101] (steps 1-5), using acetone as the de-greasing solvent and replacing the Teflon mounting flap with Mylar adhesive tape. Also, liquid electric tape was applied to protect the wire leads soldered to the attached

strain gages. For thermal monitoring, each of the test specimens were equipped with an installed thermocouple (URBEST® K Type 800C). In the case of the fused silica reference sample, the thermocouple was inserted into a ~1.5 cm hole bored into the body, and held in place using autoclave adhesive, while the Aluminum 6061 sample utilized an external thermocouple held in place with autoclave adhesive. This setup is in **Figure 39**. The resulting temperature and strain data captured through the course of this particular experiment and all following CTE derivation experiments were analyzed using the procedures described within [102] to determine the CTE values of the specimens tested.

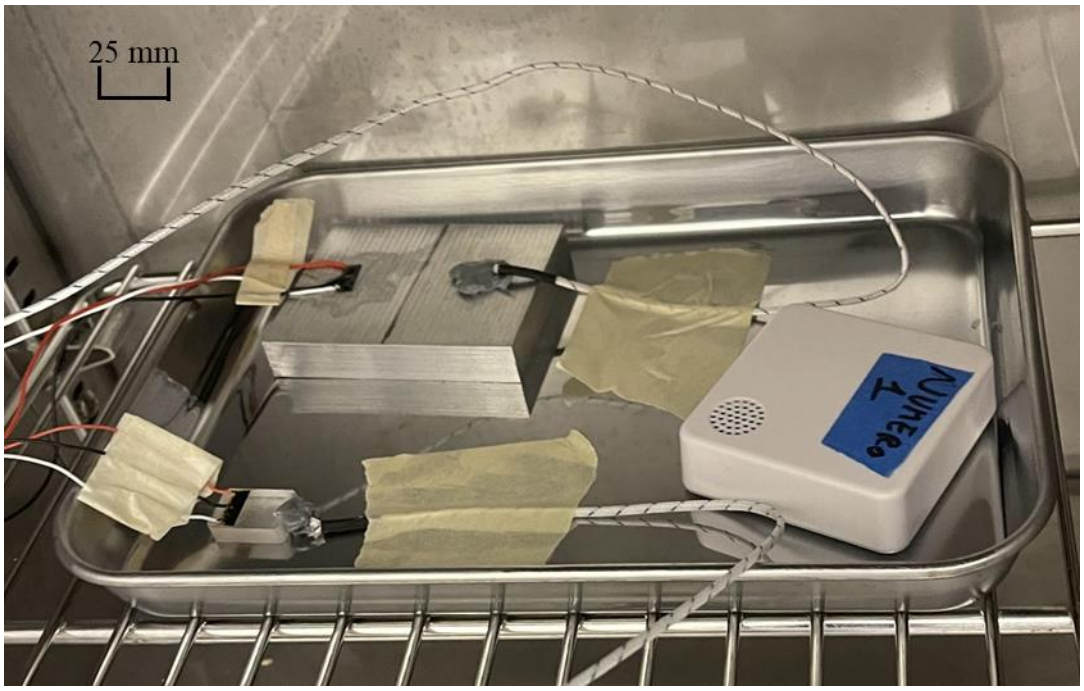

Figure 39. Aluminum 6061 CTE validation test run experimental setup.

After the procedure validation was completed, the first of the AM structural elements that were analyzed was a simple shape FFF thermoplastic test body, composed of PLA generated as a solid (100% infill) rectangular block. For this experimental effort, we created seven (7) 3D-

printed test specimens, using 3DXTECH's EcoMax Natural Color Polylactic Acid (PLA) semicrystalline Thermoplastic Polymer [28]. This particular filament was chosen for use in the research effort due to 1) the purity of the PLA filament (low levels of additives with >99% PLA concentration resin) [103], 2) the fact that PLA is the most common filament for use in FFF printers with applications across many engineering disciplines [104]. This ensures that the data obtained through this effort will be useful and applicable to a wide range of AM technologies. All seven (7) of the simple rectangular block 3D-printed test specimens were produced using the same Ultimaker 2+ printer, and were manufactured using the same spool of PLA filament. Each test specimen measured 40 x 20 x 5 mm^3, and was constructed as a solid body with 100% infill.

Once manufactured, an external strain gage was installed onto the surface of each of the simple shape PLA test specimens. The strain gages were installed using the same process and materials as those used to install gages onto the aluminum samples, with a ~1.5 cm hole bored into the test specimens to install the thermocouples, and autoclave adhesive. An example of the final prepared PLA and SiO_2 test specimens are shown in **Figure 40.**

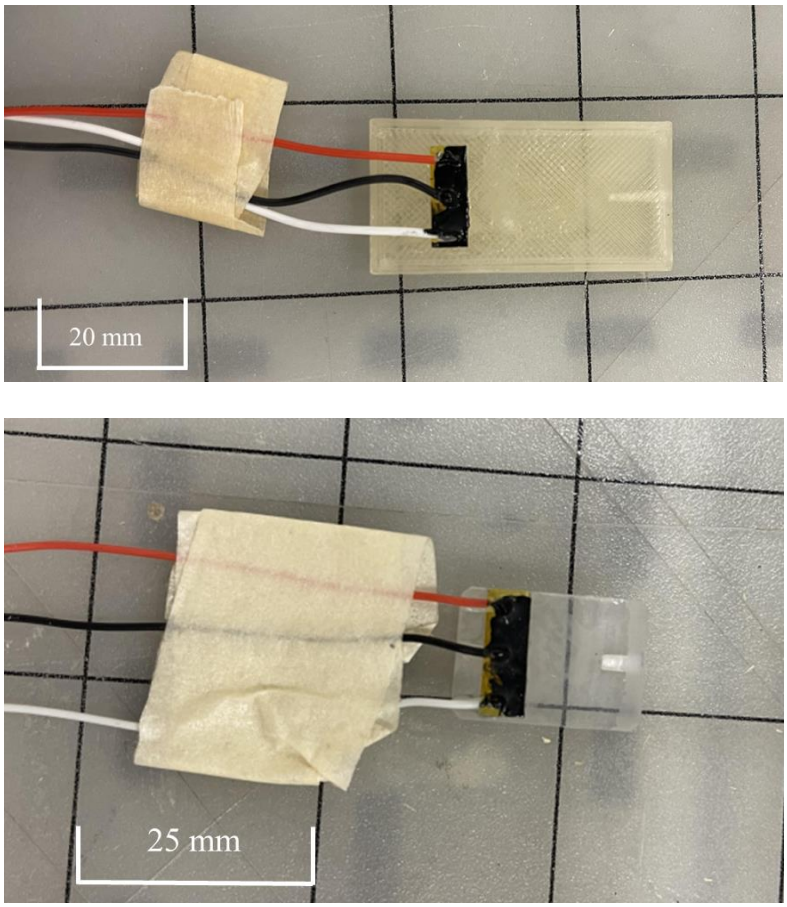

Figure 40. (Top) PLA and (bottom) silica test specimens with strain gage attached and thermocouple bore hole.

Overall, six (6) simple shape PLA specimens were successfully tested against a single silica reference sample within the environmental chamber (one strain gage failure was detected for one sample during pre-test checkout, causing the removal of that test specimen from evaluation).

The next phase of the study was to demonstrate this same process on structures that are larger and possess more complex geometries. To accomplish this, five (5) test specimens in the shape of a Möbius strip were created using 3DXTECH's EcoMax Natural Color PLA, using the same spool of PLA, and with the same Ultimaker S5 printer. This shape was selected in order to determine the overall utility of the described processes on a body with an outer surface made up

of continuous curvature in two axes, shown in **Figure 41** with strain gage attached. For each of the complex test specimens, and the reference SiO_2 sample used for this effort, an external strain gage (Micro-Measurements WK-06-250BG-350) was attached to the surface of the materials tested utilizing the previously described techniques. Additionally, each specimen utilized an external thermocouple held in place with autoclave adhesive. Overall, four (4) of these complex shape test specimens were evaluated against a single silica reference sample within the environmental chamber (one strain gage failed and caused the removal of that specimen from evaluation).

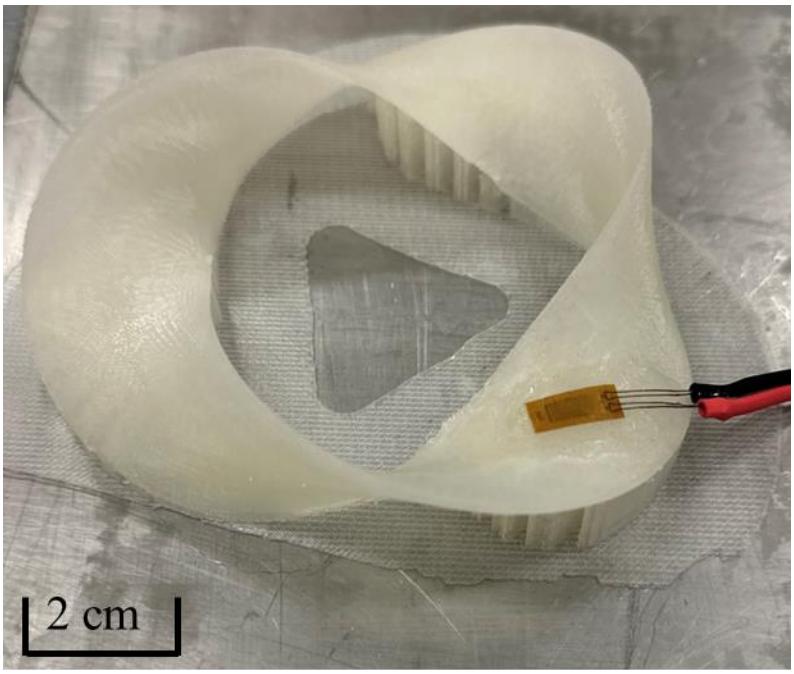

Figure 41. Complex PLA shape (Möbius strip), with strain gage attached.

EXPERIMENTAL CTE DETERMINATION - RESULTS

Over the course of this research study, aluminum samples were evaluated as a way to validate the experimental construct, process functionality, and analysis procedures utilized.

Three (3) total aluminum samples were evaluated (two (2) using the Omega SGT-3BH/350-XY41 strain gage and one (1) using the Micro-Measurements WK-06-250BG-350 strain gage). The experimentally derived CTE value for the aluminum reference samples, as well as the PLA test samples (simple and complex shapes), was found by examining the linear response region of the measured strain versus temperature data captured during experimentation, and utilizing the following equation [102]:

$$\boldsymbol{\alpha_s - \alpha_r = \frac{(\varepsilon_s - \varepsilon_r)}{\Delta T} = \frac{\varepsilon_m}{\Delta T}} \quad (1)$$

where $\boldsymbol{\alpha_{s/r}}$ is the CTE of the sample and reference material respectively, $\boldsymbol{\alpha_r} = 0.57\ \boldsymbol{\frac{\mu m}{m \times K}}$, $\boldsymbol{\varepsilon_{s/r}}$ is the strain of the sample and reference material respectively, $\boldsymbol{\varepsilon_m}$ is the measured strain output of the Wheatstone bridge, $\boldsymbol{\Delta T}$ is change in temperature during the evaluation period.

For the two (2) aluminum samples tested using the Omega SGT-3BH/350-XY41 strain gage, the median CTE value was found to be 23.363 $\frac{\mu m}{m \times K}$. The aluminum sample tested using the Micro-Measurements WK-06-250BG-350 strain gage produced a calculated CTE value of 22.96 $\frac{\mu m}{m \times K}$. Both of these experimental results correspond very well to the published CTE value of aluminum 6061 at 23.6 $\frac{\mu m}{m \times K}$ [105]. Use of this analysis provides an overall error rate of 1.0% for the Omega SGT-3BH/350-XY41 strain gage setup, and an error rate of 2.9% for the Micro-Measurements WK-06-250BG-350 strain gage setup. These results provided confidence in the validity of the overall experimental construct, and allowed us to proceed forward with the determination of the unknow PLA CTE values.

Overall, the data obtained through the experimental conduct was found to be consistent amongst the six (6) simple shape PLA test specimens that underwent testing. By assessing each

simple shape test specimen independently and determining a CTE value for each test run it is possible to generate the global median CTE value for the simple shape PLA specimens which is computed to be 73.11 $\frac{\mu m}{m \times K}$. For the complex shape PLA test specimens, the data obtained from the testing of the four (4) viable candidate structures also produced consistent results amongst the specimens evaluated. In the case of the complex shape PLA test specimens the experimental median CTE value calculated was found to be 68.66 $\frac{\mu m}{m \times K}$. In addition to the dissimilar CTE evaluation conducted, PLA test specimens comprised of using 3DXTECH's EcoMax Natural Color PLA were subjected to a material evaluation conducted at Texas A&M University (TAMU), under the advising of Dr. Anastasia Muliana, using a TA Instruments Q400 Thermomechanical Analyzer. This dedicated independent testing found the experimental median CTE value of the PLA specimens to be 83.42 $\frac{\mu m}{m \times K}$. There are many factors that could lead to the differences found in this data: slight differences among the individual strain gages, causing strain variability, thermal measurement accuracy, macro-scale thermomechanical interlayer interactions, and environmental differences during each measurement and during the manufacturing process (variations in humidity – hygrothermal effects), [97].

Figure 42 shows the individual test specimen calculated CTE values along with the variation in the results obtained with respect to each experimental method. Overall, the variation in experimental results between the two methods appears to produce slightly lower results than those results produced by the TAMU Thermomechanical Analyzer.

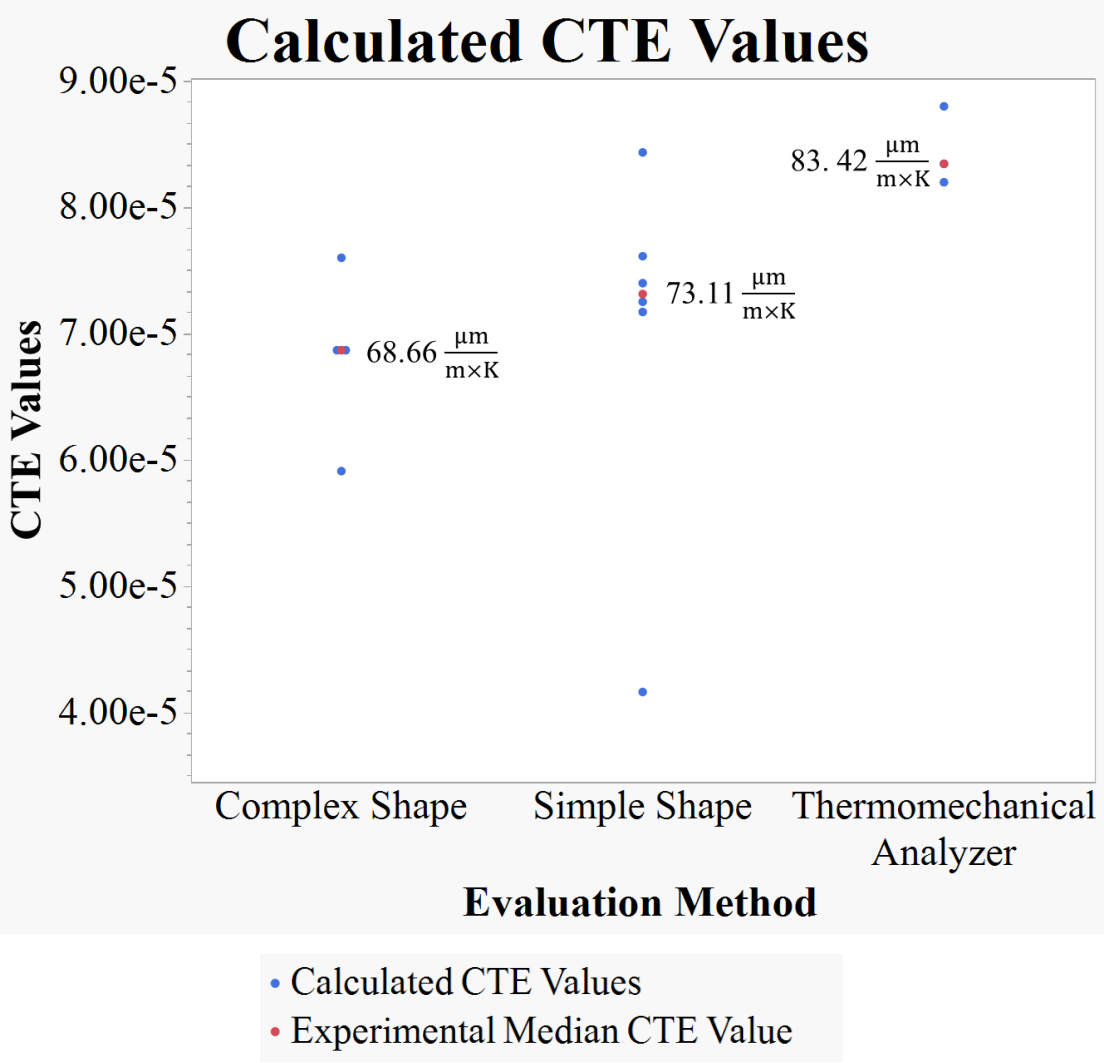

Figure 42. Experimental data variation as a function of experimental methodology.

We can further analyze these data using non-parametric statistical tests to determine if there is a significant difference in the location of the distributions for each examination methodology. This will help us to conclude whether calculated CTE values differ based on examination type. Through the use of a Kruskal-Wallis Test it is possible to show, given our experimental samples, that there is no statistically significant difference in the locations of the CTE value distributions obtained. This further supports the use of the experimental process demonstrated for use AM polymer structures.

CONCLUSIONS

The CTE determination technique utilized within this study showed an outstanding ability to generate useful and consistent mechanical properties from AM polymer structures of both simplistic and complex geometries. Specifically, the ability to utilize as-manufactured structures comprised of complex geometries to determine the macro-scale CTE behavior of the overall body is of great importance to researchers pursuing the advancement of AM technologies, and practitioners utilizing these technologies. This is especially true when employing fiber-reinforced base materials within an AM construct. Issues associated with fiber-matrix and bead-bead bonding, as well as orientation differences throughout the body, can lead to large unknowns with respect to the overall macro-scale mechanical properties of structures created with these AM processes and materials [12]. A process such as what we described within this article is a low-cost and easily repeatable method that can measure the CTE behavior of the as-built structure.

The processes and procedures presented were intended to demonstrate the overall viability of this experimental construct for use in AM structures, but its formalized use to derive material properties for structural design and model creation would require additional refinement. To better refine the techniques described within this document, a more in-depth follow-on study is recommended. This study should consist of a statistically relevant number additively manufactured bodies whose CTE values can be determined. The nature of the AM process (from environmental print-to-print variations) can result in a high variation in the macro-scale material and structural properties of the parts produced [106,107] requiring the evaluation of multiple test specimens. Such a study should explore the effect of printing parameters and strain gage placement on the body of the test specimen to the CTE values obtained. This would lead to a

greater understanding of the effect (if one exists) of the manufacturing parameters employed on the expression of a critical material/mechanical property of the AM structure of interest.

If one were to work to employ this CTE analysis technique in practice, on an unknown test structure, it would be recommended to place multiple strain sensing devices at various locations on the surface of the body, or at positions of high interest. This would allow for a more comprehensive determination of the CTE value of the overall structure or region of interest for a given design. Use of multiple sensing devices on each specimen analyzed would provide for a statistically relevant determination to be made on the CTE value obtained. This is especially true of AM structures that possess complex geometries, where the orientation of the material deposition would locally vary. Additionally, use of this technique would be dependent on the formulation and determination of the best possible process for attaching strain sensing devices on the particular body/material composition of interest.

Acknowledgements

The authors would like to acknowledge the support received from the Defense Innovation Unit (DIU), UC Davis Engineering and Student Design Center (Jose Mojica and Sherry Batin), UC Davis Craft Center (Jared Tolla and Sanne Stark Fetting), USAF Research Lab (Mr. Andrew Abbott, Mr. Tyler Lesthaeghe, Dr. Craig Przybyla, Dr. Lorianne Groo, and Dr. Eric Lindgren), Dr. David Slaughter, Dr. Anastasia Muliana, Aryabhat Darnal, and the members (Nickolas Loftus) of the UC Davis Advanced Composites Research, Engineering and Science (ACRES) laboratory who provided critical support and expertise during the development of this study.

CHAPTER 5 – CONCLUSIONS

The research, analysis, and conclusions within this PhD dissertation describe in detail:

1) a novel experimental and analysis construct to map and quantify the surface displacements resultant from manufacturing-induced residual stresses that can be utilized by researchers and manufacturers alike, to generate a deeper understanding of the warping/deformation behavior of a particular filament material or manufacturing system;

2) the adaptation of a low-overhead methodology able to accommodate AM samples of a variety of sizes and manufacturing systems, to quickly and capably derive its CTE.

With respect to the development of this novel process, this research effort has shown that it is possible to install an *in situ* DIC remote measurement capability able to document full-field displacements of a small-scale AM structure during the entirety of the manufacturing process. This capability was able to deliver data products that documented:

1) the spatial and temporal temperature flow on any point of the surface of a FFF structure during its print process;

2) the spatial and temporal material displacements for the entirety of the surface imaged, caused by these temperature gradients.

These data products provide insight into the manifestation of manufacturing-induced residual stresses, allowing for the exploration of the deformation effects and interactions resultant from a range of print parameter factors. This explicit ability to determine the singular and combined effects of discrete manufacturing parameters will empower users of this technology to tailor the manufacturing processes employed to best balance the equities of production throughput, production accuracy, and material selection. Additionally, this work has the potential to greatly

empower researchers to overcome the previously stated shortcomings in the existing numerical and analytical AM modeling capabilities. The data outputs of this developed construct can be utilized to generate experimentally-based boundary conditions, specifically actual displacement and temperature values. These boundary conditions can provide a method to develop and validate more capable and complete modelling capabilities. Finally, the usage of this experimental construct is not solely limited to neat polymer filaments employed within FFF manufacturing systems. For the purpose of initially devising and validating the data capture and analysis techniques described within this dissertation, I restricted myself to the use of a neat amorphous polymer filament, to avoid any potential confounding effects that could be caused by crystallization or fiber/matrix interactions. Now that the experimental and analytical methodologies have been developed and demonstrated, it is entirely appropriate that the use of this construct be expanded, and employed in the assessment of ever more complex and structurally significant filament formulations (high strength semi-crystalline polymers such as Polyether ether ketone (PEEK) and Polyether ketone ketone (PEKK) in addition to the inclusion of chopped or continuous fibers).

In addition to the work accomplished here, my dissertation also provided an in-depth presentation of a low-cost process to capably derive the CTE of AM structures. This effort concentrated on the determination of a key macroscale material property of as-manufactured 3D printed test specimens. This effort proved to be highly successful in providing a repeatable standardized methodology, to accurately derive a material property that is critical to understanding both the behavior of the structure during the manufacturing process, as well as the performance of the finished part during its operational life cycle. This provides the ability to develop a greater understanding of the overall thermomechanical behavior of a given AM

structure. This methodology proved robust and flexible enough for viable results on metallic- and polymer-based structures, regardless of the complexity of design. By producing a series of test specimens and subjecting them to the experimental and analysis methodology described, it is possible to build an understanding of a newly formulated AM mixture, to better inform design, manufacturing, and employment choices.

Overall, the research detailed within this dissertation resulted in the creation of a means to obtain displacement measurement data, and provide the AM community with critical data to enable informed manufacturing and further research progress. This groundbreaking experimental and analysis construct establishes a foundational level of understanding to facilitate research efforts into the development of new advanced materials, production systems, and modeling capabilities.

REFERENCES

[1] Singh, S., Singh, G., Prakash, C., and Ramakrishna, S. “Current Status and Future Directions of Fused Filament Fabrication.” *Journal of Manufacturing Processes*, Vol. 55, 2020, pp. 288–306. https://doi.org/10.1016/J.JMAPRO.2020.04.049.

[2] Heller, B. P., Smith, D. E., and Jack, D. A. “Effects of Extrudate Swell and Nozzle Geometry on Fiber Orientation in Fused Filament Fabrication Nozzle Flow.” *Additive Manufacturing*, Vol. 12, 2016, pp. 252–264. https://doi.org/10.1016/j.addma.2016.06.005.

[3] Brenken, B., Barocio, E., Favaloro, A., Kunc, V., and Pipes, R. B. “Fused Filament Fabrication of Fiber-Reinforced Polymers: A Review.” *Additive Manufacturing*, Vol. 21, 2018, pp. 1–16. https://doi.org/10.1016/j.addma.2018.01.002.

[4] Ahmadifar, M., Benfriha, K., Shirinbayan, M., and Tcharkhtchi, A. “Additive Manufacturing of Polymer-Based Composites Using Fused Filament Fabrication (FFF): A Review.” *Applied Composite Materials*, Vol. 28, No. 5, 2021, pp. 1335–1380. https://doi.org/10.1007/s10443-021-09933-8.

[5] Vaes, D., and van Puyvelde, P. “Semi-Crystalline Feedstock for Filament-Based 3D Printing of Polymers.” *Progress in Polymer Science*, Vol. 118, No. 101411, 2021. https://doi.org/10.1016/j.progpolymsci.2021.101411.

[6] Liao, Y., Liu, C., Coppola, B., Barra, G., di Maio, L., Incarnato, L., and Lafdi, K. “Effect of Porosity and Crystallinity on 3D Printed PLA Properties.” *Polymers*, Vol. 11, No. 9, 2019. https://doi.org/10.3390/polym11091487.

[7] Spoerk, M., Sapkota, J., Weingrill, G., Fischinger, T., Arbeiter, F., and Holzer, C. “Shrinkage and Warpage Optimization of Expanded-Perlite-Filled Polypropylene Composites in Extrusion-Based Additive Manufacturing.” *Macromolecular Materials and Engineering*, Vol. 302, No. 10, 2017. https://doi.org/10.1002/mame.201700143.

[8] Li, J., Durandet, Y., Huang, X., Sun, G., and Ruan, D. “Additively Manufactured Fiber-Reinforced Composites: A Review of Mechanical Behavior and Opportunities.” *Journal of Materials Science & Technology*, Vol. 119, 2022, pp. 219–244. https://doi.org/10.1016/J.JMST.2021.11.063.

[9] Zhang, C., Chen, Y., Chen, H., and Chong, D. “Industry 4.0 and Its Implementation: A Review.” *Information Systems Frontiers*, 2021. https://doi.org/10.1007/s10796-021-10153-5.

[10] Haleem, A., and Javaid, M. “Additive Manufacturing Applications in Industry 4.0: A Review.” *Journal of Industrial Integration and Management*, Vol. 04, No. 04, 2019, p. 1930001. https://doi.org/10.1142/S2424862219300011.

[11] Pal, A. K., Mohanty, A. K., and Misra, M. “Additive Manufacturing Technology of Polymeric Materials for Customized Products: Recent Developments and Future Prospective.” *RSC Advances*, Vol. 11, No. 58, 2021, pp. 36398–36438. https://doi.org/10.1039/D1RA04060J.

[12] Papon, E. A., and Haque, A. “Review on Process Model, Structure-Property Relationship of Composites and Future Needs in Fused Filament Fabrication.” *Journal of Reinforced Plastics and Composites*, Vol. 39, Nos. 19–20, 2020, pp. 758–789. https://doi.org/10.1177/0731684420929757.

[13] Armillotta, A., Bellotti, M., and Cavallaro, M. “Warpage of FDM Parts: Experimental Tests and Analytic Model.” *Robotics and Computer-Integrated Manufacturing*, Vol. 50, 2018, pp. 140–152. https://doi.org/10.1016/j.rcim.2017.09.007.

[14] Sreejith, P., Kannan, K., and Rajagopal, K. “A Thermodynamic Framework for Additive Manufacturing, Using Amorphous Polymers, Capable of Predicting Residual Stress, Warpage and Shrinkage.” *International Journal of Engineering Science*, Vol. 159, 2021, p. 103412. https://doi.org/10.1016/j.ijengsci.2020.103412.

[15] Xia, H., Lu, J., Dabiri, S., and Tryggvason, G. “Fully Resolved Numerical Simulations of Fused Deposition Modeling. Part I: Fluid Flow.” *Rapid Prototyping Journal*, Vol. 24, No. 2, 2018, pp. 463–476. https://doi.org/10.1108/RPJ-12-2016-0217.

[16] Xia, H., Lu, J., and Tryggvason, G. “Fully Resolved Numerical Simulations of Fused Deposition Modeling. Part II – Solidification, Residual Stresses and Modeling of the Nozzle.” *Rapid Prototyping Journal*, Vol. 24, No. 6, 2018, pp. 973–987. https://doi.org/10.1108/RPJ-11-2017-0233.

[17] Zhang, Y., and Chou, K. “A Parametric Study of Part Distortions in Fused Deposition Modelling Using Three-Dimensional Finite Element Analysis.” *The Journal of Engineering Manufacture*, Vol. 222, No. 8, 2008, pp. 959–968. https://doi.org/10.1243/09544054JEM990.

[18] Wang, T.-M., Xi, J.-T., and Jin, Y. “A Model Research for Prototype Warp Deformation in the FDM Process.” *International Journal of Advanced Manufacturing Technology*, Vol. 33, No. 1097, 2007. https://doi.org/10.1007/s00170-006-0878-7.

[19] Watanabe, N., Shofner, M. L., Treat, N., and Rosen, D. W. A MODEL FOR RESIDUAL STRESS AND PART WARPAGE PREDICTION IN MATERIAL EXTRUSION WITH APPLICATION TO POLYPROPYLENE. 2016.

[20] Moumen, A. el, Tarfaoui, & M., and Lafdi, & K. “Modelling of the Temperature and Residual Stress Fields during 3D Printing of Polymer Composites.” *The International*

Journal of Advanced Manufacturing Technology, Vol. 104, 2019, pp. 1661–1676. https://doi.org/10.1007/s00170-019-03965-y.

[21] Kantaros, A., and Karalekas, D. "Fiber Bragg Grating Based Investigation of Residual Strains in ABS Parts Fabricated by Fused Deposition Modeling Process." *Materials & Design*, Vol. 50, 2013, pp. 44–50. https://doi.org/10.1016/j.matdes.2013.02.067.

[22] Li, J., Xie, H., and Ma, K. "In-Situ Monitoring of the Deformation during Fused Deposition Modeling Process Using CGS Method." *Polymer Testing*, Vol. 76, 2019, pp. 166–172. https://doi.org/10.1016/j.polymertesting.2019.03.030.

[23] Li, F., Yu, Z., Yang, Z., and Shen, X. "Real-Time Distortion Monitoring during Fused Deposition Modeling via Acoustic Emission." *Structural Health Monitoring*, Vol. 19, No. 2, 2020, pp. 412–423. https://doi.org/10.1177/1475921719849700.

[24] Zhang, W., Wu, A. S., Sun, J., Quan, Z., Gu, B., Sun, B., Cotton, C., Heider, D., and Chou, T. W. "Characterization of Residual Stress and Deformation in Additively Manufactured ABS Polymer and Composite Specimens." *Composites Science and Technology*, Vol. 150, 2017, pp. 102–110. https://doi.org/10.1016/j.compscitech.2017.07.017.

[25] Casavola, C., Cazzato, A., Moramarco, V., and Pappalettera, G. "Residual Stress Measurement in Fused Deposition Modelling Parts." *Polymer Testing*, Vol. 58, 2017, pp. 249–255. https://doi.org/10.1016/j.polymertesting.2017.01.003.

[26] Spencer, R., Hassen, A. A., Baba, J., Lindahl, J., Love, L., Kunc, V., Babu, S., and Vaidya, U. "An Innovative Digital Image Correlation Technique for In-Situ Process Monitoring of Composite Structures in Large Scale Additive Manufacturing." *Composite Structures*, Vol. 276, No. 114545, 2021. https://doi.org/10.1016/j.compstruct.2021.114545.

[27] ASTM International. "D6272 − 17 Standard Test Method for Flexural Properties of Unreinforced and Reinforced Plastics and Electrical Insulating Materials by Four-Point Bending 1." 2020. https://doi.org/10.1520/D6272-17E01.

[28] 3DXTech Advanced Materials. PLA-TDS-V03. *ECOMAX PLA 3D Printing Filament Technical Data Sheet*. https://www.3dxtech.com/. Accessed Dec. 1, 2021.

[29] Emile S. Greenhalgh. *Failure Analysis and Fractography of Polymer Composites*. Woodhead Publishing Limited, 2009.

[30] Park, S., and Fu, K. (Kelvin). "Polymer-Based Filament Feedstock for Additive Manufacturing." *Composites Science and Technology*, Vol. 213, 2021, p. 108876. https://doi.org/10.1016/J.COMPSCITECH.2021.108876.

[31] Hassanin, H., Sheikholeslami, G., Sareh, P., and Ishaq, R. B. “Microadditive Manufacturing Technologies of 3D Microelectromechanical Systems.” *Advanced Engineering Materials*, Vol. 23, No. 12, 2021, p. 2100422. https://doi.org/10.1002/adem.202100422.

[32] Nikitakos, N., Dagkinis, I., Papachristos, D., Georgantis, G., and Kostidi, E. Economics in 3D Printing. In *3D Printing: Applications in Medicine and Surgery*, Elsevier, 2020, pp. 85–95.

[33] Kumar, S., Singh, R., Singh, T., and Batish, A. “Fused Filament Fabrication: A Comprehensive Review.” *Journal of Thermoplastic Composite Materials*, 2020. https://doi.org/10.1177/0892705720970629.

[34] Dey, A., Roan Eagle, I. N., and Yodo, N. “A Review on Filament Materials for Fused Filament Fabrication.” *Journal of Manufacturing and Materials Processing*, Vol. 5, No. 3, 2021, p. 69. https://doi.org/10.3390/jmmp5030069.

[35] Wijnen, B., Sanders, P., and Pearce, J. M. “Improved Model and Experimental Validation of Deformation in Fused Filament Fabrication of Polylactic Acid.” *Progress in Additive Manufacturing*, Vol. 3, 2018, pp. 193–203. https://doi.org/10.1007/s40964-018-0052-4.

[36] Chen, L., He, Y., Yang, Y., Niu, S., and Ren, H. “The Research Status and Development Trend of Additive Manufacturing Technology.” *The International Journal of Advanced Manufacturing Technology*, Vol. 89, Nos. 9–12, 2017, pp. 3651–3660. https://doi.org/10.1007/s00170-016-9335-4.

[37] Ramos, N., Mittermeier, C., and Kiendl, J. “Experimental and Numerical Investigations on Heat Transfer in Fused Filament Fabrication 3D-Printed Specimens.” *International Journal of Advanced Manufacturing Technology*, Vol. 118, Nos. 5–6, 2022, pp. 1367–1381. https://doi.org/10.1007/S00170-021-07760-6.

[38] Fitzharris, E. R., Watanabe, N., Rosen, D. W., and Shofner, M. L. “Effects of Material Properties on Warpage in Fused Deposition Modeling Parts.” *International Journal of Advanced Manufacturing Technology*, 2018. https://doi.org/10.1007/s00170-017-1340-8.

[39] Dinwiddie, R. B., Kunc, V., Lindal, J. M., Post, B., Smith, R. J., Love, L., and Duty, C. E. Infrared Imaging of the Polymer 3D-Printing Process. No. 9105, F. P. Colbert and S.-J. (Tony) Hsieh, eds., 2014, pp. 910502.

[40] Costa, S. F., Duarte, F. M., and Covas, J. A. “Thermal Conditions Affecting Heat Transfer in FDM/FFE: A Contribution towards the Numerical Modelling of the Process: This Paper Investigates Convection, Conduction and Radiation Phenomena in the Filament Deposition Process.” *Virtual and Physical Prototyping*, Vol. 10, No. 1, 2015, pp. 35–46. https://doi.org/10.1080/17452759.2014.984042.

[41] Fu, Y., Downey, A., Yuan, L., Pratt, A., and Balogun, Y. “In Situ Monitoring for Fused Filament Fabrication Process: A Review.” *Additive Manufacturing*, Vol. 38, 2021, p. 101749. https://doi.org/10.1016/j.addma.2020.101749.

[42] Nascimento, M., Inácio, P., Paixão, T., Camacho, E., Novais, S., Santos, T., Fernandes, F., and Pinto, J. “Embedded Fiber Sensors to Monitor Temperature and Strain of Polymeric Parts Fabricated by Additive Manufacturing and Reinforced with NiTi Wires.” *Sensors*, Vol. 20, No. 4, 2020, p. 1122. https://doi.org/10.3390/s20041122.

[43] Schreier, H., Orteu, J.-J., and Sutton, M. A. *Image Correlation for Shape, Motion and Deformation Measurements*. Springer US, Boston, MA, 2009.

[44] Holzmond, O., and Li, X. “In Situ Real Time Defect Detection of 3D Printed Parts.” *Additive Manufacturing*, Vol. 17, 2017, pp. 135–142. https://doi.org/10.1016/j.addma.2017.08.003.

[45] Saluja, A., Xie, J., and Fayazbakhsh, K. “A Closed-Loop in-Process Warping Detection System for Fused Filament Fabrication Using Convolutional Neural Networks.” *Journal of Manufacturing Processes*, Vol. 58, 2020, pp. 407–415. https://doi.org/10.1016/j.jmapro.2020.08.036.

[46] Weisz-Patrault, D., Margerit, P., and Constantinescu, A. “Residual Stresses in Thin Walled-Structures Manufactured by Directed Energy Deposition: In-Situ Measurements, Fast Thermo-Mechanical Simulation and Buckling.” *Additive Manufacturing*, Vol. 56, 2022, p. 102903. https://doi.org/10.1016/j.addma.2022.102903.

[47] Dong, Y. L., and Pan, B. “A Review of Speckle Pattern Fabrication and Assessment for Digital Image Correlation.” *Experimental Mechanics*, Vol. 57, No. 8, 2017, pp. 1161–1181. https://doi.org/10.1007/s11340-017-0283-1.

[48] Ahmadifar, M., Benfriha, · K, Shirinbayan, · M, and Tcharkhtchi, · A. “Additive Manufacturing of Polymer-Based Composites Using Fused Filament Fabrication (FFF): A Review.” *Applied Composite Materials*, 2021. https://doi.org/10.1007/s10443-021-09933-8.

[49] Colorfabb. *TDS_ColorFabb_PETG_Economy*. 2017.

[50] Correlated Solutions. *Speckle Pattern Fundamentals - Application Note*. 2021.

[51] Correlated Solutions. *Vic-2D Software Manual*. 2021.

[52] nScript. *2021-3Dn-Technical Overview*. 2021.

[53] Khoo, S. W., Karuppanan, S., and Tan, C. S. A Review of Surface Deformation and Strain Measurement Using Two-Dimensional Digital Image Correlation. *Metrology and Measurement Systems*. 3. Volume 23, 461–480.

[54] Dracast. *LED500 PLUS SERIES TDS*. 2015.

[55] Saouma, V., and Cintron, R. *Strain Measurements with Digital Image Correlation System Vic-2D Probabilistic and Performance Based Assessment of Concrete Dams (PPACD) View Project Fragility Analysis of Concrete Dams View Project*. Boulder, CO, 2008.

[56] Bigger, R., Blaysat, B., Boo, C., Grewer, M., Hu, J., Jones, A., Klein, M., Raghavan, K., Reu, P., Schmidt, T., Siebert, T., Simenson, M., Turner, D., Vieira, A., and Weikert, T. *A Good Practices Guide for Digital Image Correlation*. 2018.

[57] Carrete, I. A., Bermudez, D., Aguirre, C., Alvarez-Primo, F. A., Anil-Kumar, S., Chinolla, P., Gamboa, M., Gonzalez, S. A., Heredia, H. E., Hernandez, A. M., Levario, E., Lindquist, J. R., Luna, V. C., Martinez, L. M., Mendez, V. E., Slager, J. J., Ugarte-Sanchez, L., Urquidi, Y. A., Zamora, A., and Roberson, D. A. "Failure Analysis of Additively Manufactured Polyester Test Specimens Exposed to Various Liquid Media." *Journal of Failure Analysis and Prevention*, Vol. 19, No. 2, 2019, pp. 418–430. https://doi.org/10.1007/s11668-019-00614-0.

[58] Fang, L., Yan, Y., Agarwal, O., Kang, S. H., Yao, S., and Seppala, J. E. "Effects of Environmental Temperature and Humidity on the Geometry and Strength of Polycarbonate Specimens Prepared by Fused Filament Fabrication." *Materials*, Vol. 13, No. 19, 2020, pp. 1–16. https://doi.org/10.3390/ma13194414.

[59] Elitech. *Tlog Series Temperature Data Logger User Manual*.

[60] Brereton, R. G. "ANOVA Tables and Statistical Significance of Models." *Journal of Chemometrics*, Vol. 33, No. 3, 2019, p. e3019. https://doi.org/10.1002/cem.3019.

[61] Kutner, M. H., Nachtsheim, C., Neter, J., and Li, W. *Applied Linear Statistical Models*. 2005.

[62] Hull, C. W., and Arcadia, C. United States Patent (19) Hull (54) (75) (73) 21) 22 (51) 52) (58) (56) APPARATUS FOR PRODUCTION OF THREE-DMENSONAL OBJECTS BY STEREOLITHOGRAPHY, , 1984.

[63] Abdulhameed, O., Al-Ahmari, A., Ameen, W., and Mian, S. H. "Additive Manufacturing: Challenges, Trends, and Applications Manufacturing Processes." Vol. 11, No. 2, 2019, pp. 1–27. https://doi.org/10.1177/1687814018822880.

[64] Prashar, G., Vasudev, H., and Bhuddhi, D. “Additive Manufacturing: Expanding 3D Printing Horizon in Industry 4.0.” *International Journal on Interactive Design and Manufacturing*, 2022. https://doi.org/10.1007/s12008-022-00956-4.

[65] Godina, R., Ribeiro, I., Matos, F., Ferreira, B. T., Carvalho, H., and Peças, P. “Impact Assessment of Additive Manufacturing on Sustainable Business Models in Industry 4.0 Context.” *Sustainability (Switzerland)*, Vol. 12, No. 17, 2020. https://doi.org/10.3390/su12177066.

[66] Holmes, M. “Additive Manufacturing Continues Composites Market Growth.” *Reinforced Plastics*, Vol. 63, No. 6, 2019, pp. 296–301. https://doi.org/10.1016/j.repl.2018.12.070.

[67] Altıparmak, S. C., and Xiao, B. A Market Assessment of Additive Manufacturing Potential for the Aerospace Industry. *Journal of Manufacturing Processes*. Volume 68, 728–738.

[68] Bourell, D. L. Perspectives on Additive Manufacturing. *Annual Review of Materials Research*. Volume 46, 1–18.

[69] Srivastava, M., and Rathee, S. Additive Manufacturing: Recent Trends, Applications and Future Outlooks. *Progress in Additive Manufacturing*. 2. Volume 7, 261–287.

[70] Guo, N., and Leu, M. C. Additive Manufacturing: Technology, Applications and Research Needs. *Frontiers of Mechanical Engineering*. 3. Volume 8, 215–243.

[71] Ebnesajjad, S. Introduction to Plastics. In *Chemical Resistance of Commodity Thermoplastics*, Elsevier, 2016, pp. xiii–xxv.

[72] Spoerk, M., Gonzalez-Gutierrez, J., Sapkota, J., Schuschnigg, S., and Holzer, C. “Effect of the Printing Bed Temperature on the Adhesion of Parts Produced by Fused Filament Fabrication.” *Plastics, Rubber and Composites*, Vol. 47, No. 1, 2018, pp. 17–24. https://doi.org/10.1080/14658011.2017.1399531.

[73] Freddi, A., Olmi, G., and Cristofolini, L. *Experimental Stress Analysis for Materials and Structures Stress Analysis Models for Developing Design Methodologies*. 2015.

[74] Bárány, T., Földes, E., and Czigány, T. “Effect of Thermal and Hygrothermal Aging on the Plane Stress Fracture Toughness of Poly(Ethylene Terephthalate) Sheets.” *Express Polymer Letters*, Vol. 1, No. 3, 2007, pp. 180–187. https://doi.org/10.3144/expresspolymlett.2007.28.

[75] Fuentes, J. M., Arrieta, M. P., Boronat, T., and Ferrándiz, S. “Effects of Steam Heat and Dry Heat Sterilization Processes on 3D Printed Commercial Polymers Printed by Fused Deposition Modeling.” 2022. https://doi.org/10.3390/polym14050855.

[76] Kováčová, M., Kozakovičová, J., Procházka, M., Janigová, I., Vysopal, M., Ivonačerničková, I. I., Krajčovič, J., and Špitalský, Z. "Novel Hybrid PETG Composites for 3D Printing." *Applied Sciences*, 2020. https://doi.org/10.3390/app10093062.

[77] Wohlers, T., and Gornet, T. *History of Additive Manufacturing*. 2016.

[78] Besnea, D., Dinu, E., Moraru, E., Spanu, A., Rizescu, C., and Constantin, V. "Experimental Researches Regarding the Manufacturing of New Thermoplastic Materials Used in Additive Technologies." *Materiale Plastice*, Vol. 56, 2019, pp. 167–170.

[79] Valente, M., Sibai, A., and Sambucci, M. "Extrusion-Based Additive Manufacturing of Concrete Products: Revolutionizing and Remodeling the Construction Industry." *Journal of Composites Science*, Vol. 3, No. 3, 2019, p. 88. https://doi.org/10.3390/jcs3030088.

[80] Shakor, P., Nejadi, S., Paul, G., and Malek, S. "Review of Emerging Additive Manufacturing Technologies in 3D Printing of Cementitious Materials in the Construction Industry." *Frontiers in Built Environment*, Vol. 4, 2019. https://doi.org/10.3389/fbuil.2018.00085.

[81] Pelz, J. S., Ku, N., Meyers, M. A., and Vargas-Gonzalez, L. R. "Additive Manufacturing of Structural Ceramics: A Historical Perspective." *Journal of Materials Research and Technology*, Vol. 15, 2021, pp. 670–695. https://doi.org/10.1016/j.jmrt.2021.07.155.

[82] Patel, F., and Badheka, V. "Overview on Printability of Metals and Alloys." *Materials Today: Proceedings*, Vol. 62, No. P13, 2022, pp. 7302–7307. https://doi.org/10.1016/j.matpr.2022.03.731.

[83] Ngo, T. D., Kashani, A., Imbalzano, G., Nguyen, K. T. Q., and Hui, D. "Additive Manufacturing (3D Printing): A Review of Materials, Methods, Applications and Challenges." *Composites Part B: Engineering*, Vol. 143, 2018, pp. 172–196. https://doi.org/10.1016/j.compositesb.2018.02.012.

[84] Jandyal, A., Chaturvedi, I., Wazir, I., Raina, A., and Ul Haq, M. I. "3D Printing – A Review of Processes, Materials and Applications in Industry 4.0." *Sustainable Operations and Computers*, Vol. 3, 2022, pp. 33–42. https://doi.org/10.1016/j.susoc.2021.09.004.

[85] Peng, T., Kellens, K., Tang, R., Chen, C., and Chen, G. "Sustainability of Additive Manufacturing: An Overview on Its Energy Demand and Environmental Impact." *Additive Manufacturing*, Vol. 21, 2018, pp. 694–704. https://doi.org/10.1016/j.addma.2018.04.022.

[86] Javaid, M., Haleem, A., Singh, R. P., Suman, R., and Rab, S. "Role of Additive Manufacturing Applications towards Environmental Sustainability." *Advanced Industrial*

and Engineering Polymer Research, Vol. 4, No. 4, 2021, pp. 312–322. https://doi.org/10.1016/j.aiepr.2021.07.005.

[87] Zhao, L., Jiang, Z., Zhang, C., and Jiang, Z. "Development Model and Experimental Characterization of Residual Stress of 3D Printing PLA Parts with Porous Structure." *Applied Physics A: Materials Science and Processing*, Vol. 127, No. 2, 2021. https://doi.org/10.1007/s00339-020-04238-2.

[88] Syrlybayev, D., Zharylkassyn, B., Seisekulova, A., Perveen, A., Talamona, D., Bruno, C., Fernandes, P., Faroughi, A., Ferrás, L. L., and Afonso, A. M. "Optimization of the Warpage of Fused Deposition Modeling Parts Using Finite Element Method." 2021. https://doi.org/10.3390/polym13213849.

[89] Pei, C., and Yuan, H. "Microstructural Characteristics and Its Correlation to Mechanical Properties of Additively Manufactured Nickel-Base Superalloy upon Heat Treatments." *Fatigue and Fracture of Engineering Materials and Structures*, 2022. https://doi.org/10.1111/ffe.13914.

[90] Harris, M., Potgieter, J., Archer, R., and Arif, K. M. Effect of Material and Process Specific Factors on the Strength of Printed Parts in Fused Filament Fabrication: A Review of Recent Developments. *Materials*. 10. Volume 12.

[91] Cano, S., Lube, T., Huber, P., Gallego, A., Naranjo, J. A., Berges, C., Schuschnigg, S., Herranz, G., Kukla, C., Holzer, C., and Gonzalez-Gutierrez, J. "Influence of the Infill Orientation on the Properties of Zirconia Parts Produced by Fused Filament Fabrication." *Materials*, Vol. 13, No. 14, 2020. https://doi.org/10.3390/ma13143158.

[92] Rashed, K., Kafi, A., Simons, R., and Bateman, S. "Fused Filament Fabrication of Nylon 6/66 Copolymer: Parametric Study Comparing Full Factorial and Taguchi Design of Experiments." *Rapid Prototyping Journal*, Vol. 28, No. 6, 2022, pp. 1111–1128. https://doi.org/10.1108/RPJ-06-2021-0139.

[93] Cerda-Avila, S. N., Medellín-Castillo, H. I., Cervántes-Uc, J. M., May-Pat, A., and Rivas-Menchi, A. "Fatigue Experimental Analysis and Modelling of Fused Filament Fabricated PLA Specimens with Variable Process Parameters." *Rapid Prototyping Journal*, Vol. ahead-of-print, No. ahead-of-print, 2023. https://doi.org/10.1108/RPJ-10-2022-0354.

[94] Alvarez C., K. L., Lagos C., R. F., and Aizpun, M. "Investigating the Influence of Infill Percentage on the Mechanical Properties of Fused Deposition Modelled ABS Parts." *Ingenieria e Investigacion*, Vol. 36, No. 3, 2016, pp. 110–116. https://doi.org/10.15446/ing.investig.v36n3.56610.

[95] Jap, N. S. F., Pearce, G. M., Hellier, A. K., Russell, N., Parr, W. C., and Walsh, W. R. "The Effect of Raster Orientation on the Static and Fatigue Properties of Filament

Deposited ABS Polymer." *International Journal of Fatigue*, Vol. 124, 2019, pp. 328–337. https://doi.org/10.1016/J.IJFATIGUE.2019.02.042.

[96] Çakan, B. G. "Effects of Raster Angle on Tensile and Surface Roughness Properties of Various FDM Filaments." *Journal of Mechanical Science and Technology*, Vol. 35, No. 8, 2021, pp. 3347–3353. https://doi.org/10.1007/s12206-021-0708-8.

[97] Poore, M. W., and Kesterson, K. F. *A STRAIN-GAGE TECHNIQUE FOR MEASURING THE THERMAL EXPANSION OF SOLIDS (Report Y-2065)*. 1977.

[98] National Instruments. "NI-DAQmx 21.3 Help." 2022, pp. 218–220.

[99] Tenney Environment, and Thermal Product Solutions. *T2 Series Specifications and Product Information*. 2020.

[100] UQG Optics. Suppliers of Custom and Stock Optics. *Corning 7980 Technical Data Sheet*. www.uqgoptics.com.

[101] Omega Engineering Inc. *SG401 and SG496 Rapid Cure Strain Gauge Adhesives User's Guide*. 2013.

[102] Vishay Precision Group, and Micro-Measurements. *Measurement of Thermal Expansion Coefficient Using Strain Gages Strain Gages and Instruments*. 2010.

[103] Kamau-Devers, K., Yanez, V. R., Medina Peralta, V. W., and Miller, S. A. "Using Internal Micro-Scale Architectures from Additive Manufacturing to Increase Material Efficiency." *Journal of Cleaner Production*, Vol. 291, 2021. https://doi.org/10.1016/j.jclepro.2021.125799.

[104] Wojtyła, S., Klama, P., and Baran, T. "Is 3D Printing Safe? Analysis of the Thermal Treatment of Thermoplastics: ABS, PLA, PET, and Nylon." *Journal of Occupational and Environmental Hygiene*, Vol. 14, No. 6, 2017, pp. D80–D85. https://doi.org/10.1080/15459624.2017.1285489.

[105] Chun, H. J., Daniel, I. M., and Wooh, S. C. "Residual Thermal Stresses in a Filamentary SiCAl Composite." *Composites Engineering*, Vol. 5, No. 4, 1995, pp. 425–436. https://doi.org/10.1016/0961-9526(95)00015-F.

[106] Sehhat, M. H., Mahdianikhotbesara, A., and Yadegari, F. "Impact of Temperature and Material Variation on Mechanical Properties of Parts Fabricated with Fused Deposition Modeling (FDM) Additive Manufacturing." *International Journal of Advanced Manufacturing Technology*, Vol. 120, Nos. 7–8, 2022, pp. 4791–4801. https://doi.org/10.1007/s00170-022-09043-0.

[107] Charlon, S., and Soulestin, J. “Thermal and Geometry Impacts on the Structure and Mechanical Properties of Part Produced by Polymer Additive Manufacturing.” *Journal of Applied Polymer Science*, Vol. 137, No. 35, 2020. https://doi.org/10.1002/app.49038.